Automatic Breast Cancer Classification Using Novel Feature Extraction for Magnetic Resonance Imaging and Image Processing Technique

Alshanbari, Hanan Saad J

Award date:
2014

Awarding institution:
Coventry University

Automatic Breast Cancer Classification Using Novel Feature Extraction for Magnetic Resonance Imaging and Image Processing Technique

Hanan Alshanbari

Automatic Breast Cancer Classification Using Novel Feature Extraction for Magnetic Resonance Imaging and Image Processing Technique

By
Hanan Alshanbari

April 2013

A report submitted in partial fulfilment of the University's requirements for the Degree of Doctor of Philosophy

Coventry University | Doctoral College | Centre for Research Capability and Development

Library Declaration and Deposit Agreement

Title: Ms	**Forename:** Hanan	**Family Name:** Alshanbari
Student ID: 3946316	**Faculty:** ECC	**Award:** PhD

Thesis Title:
Automatic Breast Cancer Classification Using Novel Feature Extraction for Magnetic Resonance Imaging and Image Processing Technique

Freedom of Information:
Freedom of Information Act 2000 (FOIA) ensures access to any information held by Coventry University, including theses, unless an exception or exceptional circumstances apply.

In the interest of scholarship, theses of the University are normally made freely available online in the Institutions Repository, immediately on deposit. You may wish to restrict access to your thesis for a period of up to three years. Reasons for restricting access to the electronic thesis should be derived from exemptions under FOIA.
(Please also refer to the University Regulations Section 8.12.5)

Do you wish to restrict access to thesis/submission:	No

Please note: If your thesis includes your publications in the appendix, please ensure you seek approval from the publisher first, and include their approval with this form. If they have not given approval, they will need to be removed from the version of your thesis made available in the Institutional Repository.

If Yes please specify reason for restriction:

Length of restriction:	
Does any organisation, other than Coventry University, have an interest in the Intellectual Property Rights to your work?	No
If Yes please specify Organisation:	
Please specify the nature of their interest:	
Signature: 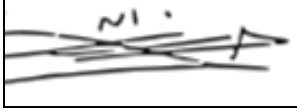	**Date:** 29/1/2018

For Doctoral College and Centre for Research Capability and Development use	
Date Final Thesis Submitted	
Date of Thesis release to Library	

Certificate of Ethical Approval

Applicant:

Hanan Alshanbari

Project Title:

Automatic Breast Cancer Classification Using Novel Feature Extraction for Magnetic Resonance Imaging

This is to certify that the above named applicant has completed the Coventry University Ethical Approval process and their project has been confirmed and approved as Low Risk

Date of approval:

19 June 2017

Project Reference Number:

P57934

ABSTRACT

Determining the appropriate methodologies for the early detection of breast cancer is still an open research problem in the scientific community. Breast cancer continues to be a significant problem in the contemporary world. After 40 years of age, people tend to be more able to developing cancer, and nearly 25% of cancers are detected in women between the age of 40–49 years (Health Quality Ontario, 2007). Early detection and treatment are currently the only proven means to reduce breast cancer's related mortality rates.

Computer-aided detection is suggested as an adjunct to screening mammogram to decrease perception-based errors. Medical image processing tools were demonstrated to be effective methods for helping radiologists identify suspicious tissues in different medical imaging modalities such as Mammograms, Magnetic Resonance Imaging (MRI), and ultrasound. Since there are several types of abnormalities in the breast, they require special focus for detection; however, even trained specialists are frequently unable to detect them.

Moreover, medical experts might make mistakes, as they are only human; they may be over-worked or may make common errors, which can result in even bigger issues (or translate into death) for the patient. Hence, to lessen the burden on those physicians who face these problems, as well as higher workloads, it is imperative to facilitate the diagnostic process and to also train sufficient numbers of residents to interpret mammograms, (MRI), or other imaging modalities in the future.

MRI-based imaging provides far superior clarity and resolution when compared to other imaging modalities. The clear and precise information offered by MR imaging serves as the basis for correctly detecting cancers, while also identifying their specific type. Various imaging modalities (including MRI) provide outputs that do not give clear information or that do not clarify hidden information associated with breast cancer; in fact, it is often not possible for people to detect these unclear outputs. A specialist may

find it difficult to correctly predict the cancer type, which could lead to the wrong diagnosis. This prediction can be improved by computer-aided technologies, which also minimizes human intervention. In this study, we tried provide an automatic detection breast cancer detection system using samples of MRI breast images.

One of the fundamental issues in the design of a detection system is to determine the efficient features that should be used together to improve the accuracy of said system. Depending on the type of feature (bad to best) that is used in system design, the detection scheme can provide classification accuracy results (0 to 100%). The use of a good classifier is also necessary to deal with non-linear classification.

This research work proposes pre-processing methods for MR images, as well as novel methods to detect cancer in those images. This work also proposed new methods to retrieve discriminative features from suspicious MR images, and also utilizes the neural network classifiers on them to create an automatic decision making system. An extensive test is conducted on the classifier to assess its ability to provide false-positive and false-negative readings, and also evaluated its accuracy rates.

The proposed research starts with a detailed study to understand the suspicious patterns observed in MR images. In order to overcome some of the bottlenecks in the existing methods, this study tries to improve the suspicious MRI pattern detection by devising novel techniques (novel features). In this investigation, this study further offers an exploration of the current theoretical approaches to segmentation, and then aim to assess the impact of a watershed transform algorithm on magnetic resonance (MR) image quality in the early detection of breast cancer to confirm the efficiency of this auto segmentation method. Moreover, five features are tested to classify the tumours. Further, ANN-based classifiers are used on these features to improve detection and to generate correct cancer classifications. This study further incorporates the support vector machine (SVM) classifier and test correct classification ability of proposed system. Different kernels of SVM are tested to find out the best results. SVM outperforms the ANN classifier in terms of accuracy by 98.52%. This study successfully classifies the type of a tumour with high accuracy using MRI of breast

images. MRI data for this study is collected from King Abdullah medical city (KAMC) (http://www.kamc.med.sa/index.php/en/).

CONTENTS

List of Figures

List of Table

ACRONYMS

ABCDS	Automatic Breast Cancer Detection System
ACDS	Automated Cancer Detection System
ACO	Ant Colony Optimization
AD	Architectural distortion
AMGA	Adaptive merging and Growing Algorithm
AND	Anisotropic Nonlinear Diffusion
ANFIS	Adaptive Neuro Fuzzy inference System
ANN	Artificial Neural Network
AnSR	Anisotropic Smoothing Regularize
ART	Adaptive Resonance Theory
AWGN	Additive with Gaussian nose channel
BPN	Back Propagation Neural Network
BSE	Breast Self-Examination
CAD	Computer-Aided Detection
CBR	Construction Products Regulation
CC	Cranio-Caudal
CPP	Combined Patch and Pixel
CPU	Central Processing Unit
CSF	Cerebrospinal Fluid
CT-Scan	Computed Tomography Scan
DCIS	Ductal Carcinoma in Situ
DCT	Discrete Cosine Transforms
DIP	Digital Image Processing
EHR	Electronic Health Records
FA	Firefly Algorithm
FCM	Fuzzy C-Means
FDS	Food and Drug Administration
FFANN	Feed-Forward Artificial Neural Network

GA	Genetic Algorithm
GaSR	Gaussian Smoothing Regularize
GB	Gigabyte
GBM	Glioblastoma
GHz	Gigahertz
GM	Grey Matter
GPC	Graph Proximity Cleansing
IMF	Interpolate Median Filter
IQ	Intelligent Quotient
KCGA	K-means with Chaos Genetic Algorithm
LCIS	Lobular Carcinoma In Situ
LITT	Laser-induced Interstitial Thermal Therapy
LVQ	Learning Vector Quantization
MATLAB	Matrix Laboratory
MC	Micro-Calcifications
MFNN	Mixed Feature based Neural Network
MLO	Medio-Lateral Oblique
MM	Min Max
MMRF	Markov Random Field
MRI	Magnet Resonance Imaging
NLM	Non Local Means
NLST	Non linear Structure Tensor
NMP	Nuclear Magnetic Resonance
OTVF	Optimized Total Variation Filter
PDE	Partial Differential Equation
PET	Positron Emission Tomography
PSO	Particle Swarm Optimization
RAM	Random Access Memory
RBF	Radial Basis Function
RF	Radio Frequency
RNLM	Rican non-local filter

ROI	Extract Regions of Interest
SEL	Successive Enhancement Learning
SNR	Signal-to-Noise Ratio
SOM	Self Organization Map
SPECT	Single Photon Emission Computed Tomography
SVM	Support Vector Machine
TDLU	Terminal Ductal Lobular Unite
TIM	Threshold Internal Method
TV	Total Variation
UDWT	Undecimated Wavelet Transform
USA	United States of America
WM	White Matter
WML	White Matter Lesion
X-Ray	X-Radiation

ACKNOWLEDGEMENTS

First of all, I would like to thank my supervisor, Dr. ***Saad Amin***. I feel privileged to express my deep sense of gratitude to my supervisor for his valuable guidance, endless support, and constant encouragement throughout the course of my research work. His truly scientific intuition and broad vision inspired and enriched my growth as a student and researcher. I humbly acknowledge a lifetime of gratitude to him. I would also like to thank Dr. ***James Sheterworth*** for providing critical feedback and comments during our discussions, which are deeply acknowledged.

I express my regards to Dr. ***Khaled Salman*****,** Director of the **King Abdullah Medical City Hospital, Saudi Arabia** Research Center, and Mr. ***Shadi Musalm***, who supported and made my research data collection possible.

I am highly indebted to my dear ***husband*** for his great guidance and sacrifice throughout the course of my research work. Further, I am highly indebted to him and to my daughters, ***Nouf*** and ***Haya***, for being a constant source of love and motivation for me, particularly in times of hardship and difficulty. They have always been a source of true guidance, inducing the feeling of eternal divine power within me.

I would like to thank my wonderful ***parents*** for their unrelenting support and trust. I would not have made it this far without you. I greatly appreciate your efforts in leading my siblings and myself to intellectual pursuits, and I cherish your ideals for being extraordinary individuals who do not just see the world the way it is, but you also see it the way it should be.

Thanks to other members of my family, especially my sisters and brother. Their kind words of encouragement will remain forever etched in my memory and consciousness.

I would like to express my sincere thanks to the many anonymous reviewers of the various Conferences and Journals. Their constructive comments helped me to shape the course of my research work.

Finally, I would also like to thank all the readers of this work, since any piece of academia is useful if it is read and understood by others. In this way, academic works can serve as a bridge for future research.

With profound gratitude, love, and devotion, I dedicate this work to almighty Allah for the beneficence and mercy he has always bestowed upon me and to my ***Parent***.

List of Publications

This research has been documented, in part, within the following publication:

Alshanbari, H., Amain, S., Shuttelworth, J., Slman, K., & Muslam, S. (2015). Automatic segmentation in breast cancer using watershed algorithm. International Journal of Biomedical Engineering and Science, 2(2), 1-6.

CHAPTER 1

INTRODUCTION

1.1 INTRODUCTION

Computers are very efficient and helpful in carrying out mundane tasks and in processing medical data into useful information; its potential as a powerful technology can be further exploited to assist radiologists in making more accurate diagnoses (Moein, 2014; Taylor, 2008). The utilization of computers in decision making can be employed in many different forms. The vast and abundant accumulated wealth of information available within each image can be made available to radiologists to detect abnormalities and to ultimately arrive at a more consistent decision (Graber et al., 2002; Jordanov et al., 2015).

Although much attention has been paid to technical quality assurance to guarantee optimal image quality in most breast screening methods, such as mammograms and ultrasounds, many improvements can be made to enhance the quality of image interpretation, which seems to be the weakest link in the process. Thus, there is a need to develop tools or algorithms that assist radiologists in making quick and accurate decisions. To increase detection and diagnostic accuracy, and to save on the need for manual labour, computer-aided methodologies (algorithms) have been developed. These computer-aided algorithms can make diagnoses in a more quantitative, algebraic fashion, although it cannot be denied that most radiological decision making is highly subjective. Such methodologies or algorithms were also developed to help radiologists evaluate medical images and to detect abnormalities in the breast at an early stage. In general, these methodologies are procedures that employ computers to assist doctors in interpreting medical images. This is an interdisciplinary method that combines the technology of digital image processing with radiological image processing. Computer-aided algorithms combine image processing techniques and the knowledge of expert radiologists to improve the accuracy of abnormality detection. In particular, these methodologies, which are used for the automated detection (Woods et al., 2002) or classification (Fraser et al., 2014) of abnormalities in the breast, can be very useful in controlling the development of breast cancer, and they can also provide doctors with a second perspective, which is characterized by very good consistency and repeatability.

The existence of electronic health records (EHRs) has encouraged researchers to adopt the idea of an electronic healthcare system, where the components of the legacy healthcare systems come together and electronically share and transfer patient information across a nationwide public infrastructure.

1.2 AIMS AND OBJECTIVES

Novel techniques are proposed in this work to analyze suspicious tissue patterns in the early detection of breast cancer. The developed techniques are expected to help radiologists evaluate breast images and to detect breast cancer more accurately. Such systems are used in conjunction with human evaluations of a given diagnosis. These systems not only improve image quality, but they also help to increase image contrast, automatically determine lesion location, greatly reduce the human efforts required to make a diagnosis, and improve the accuracy of detection and diagnosis. The computer-aided algorithms for pre-processing help to separate suspicious regions, which may contain abnormalities, from the background parenchyma. In other words, such pre-processing methodologies partition the images acquired from magnetic resonance imaging (MRI) into several nonintersecting regions, and they also extract regions of interest (ROIs) and suspicious tissue candidates from these images. Overall, the proposed method for breast cancer detection uses image processing methods like image de-noising , image enhancement, image segmentation, classification, etc., to detect breast cancer in its early stages, as these methods assist radiologists in detecting abnormalities; they also improve the accuracy of interpretation.

The main aim of this study is to develop a system that can provide segmentation and classification of breast tumours with a high degree of accuracy. In order to achieve the same, following objectives are designed for this study:

1. To search for novel and optimal breast cancer detection features.
2. To combine these novel features with the pre-existing features from the literature in order to develop better feature data.
3. To develop a MRI-based automated breast cancer classifier.
4. To analyze a developed automated method to enhance classification accuracy.
5. To minimize the false-positive and false-negative rate during classification.

1.3 RESEARCH SCOPE

In recent years, bioinformatics has become a notable field, since it enables data analysis of an organism to diagnose various diseases, such as cancer. Cancer is a dreadful disease that is found in many living beings. Cancer studies constitute one of the most challenging areas in research; it is the second-leading cause of death worldwide (Boyle, 1997). At present, one of the most important causes of cancer-related deaths among middle-aged women is breast cancer. MRI is a commonly used imaging modality that is currently employed by radiologists in the early detection and diagnosis of cancer through images of the breast. Digital MRI has turned out to be the most effective technique for premature breast cancer detection, although fewer research initiatives have attempted the development of automated tumour detection and classification methods using MRI samples.

Digital MRI captures magnetic resonance (MR) images of the breast and accumulates all image files in a computer. MR images require noise removal, contrast enhancement, and other pre-processing methods to achieve better feature extraction and accurate breast cancer identification. Processing these MR images requires high computational capabilities. Hence, this research aims to develop effective breast cancer detection and classification methods using MRI data.

1.4 PROBLEM SPECIFICATION

Making a correct breast tumour diagnosis is a rather difficult task and requires special efforts. The early diagnosis of breast cancer provides clinicians with the chance to use the most appropriate treatments, thus resulting in better chances of survival. The World Health Organization's International Agency for Research on Cancer Working Group confirmed that early cancer detection and treatment are considered to be the most promising approaches to reduce breast cancer mortality (World Health Organization, 2007, Senkus et al., 2015). Moreover, the auto-detection of breast cancer is still an open and challenging research issue. MRI-based cancer detection is still in its very early stages, and much less research has been carried out in this domain for the automated classification of breast cancer. This study is carried out to provide a fast, yet powerful, breast cancer detection technique that can provide an effective solution to promote accurate tumour detection, while ensuring low false detection rates using MRI datasets.

Image processing methods are applied to identify the tumour area in MR image samples. The proposed feature-extraction methods are also compared with earlier proposed feature-

extraction methods (total tumour area, angular smoothness of the corners, and the counter-clockwise rotation to clockwise rotation ratio) for classification accuracy Then, a hybridization of these features is applied and tested with a well-known classifier known as the artificial neural network (ANN) to improve the classification's performance even further. The result of ANN is validated against the k-fold cross-validation test, false-positive test, and false-negative test. Figure 1.1 shows a sample of the MRI data for (a) a benign and (b) a malignant tumour. It is quite evident from the figure that benign tumour is not that dense as the malignant tumour. That is the biggest visble difference between them and can serve the basis for the development of automatic detection system.

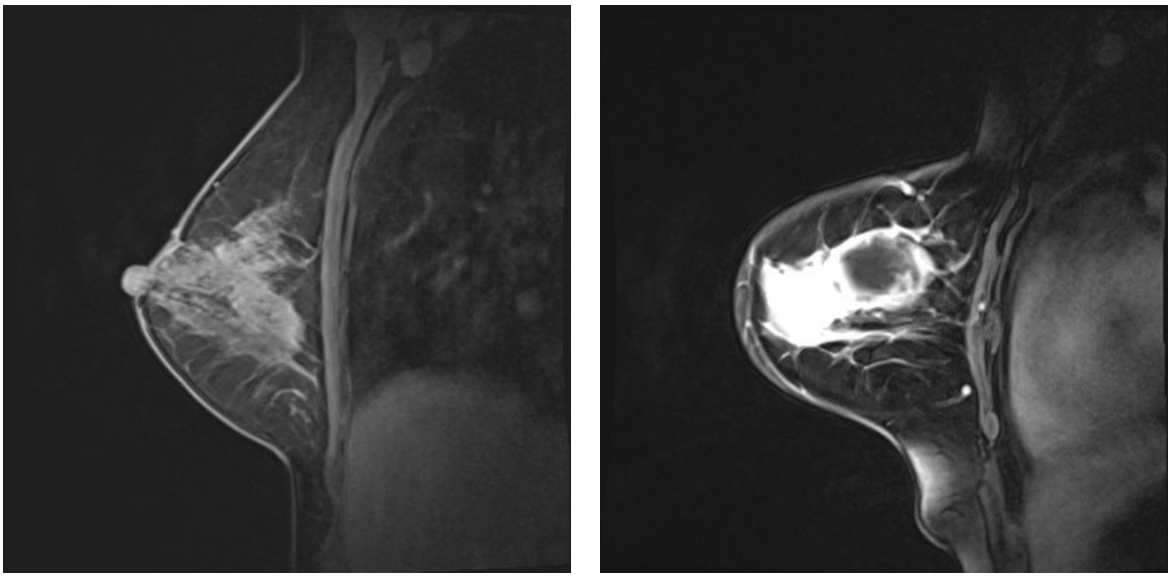

(a) (b)

FIGURE 1.1: SAMPLE MRI OF (A) A BENIGN AND (B) A MALIGNANT TUMOUR.

1.5 Thesis ORGANIZATION

The outline of this Thesis is provided below.

Chapter 1 provides an introduction to the research area, and it also details the aim of this study. This chapter also provides the scope of this research and an overview of subsequent chapters.

Chapter 2 through lights on the breast cancer, various tumour types, and different diagnostic methods and classification approach. It also features a definition of the research problem and offers an overview of the proposed approach for this research.

Chapter 3 deals with the literature review of breast cancer detection techniques, especially

mammography and MRI-based approaches. It reviews the methods currently used to identify breast cancer in its early stages, and it also discusses the different feature and classification approaches used during auto-detection.

Chapter 4 describes the methodologies that are currently used, as well as the methods explored in this study when analyzing MRI images in the early detection of breast cancer.

Chapter 5 provides an overview of the basic theories related to ANN and SVM.

Chapter 6 elaborates the automatic segmentation method proposed in this study to determine the ROI, so that feature extraction can be applied to that region.

Chapter 7 discusses the effective feature extraction and pre-processing methodologies. Then, a discussion is offered about the various classification approaches that employ the threshold method, ANN and SVM. Further, this chapter also features a classification analysis using k-fold cross-validation.

Chapter 8 concludes this Thesis by presenting experimental findings, as well as by providing the scope for future initiatives to enhance the work presented here.

CHAPTER 2

BREAST CANCER AND DETECTION METHODS

2.1 BREAST CANCER

Cancer develops when cells in a specific part of the body grow out of control. Cancer cells divide and grow indefinitely. Instead of dying, they outlive normal cells and they continue to form new abnormal cells. These cells usually form a tumour, which is nothing but the abnormal growth of tissue. There are two forms of tumours: malignant tumours and benign tumours. Malignant tumours are the most dangerous type of a tumour, which comprises cancer cells that invade the neighbouring tissues. Conversely, benign tumours grow locally and they are of a greater size; moreover, they do not invade neighbing tissues, they do not return following surgical removal, and they are not typically life threatening (Schwartz et al., 2013; Mehrabi et al., 2015).

Breast cancer is a malignant tumour that developed from cells of the breast. Breast cancers are life-threatening malignancies that develop in one or both breasts, and they represent the most common form of cancer among women aged 15–54 years (Mehrabi et al., 2015; Rodby et al., 2016).

2.2 TISSUE AND CELLULAR DIAGNOSIS OF BREAST CANCER

Tissue- and cell-based diagnoses are the most famous methods for breast cancer detection among medical professionals. This approach uses the Mammotome breast biopsy system (Burbank et al., 1996; Parker et al., 2001; Nakano et al., 2007; Pan et al., 2014; Denison and Lester, 2016), which was approved by the U.S. Food and Drug Administration (FDA) in 1996. An improved (handheld) version of the same device became available on the market in 1999. The basic principle employed in this method is as follows.

A large needle is used and inserted into the suspicious region of the human body (the breast, in the case of breast cancer) based on the findings of X-ray, ultrasound, MRI, or other similar

imaging tools (Pan et al., 2014; Denison and Lester, 2016). Then, the Mammotome is applied on the region to remove/vacate the suspicious tissue cells from the area. Additional tissues from a nearby area are also collected by rotating the device within the body. The patient remains still during the entire procedure, and either lies in the supine position (when the handheld device is used) or on the stomach (when the non-handheld device is used).

The removed tissues (specimens) are examined by a medical specialist to confirm or refute the presence of breast cancer via microscopic testing (Nakano et al., 2007).

2.2.1 The study of normal and abnormal cells

Cancerous or tumour cells are modified normal cells. This modification involves the loss of more specialized functions associated with differentiation, and they also include increased growth functions, as well as the resulting invasion and metastasis formation. The more rapid the growth, the more primitive the cell in terms of both its structure and specialized work and reproductive functions; in fact, the former function depends on the activity of the cytoplasm, while the latter depends on that of the nucleus. Cancer cells are changed in character, so they spend most of their energies on growth and little on function. Thus, cancer cells more closely resemble the biology of other cancer cells than normal cells. As cancer cells are mainly disorder of cellular reproduction, so an examination of nucleus can help us to recognize it.

The nucleus of the cancer cell is likely to be large in relation to the cytoplasm, although this relative difference is sometimes due to shrinkage of the cytoplasm rather than to an increase in the size of the nucleus. The nucleus is hyper-chromatic, owing to the increased content of nucleoprotein, which stains intensely with hematoxylin and basic aniline dyes due to the coarsening chromatin network. The nucleolus is large in proportion to the size of the nucleus, which is an important feature that may be more apparent in frozen sections of the unfixed tissue or in wet films.

The presence of numerous mitotic figures is suggestive of neoplasia, although they are also seen in granulation tissue and in other rapidly regenerating cells, so these figures are not proof of malignancy. It is important to note that the more rapid the growth, the more numerous the mitotic processes. The nucleus may be represented by a dark mass of chromatin, or the chromatin may be collected as a bar across the centre of the cell in the metaphase or monster stage (the typical appearance), or in two separate masses, one at each pole, in the anaphase or disaster stage. In highly malignant tumours, multicentric division and

other forms of typical mitosis may sometimes be seen. The chromosomes in a neoplastic cell vary in number, but in none of the malignant tumours examined has their number been normal (same as healthy cell).

As is evident, cellular diagnosis relies on an invasive method, limiting its usefulness. It will be much better if non-invasive methods can be developed for the detection of breast cancer; as such, this task is attempted in this work.

2.3 BREAST CANCER RISK FACTORS

Breast cancer continues to be a significant public health problem around the world. According to a study, women of the ages between of 40–49 years find more prone to breast cancer and approximately 25% of all breast cancer deaths occur in women of this age range (Health Quality Ontario, 2007). According to the estimation of the American Cancer Society, in 1996, approximately 184,300 women were diagnosed with breast cancer and 44,300 of them had died (Parker et al., 1996). An estimate from 2009 revealed that 192,370 new cases of invasive breast cancer were diagnosed, while about 40,610 women died in the United States. According to Ferlay et al. (2010), there are approximately 100.000 new cases of breast cancer worldwide each year; it is the second leading cause of cancer deaths in women.

Breast cancer can either be non-invasive (confined to the site of origin) or invasive (where it spreads beyond the site of origin) in nature. Non-invasive breast cancers include ductal carcinoma in situ (DCIS), which is also known as intraductal carcinoma, and lobular carcinoma in situ (LCIS). DCIS consists of cancer cells that present in the lining of the duct. DCIS is a non-invasive, early-stage cancer; however, if left untreated, it may sometimes progress to an invasive, infiltrating ductal breast cancer. Also non-invasive, LCIS is associated with an increased risk of invasive cancer development in both breasts (Sauter et al., 1997).

Although breast cancer has a very high incidence and death rate, its cause is still unknown, and there is no effective way to prevent its occurrence. Researchers have tried to trace both the environmental and genetic causes that lead to this disease, but so far, there is insufficient evidence to support the theories that implicate alcohol, unhealthy food, genetic mutations, pollution, and others in its development. Since breast cancer is a progressive disease that evolves during the various stages of cellular growth, the time at which breast cancer is detected is crucial.

The earlier breast cancer is detected, the higher the chance of survival (Goldhirsch et al., 2005; Rack et al., 2014). Determining the most appropriate methodologies for the early detection of breast cancer still remains an open problem in the research community, as the existing methods have a high miss rate and low specificity. Early detection and treatment are currently the only means proven to reduce breast cancer-related mortality rates.

2.4 LIMITATIONS OF THE CURRENT DETECTION METHODS

The detection of breast cancer is highly critical for making a proper diagnosis. According to the Independent UK Panel on Breast Cancer Screening (2012), the majority of methods used for breast cancer detection require human intervention, and that is why they are prone to error. Even experienced radiologists frequently fail to predict cancer types, so there is a need for an automated cancer detection system (ACDS). Moreover, X-ray-/ultrasound-based detection methods produce very poor results due to the poor visibility (low resolution) of the output image (Bleyer and Welch, 2012; Kelly, 2010). This limits automated detection and it also affects expert-based detection.

To satisfy the need for a large population for breast cancer detection, there is a growing demand for the low costs associated with automated and invasive methods, which require minimal human intervention and can provide accurate detection results with a minimum level of false-positive/negative diagnoses (Lee at al., 2010). The existing methods are costly and prone to errors (Hass et al., 2013; Lee at al., 2010). There are various features of breast cancer images that can be used to predict tumour class, and different researchers have proposed various means (imaging modalities) to do so. MRI has been proven to be very useful to get efficient features as compared to other modalities (Salem et al., 2013; Litjens et al., 2014).

Different features provide complementary information about the targeted region, which helps in the improvement of the classification accuracy. Due to that, there is a need to find out various features and optimal combinational methodology for superior performance. Furthermore, breast cancer detection should be automated, particularly for early-stage cancers, using the information retrieved from efficient features vectors. MRI is a highly effective technique for an early detection of breast cancer (Salem et al., 2013; Litjens et al., 2014) and the use of additional features can improve its performance even further.

2.5 A BRIEF ANATOMY OF THE BREAST

Obtaining an understanding of the anatomy of the breast is highly necessary to better understand the early detection of breast tumours, which is of primary importance in this investigation. The breast is composed of three basic structures: the skin, subcutaneous fat, and parenchyma fat. The interior of the female breast contains mostly fatty and fibrous connective tissues. It is divided into about 20 sections known as lobes, which are further subdivided into lobules. These are structures that contain milk-producing glands.

The ductal system is a branching system that extends from the alveoli to the end of the nipple; the ducts start branching as they extend closer to the nipple (within 16 mm) and can often follow a convoluted route. There are, on average, nine to 10 ducts that open onto the nipple, but this is individual and can range in number from four to 19. The diameter of the lactiferous ducts varies between individual women and can range from 1.09–5.89 mm. Upon milk ejection, the ducts shorten and widen, and their diameter expands as the breast milk flows towards the end of the nipple; they do not store milk. Milk ejection is essential when infants are breastfeeding, as only a minimal volume of milk is available to the infant before milk ejection occurs.

The areola is a pigmented circle of skin that surrounds the nipple. During pregnancy, the areola enlarges and becomes darker in pigmentation, which is associated with serum levels of prolactin and placental lactogen. The Montgomery's tubercles also called Montgomery's follicles, which are small sebaceous glands that open onto the areola, also become more prominent during pregnancy to provide lubrication and antimicrobial protection. Some tubercles can also produce tiny droplets of breast milk.

The nipple or papilla mamma is a conical elevation located in the centre of the areola and comprises a number of openings from the lactiferous ducts. The nipple tissue is composed of smooth muscle, which causes the nipple to become erect when it is stimulated and helps the newborn infant to locate the breast. It is, however, the least important part of the female breast during breastfeeding, and it simply provides a structure through which the ductal system and breast milk pass. The structure of the nipple is pertinent when establishing breastfeeding because good attachment and effective emptying of the breast are dependent on the infant taking a sufficiently large portion of breast tissue into its mouth. However, only a small proportion of this tissue includes the nipple.

Each mature female breast comprises an average of nine lobes, but this number can range between four and 19; the lobes are separated from each other by various amounts of fat. Each lobe consists of several lobules.

Each alveolus has a small duct that joins with others to form a single, much bigger lactiferous duct for each lobe. These lactiferous ducts extend towards, and individually open out, onto the surface of the nipple and are visible as distinct, albeit minuscule, orifices. It is for this reason that a blockage or inflammation of one lactiferous duct, as in cases of mastitis, will only affect one segment of the breast. Some of the breast lobes can also extend towards the underarm (known as the axillary tail or axillary tail of Spence); this tail can sometimes become tender, even painful, during menstruation and when lactation begins.

Normally, breast cancer first appears in the two functional elements: the lobules and ducts. Early forms of breast cancer are called in situ cancer. In situ cancer occurs when the cancerous cells have not yet spread beyond the initially affected area. DCIS is cancer that occurs in a woman's ducts and is more common than LCIS, which is cancer that is found in the lobes of the breast (Harris et al., 1992). The terminal ductal lobular unit (TDLU), which includes the inner branches of the lactiferous ducts, is the *basic histopathology unit* of the breast. The TDLU is important physiologically, as it is the site of milk production, and it is also the site where most breast lesions develop. An understanding of this anatomic structure, which is shown in Figure 2.1, is important when correlating it with mammographic and pathologic findings.

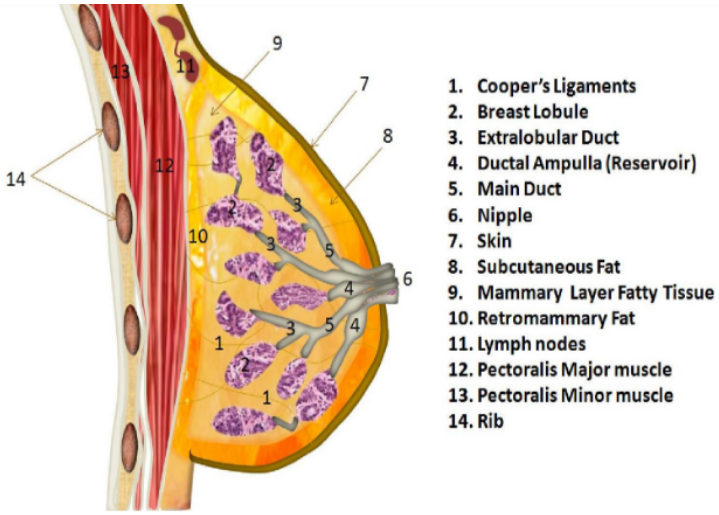

FIGURE 2.1: BREAST ANATOMY

2.6 STAGES OF BREAST CANCER

The different stages of breast cancer (Sölétormos et al., 2004) are briefly outlined in Table 2.1. Stage zero (0) describes cancer cells that are noninvasive, but which pose a long-term risk of becoming invasive. Stage one (I) describes tumours not more than 2 centimetres in diameter, and which have not yet spread beyond the breast. In stage two (II), the tumour is about 2 centimetres in diameter, but it has spread to the lymph nodes under the arm; conversely, the tumour may be about 5 centimetres in diameter, but it has not yet spread to the lymph nodes under the arm. Stage three (III) cancers are more than 5 centimetres across and they have spread to the lymph nodes or other tissues near the breast. Stage four (IV) cancers are known as metastasized cancers, and they have spread to other parts of the body. The seriousness of the diseases increases with each stage, as the survival rates decrease (McPherson et al., 2002).

Table 2.1: The different stages of breast cancer, indicated by the size and location of a patient's cancer, as reported by physicians (Harris et al., 2005)

Breast cancer is the commonest of all cancers and it is the second most common cause of cancer deaths in women, next to lung cancer (Jemal et al., 2007). It usually occurs during the involution period, i.e. in the years before menopause, and it rarely occurs before menopause. Moreover, this cancer is also rare before the age of 35 years. There is a higher incidence in nulliparous women, and the disease bears no relation to repeated suckling. Pregnancy, indeed, appears to have a protective influence. According to an estimate, 1 out of 90 female patients is likely to develop breast cancer at some time during her adult life in the USA and in Western countries (Jemal et al., 2007).

In summary, what is breast cancer?

1. Human breast cancer is a clonal disease that involves a single transformed cell, and where the end result includes a series of somatic (acquired) or germline mutations that are able to express their full malignant potential;
2. It is a malignant proliferation of the epithelial cells that line the ducts or lobules of the breast; and
3. It is a hormone-dependent disease.

2.7 BREAST ABNORMALITIES

Breast cancer is accompanied by a number of symptoms. The various abnormalities that may be seen in the breast include various masses, microcalcifications (MCs), architectural distortions, prominent lactiferous ducts, skin dimpling, or nipple thickening.

2.7.1 Masses

A breast mass is a localized swelling or lump in the breast that is described in terms of its size, shape, location, and margin characteristics. Masses are formed once the breast tissues thicken; the size of masses range from 3–30 mm, as shown in Figure 2.2. A benign mass will normally be associated with the presence of circular or oval shapes, and it will have well-defined margins. These circumscribed masses are compact and roughly elliptical. Circumscribed margins in benign breast masses will be well defined and sharply demarcated, and there will be an abrupt transition between the lesion and the surrounding tissue. Benign masses will also have a fatty halo surrounding the margin, and these masses are of medium to a low density (de Paredes, 1994). Figure 2.2 shows the different shapes of various masses: (a) an oval mass, (b) a lobular mass, (c) a circumscribed mass, and (d) a spiculated mass.

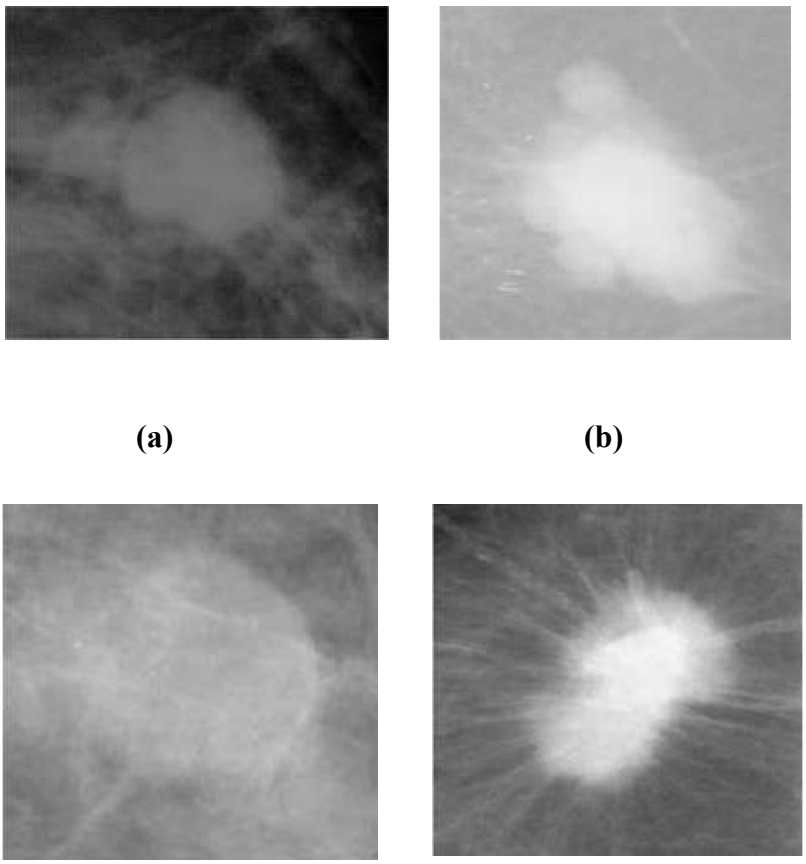

(a) **(b)**

(c) **(d)**

FIGURE 2.2: MAMMOGRAPHIC IMAGES OF (A) AN OVAL MASS, (B) A LOBULAR MASS, (C) A CIRCUMSCRIBED MASS, AND (D) A SPICULATED MASS.

Spiculated masses are more likely to represent a sign of a malignant process. The margin refers to the border of a given mass, and it should be examined carefully, as it is one of the most important criteria when determining whether a mass is benign or malignant. Malignant lesions generally have a more irregular shape than benign lesions. Spiculated lesions have a central tumour mass that is surrounded by a radiating pattern of linear spicules and ill-defined margins, which appear to be scattered. The centre of the lesion will be of medium to high density when compared to the surrounding tissues, and fine tendrils surround the tumour mass (de Paredes, 1994). Figure 2.3 shows the different types of masses.

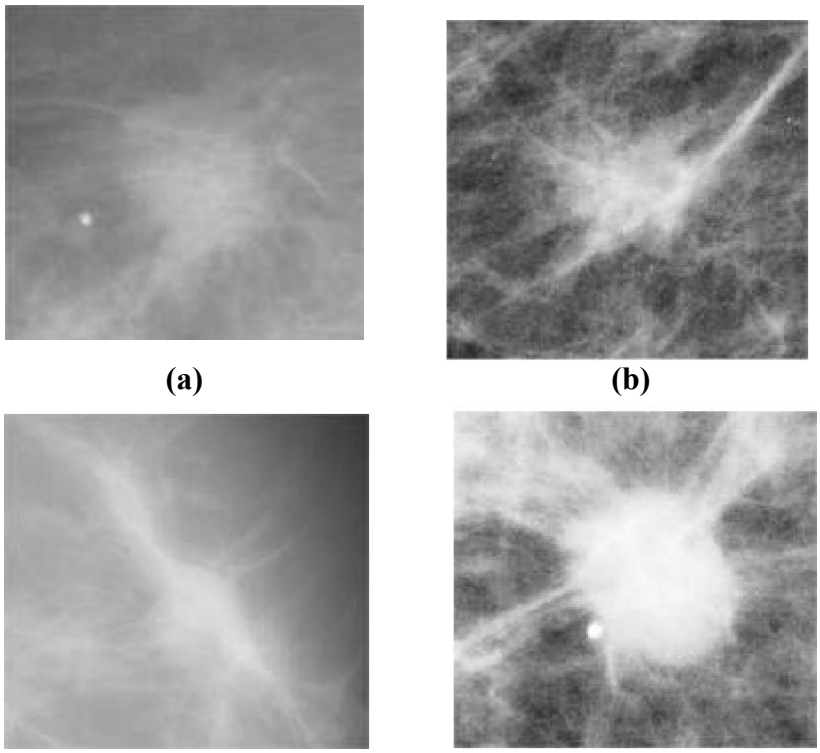

(a) **(b)**

(c) **(d)**

FIGURE 2.3: MAMMOGRAPHIC IMAGES OF (A) AN IRREGULAR MASS, (B) A MASS WITH MICRO-LOBULATED BOUNDARIES, (C) A MASS WITH OBSCURED BOUNDARIES, AND (D) A HIGH-DENSITY MASS.

2.7.2 Microcalcifications

MCs are tiny calcium deposits that range from 50 microns to several hundred microns in diameter, which usually appear in clusters. Calcifications represent an important sign of breast cancer. There are two types of calcifications: MCs and macrocalcifications. Macrocalcifications are scattered calcium deposits that are usually associated with benign conditions, and they rarely require a biopsy. MCs are isolated and appear in clusters, which are found embedded in a mass. Individual MCs typically range in size from 0.1–1.0 mm, with an average diameter of about 0.5 mm. A cluster is typically defined to be at least three MCs within a 1 cm^2 region (Boccignone et al., 2000).

Malignant calcifications may occur with or without the presence of a tumour or mass; they are typically grouped or clustered, and they vary in size and shape. Due to their high attenuation properties, MCs appear as white (or high-intensity) spots. MCs represent an early sign of breast cancer; however, only those regions in which these MCs appear as clusters

within a radius of 1 cm are MCs considered suspicious. The morphologic appearance of MCs, as illustrated in Figure 2.4, has been emphasized in the last decades. An analysis of MCs is normally based on morphological features, size, distribution, location, variability, and stability.

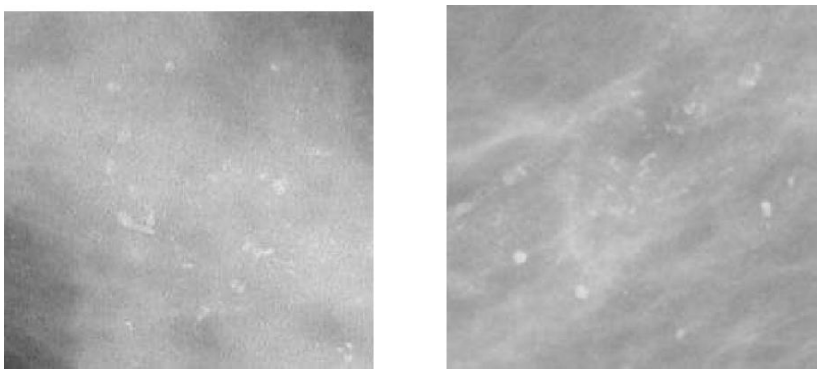

(a) **(b)**

FIGURE 2.4: MICROCALCIFICATIONS IN MAMMOGRAPHIC IMAGES.

2.7.3 Architectural Distortions

Architectural distortions (ADs) are a very important finding in the early detection of breast cancer. ADs are the third most common mammographic finding of breast cancer. As stated by Kopans (2007), "Breast cancer does not always produce a mammographically visible mass, but it frequently disrupts the normal tissues in which it develops. This distortion of architecture may be the only visible evidence of the malignant process. The probability of malignancy increases as a lesion becomes more irregular in shape. On the contrary, benign lesions are not architecturally distorted but have round, oval, or lobulated shape. Since the margins are not irregular in most benign lesions, benign masses appear encapsulated". BI-RADS (Breast imaging reporting and data system, USA) further defined AD as: "The normal architecture (of the breast) is distorted with no definite mass visible. This includes spiculations radiating from a point and focal retraction or distortion at the edge of the parenchyma. Architectural distortion can also be an associated finding." (Liberman and Menell, 2002).

The breast contains several piecewise linear structures such as ligaments, ducts, and blood vessels, which cause directionally-oriented textures in mammogram images. The presence of ADs changes the normal oriented texture of the breast. ADs appear as spiculations, retractions, and distortions. Figure 2.5 shows the appearance of an AD in a mammogram. It is difficult for radiologists to detect ADs due to the fact that their manifestations are typically subtle.

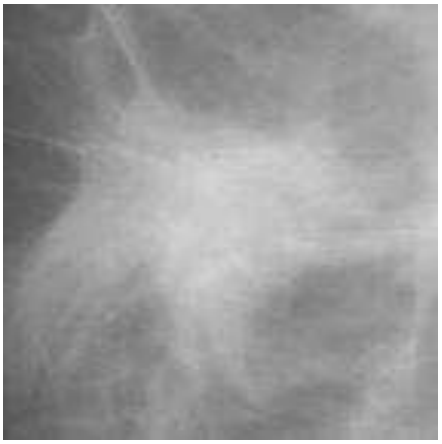

FIGURE 2.5: ARCHITECTURAL DISTORTION IN A MAMMOGRAPHIC IMAGE.

2.7.4 Bilateral Asymmetry

In bilateral asymmetry, the left and right breasts differ from each other in terms of their overall appearance in the corresponding mammographic images, as shown in Figure 2.6. The definition of asymmetry indicates the presence of a greater volume or density of breast tissue without a distinct mass; there may also be more prominent ducts in one breast when compared to the corresponding area in the other breast.

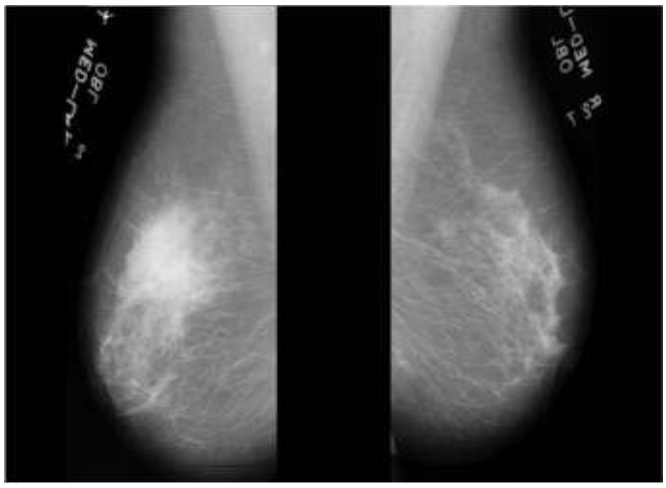

FIGURE 2.6: MAMMOGRAM SHOWING BILATERAL ASYMMETRY.

2.7.5 Other Abnormalities

Other less common signs of breast cancer include dilated lactiferous ducts and skin retraction. The lactiferous ducts may be dilated, and if these ducts are rather asymmetric, this appearance is considered to be indicative of ductal malignancy. Skin dimpling is an unusual change in the texture of the breast; in breast cancer, there may also be a change in the breast's skin colour, or there might be changes in the shape of the nipple, as shown in Figure 2.7

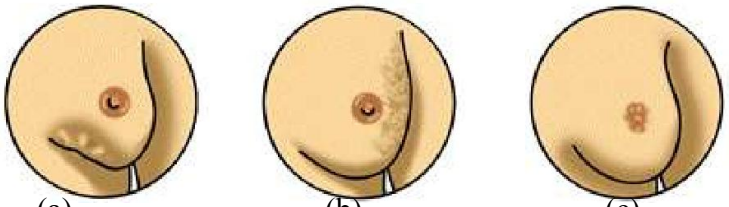

FIGURE 2.7: (A) SKIN DIMPLING, (B) A CHANGE IN SKIN COLOUR OR TEXTURE, AND (C) A CHANGE IN THE SHAPE OF THE NIPPLE.

In some cases of breast cancer, there may not be any noticeable symptoms. In fact, half of the women who get breast cancer will not experience any obvious symptoms, and they may discover their breast cancer only after undergoing a medical examination. Therefore, it is important for women to have periodic screenings for breast cancer. Breast cancer screening is vital to detecting breast cancer. The most common screening methods are mammography and sonography. There are several other breast-screening modalities, which will be discussed in the next section.

2.8 RISK FACTORS

As a matter of fact, diseases are seldom caused by a single factor (Lim et al., 2010). Certainly, the presence of the diphtheria bacillus or the tubercle bacillus in the body is not enough to produce diphtheria or tuberculosis. Three types of agents have been incriminated in the pathogenesis of breast carcinoma (Lawrence et al., 2014): hormonal stimulation, milk factors, and secretion retention.

Hormonal stimulation: The development and growth of the breast are under the influence of the ovary, the adrenal gland, and the pituitary gland (Vorherr, 2012). This is true also of mammary carcinoma. Indeed, no other tumour exhibits such a wide range of endocrine influences. Four hormones are principally involved: (1) oestrogen, (2) progesterone, (3) pituitary lactogenic hormone, and (4) pituitary–mammotrophic or mammogentic hormone (prolactin).

The endocrine organs involved in the production of this hormonal tetrad are, of course, the ovary, adrenal gland, and anterior pituitary gland. Some idea about the number of hormones being produced may be gained from measuring their excretion in the urine. When we say that mammary carcinoma is extremely susceptible to endocrine influence, it is necessarily responsible for the original induction of tumour development. Moreover, not all cancers of the breast are hormone dependent. Only 50% belong to this group although some clinicians give a figure as high as 60 per cent (Hadfield, 1958, Jozwik and Carroll, 2012)); moreover, only 40 per cent are markedly dependent. The remaining cancers have the gloomy and mysterious attribute of "autonomy", so it is often regarded as the essential biological characteristic of all malignant tumours. Unfortunately, the histology of a tumour gives no indication of its dependence. It is now recognized, however, that the enzyme content of the cancer cells may give us some leads in this respect. A histochemical study of breast tumours showed abundant esterase, lipase, and succinic dehydrogenase in well-differentiated adenocarcinomas, while lower levels were found in scirrhous carcinomas and none in medullary carcinomas. There is histochemical evidence that in oestrogen-sensitive tissues, oestrogen acts as a co-factor for transhydrogenase, thus releasing more energy for metabolic activities.

Both clinical and experimental observations support the concept of endocrine influence on breast cancer (Lawrence et al., 2014). The highest incidence of cancer is found between the ages of 40 and 49 years (Health Quality Ontario, 2007) when the influence of oestrogen is especially strong; women with delayed menopause appear to be excessively prone to developing the disease and the incidence is low in women who have had an ovariectomy. Furthermore, these tumours are 100 times more common in female than in male breast tissues (Jemal et al., 2008). If the ovaries are removed in young mice with a high mammary cancer strain, the danger of tumour development will be completely averted. The repeated injection of estrogen into mice will produce mammary cancer in a high percentage of cases, including in males of males of a non-susceptible strain (Chughtai, 1964). None of this, of course, is proof that human breast cancer is induced by hormonal stimulation, nor has cancer been produced in the higher mammals (those more closely related to humans) by the use of oestrogens (Cavalieri and Rogan, 2014).

It is of interest to note that in a series of 207 cases of cancer of the breast, in all but a few cases, there was hyperplasia of pituitary amphophils and basophils, the adrenal cortex, and the ovarian stroma, combined with thyroid atrophy with evidence of continuous oestrogen

stimulation of the epithelium of the breasts (Sommers et al., 1989). In these cases, the breasts and ovaries appeared to act as target organs. In sum, three ages are important factors in breast cancer development:

- Age at menarche: early menarche increases the risk of breast cancer by 50%–60%.
- Age at full-term pregnancy: late age (>35 years) increases the risk of breast cancer development.
- Age at menopause: late menopause increases the risks of breast cancer development by 35%.

Due to hormonal imbalances and increases in oestrogen, hypertrophy of the male breast is found in adolescence or in later life; this is called gynecomastia (Vorherr, 2012). It may occur as complications of a rare feminizing tumour of the adrenal glands, the pituitary gland, or testes. It may also arise from a tumour associated with diffuse liver disease, such as cirrhosis, as the liver is the chief organ responsible for the inactivation of estrogenic disease.

Milk Factors: The importance of heredity in the aetiology of cancer is well recognized, but Bittner (Bittner, 1941) has shown that in mouse mammary cancer, some extra chromosomal influences may be transmitted in the mother's milk (Tiede and Kang, 2011). If the young of a high breast-tumour stock are suckled by mothers of a low breast-tumour stock, the incidence of breast cancer is greatly reduced. Bittner has succeeded in extracting the cancer-producing factor in the breasts of animals with highly spontaneous carcinoma of the breast. When this factor was given to animals with a normal incidence of this tumour, the incidence rose from 1 per cent to 67 per cent. It seems certain that the carcinogenic factor is a filterable virus. It is rather startling to learn that the factor may be transmitted by both the male and female mouse.

Wood and Darling (Wood and Darling, 1943) report a family in which a number of instances of bilateral mammary carcinoma occurred in the course of four generations. In the third generation, three sisters developed breast cancer. Cancer occurred only in those women who had been nursed by their mothers, a fact suggesting the operation of a factor similar to the "milk influence" demonstrated by Bittner in mice. It is obvious that it would be most desirable to understand the extent to which Bittner's work on mouse models can be applied to the human female; however, the difficulties associated with this approach are also obvious. It is possible that a virus in the mother's milk may be the source and origin of the entire complex process that kindles the neoplastic fire in later life when conditioning factors (such

as hormonal imbalance or irritation in the ducts) prepare the stage for the final act (Yang and Jacobsen, 2008).

Breast drainage may be interfered with as the result of anomalies of the duct. The breast of the typical spinster has an underdeveloped, small, hard, fibrosed nipple, and we have already seen that cancer is commoner in those who have never borne children. According to one study (MacMahon and Feinleib, 1960), only 8.5 per cent of patients with cancer of the breast gives a normal nursing history. Bagg (Bagg, 1936) has shown that in a strain of mice with a low incidence of breast cancer, ligation of the ducts to the nipples on one side of the body halfway through pregnancy frequently produced carcinoma. By means of very rapid breeding without accompanying suckling, he also induced a high proportion of cancer cases. Of note, the animal with the most overworked mammary gland in the world – namely, the cow – never develops mammary cancer. Infiltrating carcinoma may originate de novo from normal breast tissue. In many cases, however, there is a preliminary epithelial hyperplasia followed by neoplasia within the ducts before infiltration occurs (Tiede and Kang, 2011). This may affect many groups of cells, so that a tumour may be of multicentric origin (Muir,1941).

Due to hormonal imbalances and increases in oestrogen, hypertrophy of the male breast is found in adolescence or in later life; this is called gynecomastia (Vorherr, 2012). It may occur as complications of a rare feminizing tumour of the adrenal glands, the pituitary, or testes. It may also arise from a tumour associated with diffuse liver disease, such as cirrhosis, as the liver is the chief organ responsible for the inactivation of estrogenic disease.

2.8.1 Spread

Cancer of the breast derives its evil power from its ability to invade the lymphatics, which enables it to spread even in its earliest stage (Lawrence et al., 2014). It is true that some of its forms, such as the comedo and medullary varieties, do not exhibit this tendency, but they are hopelessly outnumbered by the infiltrating scirrhous form. Spread may be accomplished by infiltration, by the lymphatics, and by the blood.

2.8.2 Infiltration

Infiltration is the means through which malignant cells spread throughout the breast. They infiltrate the tissue spaces between the fat cells and connective tissue bundles, as can be best seen in the scirrhous form of cancer. It tends to involve the skin and penetrates the pectoral muscles and even the chest wall. A tumour increases in size and invades other portions of the

breast. Adenocarcinoma and duct carcinoma show a comparatively slight tendency towards infiltration (Lawrence et al., 2014). Microscopic sections of the entire thickness of the breast show that the pectoral muscle is involved in over one-half the cases of scirrhous carcinoma at the time of operation, although no gross evidence of involvement may be apparent.

The lymphatic system propagates cancer spread by carrying the tumour cells over a distance. There are two ways in which this spread may occur (Lee et al., 2010). The cells may grow along the lymphatic system by a process originally described and named by Sampson Handley (Handley, 1931): lymphatic permeation. Conversely, they may be carried by the lymph stream in the form of tumour emboli. It is probable that embolism is a much more important method than permeation, although, for a long time, it was thought that permeation was the chief method of spread. The tumour cells reach the axillary lymph nodes early in the disease, especially in the scirrhous form of carcinoma.

Another method of spread is achieved through the blood (Yang and Jacobsen, 2008). When the bloodstream is invaded, the tumour cells are carried far and wide. It is via this route that skeletal metastasis occurs, although the initial spread may be accomplished via the lymphatic system. In order of frequency, the lumbar vertebrae, femur, thoracic vertebrae, rib, and skull are affected, and these deposits are generally osteolytic. Metastases may commonly occur in the liver, lung, and brain and occasionally in the adrenal glands and ovaries; however, they have also been described in most body sites.

2.9 SIGNS AND SYMPTOMS

The breast cancer like any other disease produces some signs and symptoms on the human body, which makes it easy to recognize in the earlier/ developing stage. As already mentioned that an earlier recognition makes the breast cancer easy curable. The general sings of breast cancer is as follows:

• Breast pain.

• Firm to a hard mass.

• Skin/nipple retraction due to pull of a scar.

• Discharge from the nipple.

• Erosion/ulceration of the nipple in Paget’s disease due to skin involvement.

• Enlargement.

• Redness.

• Generalized hardness.

• Shrinking of the breast.

• Skin tethering.

• Itching of the nipple.

The signs and symptoms of metastasis vary according to the part involved. These main signs and symptoms include:

• Weight loss.

• Bone pain.

• Back pain.

2.10 BREAST IMAGING MODALITIES

Early detection is the most successful method for dealing with breast cancer. Detection is the ability to find abnormalities and to determine where a “significant” case will prove to be malignant. Proper detection techniques will help to segregate benign cases from malignant ones. At present, the detection of breast cancer is achieved through breast self-examination (BSE), clinical evaluation, physical examination, and other screening modalities. Breast cancer screening is a professional medical examination that is performed to check a woman’s breasts for abnormalities, such as tumours and cysts, and to identify and locate any malignancies. Breast cancer screening is highly recommended, as it has been proven to significantly reduce cancer-associated fatalities. There are several breast screening modalities such as mammograms, ultrasonography, MRI, etc.

2.10.1 Advantages and disadvantages of using imaging modalities

Table 2.2 shows the advantages and disadvantages associated with using various imaging modalities for breast cancer detection.

Table 2.2: Advantages and disadvantages of pre-screening

Advantage	Disadvantage
1. Avoids expensive and toxic treatment for advanced cancer	1. Cost of additional cases
2. Extra years of productivity	2. Morbidity of test
3. Reassurance, if negative	3. Over diagnosis – e.g., DCIS (Wells et al., 2013)
4. Life years gained since more curable cancers are detected early on	4. Anxiety in positive cases and false reassurance of in false-negative cases

2.10.2 Mammography

Mammography is a periodical low-dose X-ray technique that is used to examine the breast; it is performed on women with or without complaints associated with breast cancer. An X-ray beam is passed through the tissue to record variations in the amounts of radiation that are absorbed by the tissues. However, different amounts of radiation are absorbed by different tissues, making it possible to distinguish between features and details about the examined tissues.

During the process of screening mammography, each breast is compressed onto a relatively flat surface, and an X-ray source on one side of the breast emits radiation through the breast. On the other side of the breast, the radiation is recorded on film or by an electronic device. A projection of the breast can be made from different angles. The two most common projections retrieved from mammographic screenings are cranio–caudal (CC) and medio–lateral oblique (MLO). In CC, each breast is examined from an overhead view, whereas in MLO, the breast is viewed from the side, as shown in Figure 2.8.

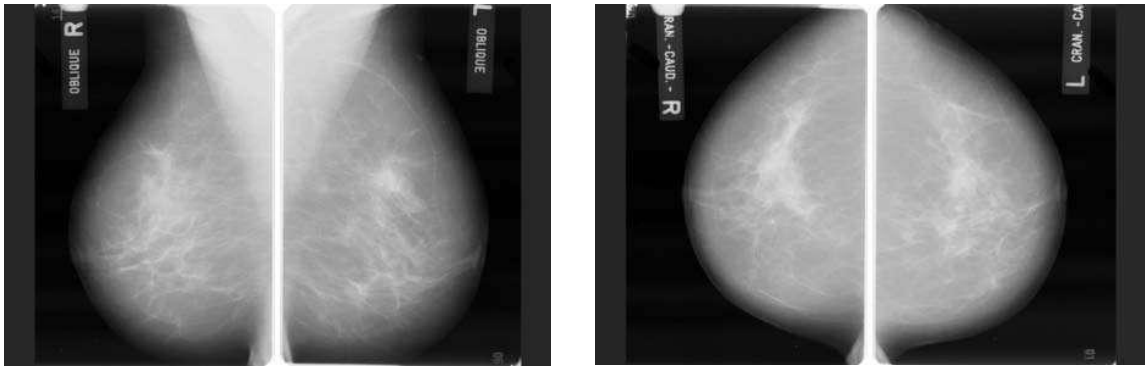

(a) **(b)**

FIGURE 2.8: (A) MEDIO–-LATERAL OBLIQUE (M LO) VIEW; (B) CRANIO–CAUDAL (CC) VIEW.

The main advantage of the MLO projection is that nearly the entire breast is visible, often including the lymph nodes. Part of the pectoral muscle will be shown in the upper part of the image. The CC view is taken from above, which yields an image that sometimes does not show the area closest to the chest wall. The standard practice of taking two views of each breast has been shown to be more sensitive and effective in detecting the signs of cancer. The main objective of screening mammography is to detect breast cancer when it is too small to be palpated by the physician or by the patient herself by means of BSE.

The most important signs of breast cancer that can be seen on a mammogram are focal masses, MCs, architectural distortions, and asymmetric breast tissue. Full-digital mammography is gaining importance when compared to conventional film-screen mammography due to the fact that digital acquisition, storage, and display processes may be conducted separately and are individually optimized.

2.10.3 Breast Ultrasound

An ultrasound is an imaging technique that sends high-frequency soundwaves through the tissues and converts them into images. The ultrasound examination places a sound-emitting probe on the breast to conduct the test without involving any radiation. In a standard ultrasound system, there are three basic types of data available for analysis: radiofrequency (RF) signals, envelope-detected signals, and B-mode images. A transmit/receive ultrasound transducer receives multiple analogue RF signals, which are converted into digital RF signals,

and beam forms into a single RF signal. The RF signal is then filtered and envelope detection is performed to yield an envelope-detected signal. Finally, the envelope-detected signal undergoes log compression, and proprietary post-processing is frequently applied to provide a greyscale representation. The resulting signals are then interpolated and rasterized to give a B-mode or display image (Noble et al., 2010).

Ultrasound is the best way to determine if the abnormality in the breast is solid (such as a benign fibroadenoma or cancer) or fluid-filled (such as a benign cyst) (Heywang et al., 1984). Wild and Neal (Sickles et al., 1983) were the first to propose the use of ultrasound imaging during a breast examination. Consequently, ultrasonography is more effective for women younger than 35 years of age. It is superior to mammography in its ability to detect local abnormalities in the dense breasts of adolescent women. From the literature, it is clear that the denser the breast parenchyma, the higher the detection accuracy of malignant tumours using ultrasound. Breast ultrasound has become an adjunct to mammography, which helps to differentiate benign from malignant lesions. It plays an increasingly important role in the evaluation of breast lesions due to the fact that it is safe (as it does not use X-rays or other types of potentially harmful radiation), portable, requires no ionizing radiation, and it is cost effective. Figure 2.9 shows an ultrasound image of a breast featuring a mass.

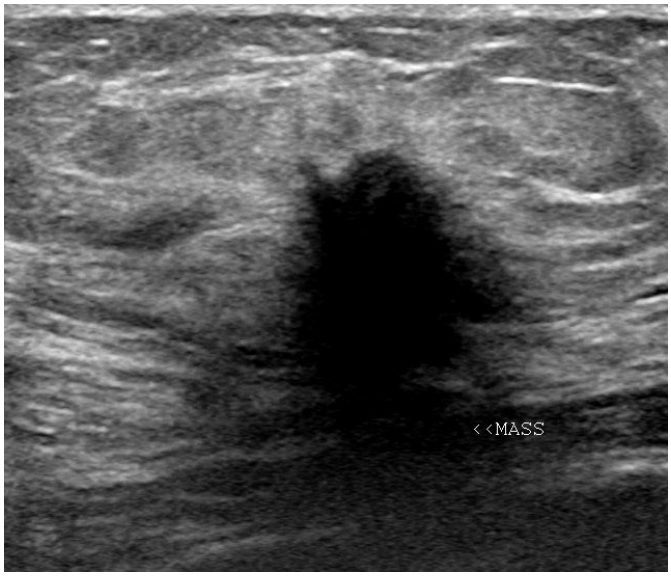

FIGURE 2.9: ULTRASOUND IMAGE SHOWING THE EXISTENCE OF A MASS.

The ultrasound image itself has some limitations, including its low resolution, low contrast, speckle noise, and blurry edges between various organs, so it is more difficult for a radiologist to read and interpret these images. In addition, ultrasound diagnosis is heavily

dependent on a doctor's personal experience. Mammography and ultrasonography are currently the most sensitive noninvasive modalities for detecting any breast cancers that have not yet spread to the lymph nodes, and these types of cancers thus have good prognoses.

A panel report issued by the Institute of Medicine and the National Research Council of National Academics (USA) says that while mammography is useful, it is not necessarily enough, and health practitioners need to investigate other complementary screening methods, such as ultrasound. The report also states that mammography depicts about three to four cancers per 1,000 women; however, in women with dense breasts, ultrasound depicts another three cancers per 1,000 women (Kolb et al., 2002). Mammography has its limitations in cancer detection in the dense breast tissues of young patients. Most cancers arise in dense tissues, so lesion detection for women in this higher risk category is particularly challenging. The breast tissue of younger women tends to be dense and full of milk glands, making cancer detection with mammography problematic. The cancers found on ultrasound are almost all small, yet invasive, cancers.

2.10.4 Magnetic Resonance Imaging (MRI)

MRI is the most promising breast cancer screening modality. In particular, dynamic contrast-enhanced (DCE) MRI shows high sensitivity in the characterization of breast cancer, whereas the specificity of the DCE-MRI is relatively low; it is also more expensive and requires the injection of a contrast agent (Hasebroock et al., 2009). MRI is able to differentiate between cancerous and noncancerous tissues due to its ability to detect the minute differences between the cells, and it can detect tumours missed by other modalities (Choe et al., 2005).

FIGURE 2.10: ORIGINAL SLICE OF AN MR IMAGE

MRI is increasingly being used in clinical settings as an adjunct to X-ray mammography and ultrasound. Of these imaging modalities, MRI has the highest sensitivity to invasive cancers and to multifocal disease. MRI is the most reliable method for assessing tumour size and extent when compared to the gold standard, histopathology. It also shows great promise for the improved screening of younger women (with denser, more radio-opaque breasts), and it holds much potential to detect cancers in women at high risk. At present, breast MRI has two major shortcomings: First, although its sensitivity is high, its specificity is relatively poor. Second, the method involves acquiring several high-resolution image volumes before, during, and after the injection of a contrast agent. A slice of an MR image can be seen in Figure 2.10. Given the large volume of data, the radiologist's ability to interpret the image becomes both complex and time consuming.

MRI is the most efficient approach for the early identification of breast tumours (Kriege et al., 2004; Theilmann et al., 2004; Barker et al., 2009; Benson et al., 2009; Van et al., 2015; Valerio et al., 2015). Breast cancer detection using MRI mainly utilizes the principle of nuclear magnetic resonance (NMR), which states that "Certain atomic nuclei can absorb and emit radio frequency energy when placed in an external magnetic field" (Slichter, 2013; Dale et al., 2015).

(a) (b)

FIGURE 2.11: AN EXAMPLE OF A DETECTED (A) BENIGN AND (B) A MALIGNANT TUMOUR USING MRI.

MRI is used to scan the breast via an external magnetic field in order to find potential tumour cells. An experienced radiologist subsequently analyzes the MRI images to classify a tumour as benign or malignant. Studies have shown that even for experienced radiologists, it is hard to make clear distinctions between tumours (Beale and Pryke, 2006, Timp et al., 2010). Figure 2.11 shows samples of MRI images taken from benign and malignant tumours.

MRI can detect lumps as small as 0.5 cm, while mammograms detect 1.1 cm lumps and

regular BSE detects lumps of about 2.1 cm. Women who are untrained in BSE have a lump that is, on average, about 3.6 cm upon detection. Table 2.2 shows the size of the tumours found by different search methods (Floyd et al, 2007, www.imaginis.com).

MRI is reported to have a sensitivity of 70%–90%. This means that the false-negative rate is between 10% and 30%. In other words, MRI can miss over one quarter of all tumours (Serres et al., 2012) when interpreted by human specialists. False negatives occur when the MRI is interpreted as negative when cancer is present. False negatives occur most often with dense breasts, which make the masses difficult to distinguish. Cancers are easier to detect in fatty breasts that are less dense (Boyd et al., 2007).

The advantages of MRI are:

- Elimination of process or artifacts
- Contrast enhancement
- Ability to perform invasive procedures more rapidly
- Potentially better resolution of the breast tissue for women younger than 50 years
- Reduced examination time for patients
- Increased examinations
- Immediate availability of images

2.10.5 Other Imaging Modalities

Breast cancer screening is commonly based on X-ray mammography, as it is cost effective and requires a very short acquisition time that provides a high throughput. Mammography, however, has a high false-negative rate and is not effective in dense breast tissue. This has

motivated the exploration of alternative imaging modalities including computed tomography (CT) (Einstein et al., 2007; Ueda et al., 2008), single photon emission CT (SPECT) (Strauss et al., 1982; Pandit-Taskar et al., 2010), and positron emission tomography (PET) (Schelling et al., 2000; Ponto et al., 2015).

Regardless of the recent advances in the early identification and surgical treatment of breast cancer, the mortality rates associated with this cancer have changed very little over the past decades, as the occult dissemination of cancer cells can occur at the early stages of carcinogenesis (Mathers et al., 2015). In this way, the mysterious dispersal of tumour cells in patients with operable malignancy can prompt the development of metastasis, yet it is typically missed by regular tumour arranging. Only 66% of these patients really have this ideal guess, while the remaining third develops the metastatic illness (Yang et al., 2013). This signifies that there is still a need to develop such methods/ tools that can detect the cancer in earlier stages with less effort and time.

2.11 SUMMARY

When examining the previously known facts about breast cancer and its associated screening modalities, it becomes clear that doctors who are performing biopsies on patients may welcome the idea of receiving additional guidance and visualization during this process. Diagnosticians that hold the training and experience required to interpret mammographic or ultrasound images are scarce. Therefore, there is an emphasis on training new radiologists to interpret these images. The situation would be more crucial if mass screening were adopted as a national policy. A detailed study of the tissue patterns formed in the breast, as well as their spatial relationships, is an area currently under consideration by research teams. The precise localization of breast tissue patterns has sparked the formulation of techniques that detect suspicious breast tissue patterns, which would aid radiologists in their diagnoses, while also providing estimations of the deviations of patient data with reference to normal data

CHAPTER 3

PROBLEM FORMULATION

3.1 INTRODUCTION

This chapter discusses the state of the art related to the proposed work – i.e., the methods used for the early detection of breast cancer. This chapter describes the works on the detection of breast cancer along with the pre-processing and segmentation methods. It also provides details about the classification algorithms which sheds light on formulating the research problem. This chapter highlights the limitations of existing work, which shows the path to carry out research by considering the limitations in the existing methods.

Performing accurate tissue segmentation using MR images is an important step in quantitative brain image analysis when detecting epilepsy. However, the accuracy of many segmentation algorithms is limited due to the presence of noise and intensity irregularity in brain MR images. Medical image segmentation has a huge impact on digital image processing, owing to its spatial resolution enhancement and image sharpening. It has been employed to derive helpful information from the medical image data which, in turn, provides the most precise and reliable method for diagnosis. This procedure is a critical challenge on account of the existence of inhomogeneities in image intensity. Eliminating spatial intensity irregularities from MR images is a difficult task since the inhomogeneities could vary with different MRI acquisition parameters, both from one patient to another and from slice to slice. The conventional method currently employed in hospitals is based on the manual segmentation of the medical image under consideration. This again relies on the physician's perceptive capabilities, as he or she will extract the required region from the image. However, this process is rendered difficult due to minute variations and the high degree of resemblance between the actual and affected biological regions in the image.

The insufficient number of radiologists and the huge volume of MR images to be analyzed result in intensive labour, and it is highly uneconomical. It also depends on the expertise of

the technician analysing the images (Beale and Pryke, 2006). The estimates also show that between 10% and 30% of tumours escape the eyes of radiologists during routine screenings. During the image acquisition stage, there are chances that the medical image might be tampered with due to issues that occur during this stage. Hence, the original image may not be useful for examination. Image segmentation can be defined as the partition or segmentation of a digital image into the same region types, with the important goal of simplifying the image under consideration into something that can be easily analysed visually. Image segmentation is a highly significant process in the whole field of medical image analysis.

There are various methods available to segment an image into subregions, so that homogeneity is maintained in each region. Due to their complexity and inaccuracy, not every technique is suitable for the examination of a medical image. Also, there are no benchmarked image segmentation techniques that can yield satisfying results. Developing an accurate segmentation method is an item of research. MR image segmentation is a highly demanding issue given its complexity. The segmentation of brain MR images is an extremely important step and it has gained much attention among many researchers over the past decade. This chapter provides a detailed account of a few of the image de-noising techniques used, as well as of the image segmentation approaches that employ clustering methods, optimized clustering techniques, and random optimized clustering approaches. This chapter offers a review of the various segmentation methods, and it also discusses their drawbacks in a comparison-based analysis.

In addition, the methods used for tumour classification are also discussed. MRI provides high-quality images over mammograms, thus providing more detailed radiology information, as described by various researchers (Saslow et al., 2009; Mann et al. 2015; Billing et al., 2015), and it is currently one of the widely accepted imaging methods used for routine breast cancer screening. The techniques used in computer-aided detection (CAD) systems have a major impact on each system's performance. The challenge with breast cancer detection is that, although many techniques have been proposed thus far, recent studies show that the performance of commercial CAD systems still needs to be improved. The development of new algorithms for CAD systems for breast cancer detection is very important. The aim of this research is to develop an efficient system for breast cancer detection. As such, the idea of

a proposed novel segmentation algorithm – which may be more accurate, effective, and rapid, and which will use MR images – will also be discussed.

3.2 PRE-PROCESSING OF MR IMAGES

The image being tested, as obtained by the acquisition device, is vulnerable to damage by the environment. Image restoration attempts have been made to minimize the effects of these degradations with the help of a filter (Aldroubi et al., 1996; Rabbani et al., 2009). Hence, a basic issue in image processing is the enhancement of image quality by noise removal. A large variety of techniques devoted to carrying out this task is available. All approaches depend on the type of noise present in the images (Malladi and Sethian, 1996). Image pre-processing techniques are useful for improving image quality before an image is processed in a given application. This utilizes a small neighbourhood of a pixel in an input image to obtain a new brightness value in the output image. These pre-processing methods are also referred to as filtration and resolution enhancement. The primary medical image quality parameters are noise and resolution. The important aim of this section is to improve image quality by de-noising and enhancing its resolution. It is necessary to preserve the edges and contour information of each medical image. To do so, effective de-noising and improved enhancement techniques are necessary as most of the imaging techniques get disturbed by noise. Image de-noising techniques, their associated illustrations, and their corresponding works are represented in Figure 3.1. (Buades et al., 2005, Mohan et al., 2014).

FIGURE 3.1: PRE-PROCESSING USING FILTERING APPROACHES.

The de-noising of MR images is a significant issue that needs to be resolved. It has been under discussion recently due to its importance for many clinical and research purposes. One technique that has found extensive application in MRI pre-processing is the Gaussian filter (Jones et al., 2005; Kalavathi and Sowdeeswari, 2016). Even though it is able to reduce some image noise (particularly in homogeneous areas), this technique also eliminates high-frequency signal components, producing blurred edges in the images. Hence, this filter has generally been used for regularization purposes, such as in voxel-based morphometry (VBM) (Ashburner and Friston, 2000), to reduce anatomical irregularities. Many edge-preserving techniques (Garnica et al., 2000) were proposed to overcome the observed blurring effects. Still, this filter requires a great deal of time to remove noise; a few significant details would also be reduced in the de-noising process. Some of these algorithms were threshold-based and Hough transformation-based, as these algorithms are used in instances when the edges are ragged; as such, these approaches tend not to include the extreme edges of the pectoral muscle.

Other transform methods that have been employed when de-noising images are principal component analysis (PCA) (Eyal et al., 2009) and discrete cosine transforms (DCT) (Stark et al., 2010). Most of the transform-domain filters have evolved from variations of the transform threshold-inverse transform principle. Based on this principle, local transform approaches (i.e., a sliding window with or without overlapping) have yielded very good results recently (Guleryuz, 2003; Guleryuz, 2007; Yaroslavsky et al., 2000). In Guleryuz's (2007) technique for Gaussian noise reduction, the image noise is eliminated by making use of overcomplete linear transforms and thresholding. Actually, Guleryuz employed a classical sliding-window DCT thresholding approach, as in Yaroslavsky et al. (2000), but the adaptive combination of overlapping estimations was applied for the reduction of the Gibbs effects.

Other recently introduced approaches make use of learned image patch dictionaries (Aharon et al., 2006; Elad and Aharon, 2006; Mairal et al., 2008) in the place of DCT when de-noising images. All of these approaches have emerged from the fact that an image can be represented as the linear combination of a set of images, with fewer non-null coefficients. This characteristic, referred to as sparseness, is the heart of the JPEG and JPEG2000 compression standards. For instance, anisotropic diffusion filters (Gerig et al., 1992) are capable of removing noise by making use of gradient information without damaging important image structures.

Even though many algorithms have been innovated to de-noise images, the issue of noise

image suppression has remained an unresolved challenge, since noise removal brings in artifacts and blurs the images. A few of the more popular de-noising filters for MRI are non-local means, anisotropic diffusion, bilateral filtering, and the total variation filter. In this section, these four filtering methods will be discussed in terms of how they reduce artifacts and noise in MR images.

Kaur and Mittal (2014) examined an MRI tumour detection technique where de-noising was performed with a 3*3 mean filter. In this technique, a de-noising filter was applied to all images to eliminate white Gaussian noise. A two-dimensional (2D)-mean filter was utilized to de-noise the image. Here, the elements were summated and then divided by their number; the output is referred to as the average or means output. The 2D window or mask that was selected for the filtering process was 3*3 in size. The choice of window size only determined element selection. Image de-noising was performed using a mean filter rather than a median filter, as it smoothes the greyscale image data with more accuracy, conducts spatial filtering on each unique pixel, and then chooses the average value (and not just the median value) of the window elements. However, the only drawback is that this approach enables autocorrelations. This may also result in misguided visual impressions of importance, as the smoothness of the resulting curve may often be taken as an indication that few visible features are important, even if they are just normal noise.

Hence, the non-local means (NLM) filter, a novel technique proposed by Buades et al. (2005), has emerged as a very easy and effective means of limiting noise with minimal deterioration of the actual structures in the image. This method is performed in accordance with the original redundancy of patterns within the images. The NLM filter has been employed to de-noise MR images, and it has yielded better results in comparison with other available methods (Coupé et al., 2008; Manjón et al., 2010; Wiest-Daesllé et al., 2008).

De-noising techniques using NLM (Perona and Malik, 1990) were employed to raise the MRI SNR by decreasing the variations between pixels in the image with near similarity indices (Nowak, 1999). The reliability of the evaluation of pixel similarity is improved by comparing small image regions with a centre at each pixel, instead of performing pixel-by-pixel comparisons. The performance obtained by the realisation of NLM is good for images degraded by both Gaussian and Rician noise. However, the computational complexity is huge, since a large number of elementary operations are necessary to de-noise each pixel.

Zhang et al. (2014) examined a Rician NLM (RNLM) filter that employs combined patch and

pixel (CPP) similarity, where only those pixels that simultaneously share pixel and neighbouring similarities will be assigned higher weights in the average. To conclude, the enumerated results indicated that the RNLM-CPP algorithm can maintain small high-contrast particle details, which are clinically related, but generally blurred by the actual RNLM algorithm.

Hu et al. (2012) presented the integration of DCT into the NLM filter to address the limitations of the latter, which resulted in a new filter. In this new filter, image patches are transformed from the time domain to the frequency domain during the de-noising process, thus making use of DCT; then, lower-dimensional frequency coefficients of the subspace of DCT are obtained by a Zig-zag scan. As a result, similarity weights are calculated in this subspace with being hard to noise instead of the full space. Hence, the accuracy of similarity weights is enhanced, and more of the same kinds of pixels can be found in the search window. Lastly, taking the characteristics of Rician noise into consideration in the MR image, the unbiased correction operation is carried out to eliminate the biased deviation. The proposed filter has been compared with many methods introduced recently, and it was shown that the proposed filter outperforms the other methods with regard to both vision and complexity.

Hwuang et al. (2013) evaluated the anisotropic smoothing regularizer (AnSR), which uses edge detection and de-noising within a Demons framework to regularize the deformation field at each iteration of the registration in a more aggressive manner in homogeneously-oriented displaced regions. It simultaneously regularizes the images in a less aggressive manner in areas comprised of non-homogeneous local deformation and tissue interfaces. Conversely, the traditional Gaussian smoothing regularizer (GaSR) performs uniformly averaging over the entire deformation field, without considering transitions across tissue boundaries and local displacements in the deformation field. In this work, AnSR is applied within the Demons algorithm, and it performs pairwise registration on 2D synthetic brain MR images, with and without noise, after inducing a deformation that simulates shrinking of the target region anticipated from laser-induced interstitial thermal therapy (LITT). The Demons, in conjunction with AnSR, are employed to register clinical T1-weighted MR images for one epilepsy and one glioblastoma (GBM) patient pre- and post-LITT.

Tristán-Vega et al. (2012) introduced a method that heavily accelerates the computation of patch distances in NLM, considering only the differences between important features, as

related to the pixels to be weighed. In comparison to other related works, the technique has a number of key benefits that are tested over the usual MRI datasets: first, the calculation maintains the statistical characterization of patches in the original NLM, thus retaining its optimality properties. However, this approach is chiefly oriented to MRI, which is implicitly non-textured.

Gopinath (2011) innovated a graph-based MRI image segmentation approach where pre-processing is conducted by making use of anisotropic filtering. An anisotropic filter helps to smooth the regions of an image without blurring the edges. For a normalized MR image of the prostate, the intensity values and its standard deviation values are replaced in the diffusion equation; the diffusion equation smoothes within a region rather than across boundaries. This equation will not result in any inter-regional blurring, as is frequently caused by Gaussian smoothing. An anisotropic diffusion filter maintains the edges of an image, but it eliminates small features and produces a mask effect in various regions of the denoised images in a uniform manner. These de-noising methods substantially eliminate noise; however, one setback is that they produce blurred images and add artifacts.

Deepika (2014) introduced a segmentation method for noisy MR images using an anisotropic diffusion filter for brain tumours. The anisotropic diffusion filter performs better than other filtering techniques when de-noising medical images. Furthermore, de-noising performance can be enhanced by modifying some of the parameters of a given filtering technique. Gallea et al. (2008) assessed a method with the purpose of achieving noise removal in MRI. Implementation of an improved version of Perona and Malik's anisotropic diffusion filter was realized. In this schema, the modified diffusion equation of the filter is useful when considering the edge's direction. This permits the filter to blur uniform areas while preserving the edges. Palma et al. (2014) provided a quantitative analysis that describes the limitations of ADF, and it also offers a new framework on the basis of both the strongest edges and on the planar regions of the image to determine the optimal parameter settings.

Furthermore, Tabik et al. (2006) studied the parallel implementation of the anisotropic nonlinear diffusion (AND) algorithm for 3D image filtering. AND is a highly capable noise-reduction technique in the domain of computer vision. This method is performed in accordance with a partial differential equation (PDE) that is tightly mated with a massive set of eigen systems. De-noising large (3D) images in biomedicine and structural cellular biology using the AND filter involves a huge computational burden. As a consequence, a

suitable parallel realization of AND is the best technique for reducing its runtime. Greenberg et al. (2006) suggested improving the structure-adaptive anisotropic filtering approach on the basis of the non-linear structure tensor (NLST) analysis technique. Based on the anisotropic measurements of image structures, a novel kernel construction approach is developed, which fine tunes the filter shape into image characteristics. Through the accurately estimated orientation of the image structures, the filtering process is carried out by properly aligning the filter kernels. Nevertheless, the conventional anisotropic diffusion filter has many drawbacks, such as its sensitivity to noise.

McPhee et al. (2011) presented the use of a bilateral filter with the aim of performing high-pass filtering of magnetic resonance phase images, as its implementation is easy. A bilateral filter weighs a pixel's vicinity based on spatial distance and similarities in intensity. Bhonsle et al. (2012) demonstrated the implementation of bilateral filtering in medical image de-noising . Its conceptualization and execution are simple, but the performance of a bilateral filter relies on its specific parameters. Hence, to yield optimal results, the parameter must be estimated. Bilateral filtering is applied to medical images that are degraded by additive white Gaussian noise with different variance values. The filter acts as a spatial Gaussian filter in areas that share the same pixel values, but it limits artifacts at boundaries between areas that are characterized by pixel values with huge differences, such as on the brain's surface.

Ryan and Laidlaw, (2014) studied and assessed a bilateral filter in the smoothing of diffuse MRI fibre orientations while preserving anatomical boundaries and supporting multiple fibres per voxel. In this technique, the distances and local estimators of weighted collections of multi-fibre models are defined, and it was shown that these estimators serve as a foundation for an effective bilateral filtering algorithm for orientation data. This method has significant applications in diffusion MR tractography, brain connectivity mapping, and cardiac modelling.

Wang and Zhou (2006) studied a de-noising algorithm for medical images that used a combination of the total variation minimization technique and the wavelet scheme. The scheme offers good noise removal in really noisy medical images, while still preserving object sharpness. This scheme allows radiologists to employ an efficient automatic stopping time criterion.

Varghees et al. (2012) suggested an automatic, adaptive image de-noising approach to eliminate Rician noise from MR images. The suggested technique is performed in accordance

with the discretized total variation (TV) minimization model and the local noise estimation scheme. The regularization parameter of the TV-based de-noising technique is in alignment with the standard deviation of noise in an MR image. The performance of the presented technique is assessed using brain MR images affected by Rician noise, and it features a standard deviation in the range of 2–30. The quality of the denoised image is validated by both subjective visualization tests and objective quality metrics. The experimental results reveal that the proposed method yields substantial improvements in maintaining the edges, while simultaneously reducing the Rician noise from an MR image. The adaptive TV filtering technique demonstrates reasonably better performance when compared to the other available methods, such as the non-local filter, bilateral filter, and multiscale linear minimum mean square–error estimation (LMMSE) approaches.

Garg and Kaur (2013) developed a technique that combines both the interpolate median filter (IMF) and the anisotropic diffusion total variation FCM (ADTVFCM) to improve the segmentation accuracy of brain MR images, as this method is required to ensure that medical images are noiseless. This enables radiologists to correctly detect brain disorders or injuries to make accurate diagnoses. Hence, this presented technique is expected to provide better segmentation results when compared to the previously described methods. This filter is affected by the staircasing effect, which results in gradual contrast variations in homogeneous objects, particularly near curved edges and corners. The popularly adopted TV filter is not optimal for MR images with spatially altering noise levels or artifacts. This method selects reliable edges, and in the initial step itself, it studies the noise/artifact distribution from the noisy image. Then, the spatially variant parameters are defined based on this estimation, thus making it an adaptive method.

The proposed technique also aligns its significant parameter via a data-driven approach without the need for user inputs, thus making it automatic. Liu et al. (2014) introduced a de-noising method on the basis of the assumptions of a spatially changing Rician noise map. A two-step wavelet-domain estimation technique was designed to extract the noise map. Many experiments have been carried out on both artificial and real MR datasets to compare the proposed model with a few highly standardized de-noising techniques.

To overcome the aforementioned issues associated with the previously described de-noising techniques, an optimized total variation filter (OTVF) method is introduced. This technique boosts the actual MR images in two steps, which comprises de-noising and edge enhancement. Many of the de-noising solutions focus primarily on noise reduction, and they

further neglect edge information. Few techniques employ different algorithms for each of these two steps. This work presents a single process that performs these two operations simultaneously while making use of a combination of image pre-processing techniques. A regularization parameter known as lambda, which is a positive value that specifies the fidelity weights, controls the amount of de-noising that occurs. The smoothing and optimization of fidelity weights are performed using particle swarm optimization (PSO), as it restores a regularization parameter that ranges from 0–1.

Image pre-processing is a significant and challenging area in the CAD systems. In medical image processing, and particularly in MRI segmentation tasks, pre-processing of an image is highly necessary so that segmentation algorithms can perform correctly. The accuracy of segmentation is increased by the proper detection and segmentation of the tissue. Accurate tissue segmentation can take place only if an image is pre-processed, as based on image size and quality. Many methods of noise removal are proposed by the different researchers in past (as discussed in above sections). From the above discussion, one can easily see that none of the methods are suitable for all sorts of analysis/ cases. The best method is dependent on many factors like, sample data type, accuracy needed, time available for processing etc. For example: evolutionary algorithm based methods provide better accuracy but take more time. So, we have to use the method based on our requirement and application.

3.3 SEGMENTATION ALGORITHMS FOR MR IMAGES

Medical imaging is the methodology or process that is used to create images of the human body for the purposes of clinical or medical science; this is routine and essential practice in the field of medicine. Medical imaging techniques can also be utilized when planning or even performing surgery (Taylor et al., 2008). Medical image segmentation is the procedure of partitioning a medical image into several segments. The aim of segmentation is the simplification and/or modification of the way in which an image is represented so that it takes on a form that gives more meaning and is easy to analyze (Sonka et al., 2014). Image segmentation is generally used to locate objects and edges (lines, curves, etc.) in images. In a more precise manner, image segmentation is the process of assigning a label to each pixel in an image, where pixels with similar labels share a few visual features. The computation of medical image segmentation is done at multiple scales in the scale space and, at times, it is moved from coarse to refined scales. MR image segmentation is quite a challenging task and it requires careful mathematical operations to determine the desired region that may be

helpful in further analyses and feature extraction of the MR image. The correct segmentation approach is necessary if the aim is to obtain correct features from the image; this is why it serves as a highly essential part of an automated classification system (Lienhart et al., 2002). Much research has investigated MRI segmentation.

For instance, Sharma and Gulista (2011) introduced a segmentation process for MR images of the human brain by making use of a K means algorithm and a canny edge detection algorithm. The K-means clustering algorithm yielded a segmented MR image with the same intensity regions. K-means clustering performs the segmentation of all the three matters of the brain (i.e., grey matter [GM], white matter [WM], and cerebrospinal fluid [CSF]). Also, the edge detection algorithm is realized by creating the boundaries of the different regions of the MR image on the basis of scale and threshold values applied during segmentation.

Somasundaram and Genish (2013) demonstrated a boundary-detection method for the segmentation of the hippocampus (the subcortical structure in the medial temporal lobe) from MR images of inhomogeneous intensity without affecting their boundary and structure. The images were preprocessed by making use of a noise filter and morphology-based tasks. An optimal intensity threshold was calculated employing the K-means clustering method. Validation of the technique was performed on axial MR images of the human brain, and it was found to perform well and featured heterogeneous intensity.

Neha and Sahu (2014) introduced enhanced (ACO) Ant Colony Optimaization for tumour segmentation. Ant-based clustering is a clustering algorithm that copies the behaviour of ants. In this algorithm, an ant's direction and its inclination to move to the next site are considered when calculating the probability with which the next site is selected by the ant. Moreover, when computing the probability of the ant's next location, a balance is created between the act of the ant's direction and the amount of pheromone distribution. In this way, the algorithm finds its application for the segmentation of brain images and in the diagnosis of tumours.

Meena and Raja (2013) demonstrated the automatic localization of epileptic seizures in the brain, employed from nuclear medicine imaging techniques such as positron emission tomography (PET). This paper focuses on examining functional images to automatically

localize epileptic seizures in the brain while making use of a symmetry-based clustering technique. This technique proposes a fully automatic symmetry-based brain abnormality detection scheme for PET sequences.

Zanaty and Afifi (2013) introduced a novel modified (FCM) Fuzzy C-Mean algorithm that can boost medical image segmentation. The proposed algorithm is implemented by modifying the objective function of the traditional FCM algorithm with an adjustable penalty. This penalty is implemented in accordance with a specific data shape and size that is employed to generate fuzzy terms. Complications associated with the new algorithm are eliminated by making use of the initial seed information, and by applying this information into the objective function rather than the entire dataset. The proposed algorithm finds its application in MRI datasets. In comparison with the other available approaches, the proposed technique can be used to accomplish the most accurate results.

Tamijeselvy et al. (2013a) presented a technique that includes an enhanced classification approach for diagnosing epilepsy. The method comprises the following phases: pre-processing the 2D MR brain image utilizing the threshold interval method (TIM) and the min max (MM); normalized segmentation of the brain image employing the multiscale segmentation technique to obtain segments of the corpus callosum; and multiscale segmentation, which aims to be better at segmenting curvatures in less time and with 91% accuracy, according to entropy-shaped features (such as the corpus callosum's bend angle and Genu thickness). The intelligent quotient (IQ) is extracted from the segmented corpus callosum to diagnose epilepsy by employing CBR and genetic classification. The optimized performance of CBR classification reduces the false-positive rate. Furthermore, the CBR classification model features 96.7% prediction accuracy, while the optimized classification technique has 97.3% prediction accuracy.

FCM is a widely known clustering technique that has been extensively employed in medical image segmentation. Though, many researchers have designed multiple clustering algorithms, not one of them is perfect. The FCM algorithm operates without any previous information. Reducing the complex nature of the algorithm is achieved by making use of an initial seed rather than the whole dataset. The FCM technique also contains an automated

penalty on the basis of data shape and size, which are used to generate fuzzy terms. The results obtained from the tests prove that when the FCM algorithm is applied to actual MR images, it results in lesser noise (Madhukumar and Santhiyakumari, 2015). The superior nature of the FCM algorithm is demonstrated when comparing its performance with the K means, SOM, and hierarchical clustering (Madhukumar and Santhiyakumari, 2015). Additionally, these experiments also yielded quantitative results. The segmentation accuracy of the FCM method was evident when it was compared to the other available methods in the literature. Based on a quantitative assessment and visual investigations, it was concluded that the FCM algorithm provides reliable and accurate segmentation. Lastly, it should also be noted that even though the FCM algorithm can outperform K-means and other popular algorithms, it is expensive from a computational standpoint, and this may reduce its applications in large volumes of MR images (Madhukumar and Santhiyakumari, 2015).

Ghassabeh et al. (2007) proposed a novel technique for the effective computation of two parameters including neighbouring pixel intensities and positions. The GA Genetic Algorithm optimization method is employed and the capacity of GA in obtaining optimal values for these parameters is established. Simulation results that make use of noisy MR images proved the efficiency of the proposed method, particularly with respect to the computation of unidentified parameters and when showcasing its robustness towards the noise.

Selvy et al. (2013) studied the combination of the (PSO) Particle Swarm Optimization method with the best clustering techniques that are currently available to obtain a globally optimal solution. The extraction of centroids is performed in a random manner in clustering schemes. In the proposed method, centroids were selected on the basis of the p_best and g_best value, which offer a globally optimal solution. The sensitivity and specificity of the PSO technique have fewer false positives when compared with conventional clustering techniques.

Soesanti et al. (2011) improvised an optimized fuzzy logic technique for segmentation of MR images of the brain. This technique is based on a modified FCM clustering algorithm. The FCM algorithm incorporates spatial information into the membership function, which is

then used for clustering, whereas the traditional FCM algorithm does not make complete use of the spatial information in the image. The benefits of the algorithm are lower sensitivity to noise in comparison to other techniques, and it provides the regions with more homogeneity than those of other techniques. The originality of this research lies in the fact that the techniques are employed on normal MR images of the brain and of a tumour, while the area of a tumour is analyzed from the segmented images.

Tamijeselvy et al. (2013b) introduced an ACO and PSO technique featuring the clustering algorithm. The performance of these algorithms was compared, and it was found that FCMPSO performs better than the FCM and FCMACO algorithm. The PSO and ACO are Swarm intelligence methods that find their implementation in clustering to obtain approximated solutions for optimization issues within a reasonable amount of computation time. The function of the PSO and ACO algorithms rests in the fact that these algorithms search for optimized solutions according to the movement of the swarm.

Abinaya and Pandiselvi (2014) presented a possessing system that occurred in three phases. In the first phase, pre-processing was conducted to remove film artifacts and unnecessary skull regions in brain MR images. In the second phase, the enhancement was carried to remove noise in the brain MR image. In the third phase, the PSO was realized to segment various tissues, such as WM, GM, and CSF in brain MR images. Segmented brain MR images help radiologists better inspect brain abnormalities and tumours. The algorithm was tested with the MR images of the brain obtained from 50 real patients.

Anitha et al. (2012) showed that white matter lesions (WMLs) are small portions of dead cells that are seen in various parts of the brain. Generally, it is hard for medical experts to accuerately quantify WMLs due to the reduced contrast between WM and GM. The goal of their paper was to automatically detect WMLs, which are frequently observed in the brains of older adults. The WML detection process comprises the following stages: 1) image pre-processing; and 2) clustering (FCM, GPC, GFCM). The system was tested using a database of 208 MR images. It was found that GFCM produces a high sensitivity of 90%, specificity of 94%, and overall accuracy of 95% over FCM and GPC (Kavitha et al., 2013). The experimental results show that GFCM can better localize large lesions and it provides lower

false-positive rates in comparison with FCM and GPC, which conquer the largest loads of WML but only in the upper ventral horns of the brain.

Fuzzy clustering algorithms have some weaknesses. The primary weakness is that it tends to be trapped in local optima and it is vulnerable to initiation sensitivity. As such, a new technique was presented to solve the initialization issues associated with FCM by making use of a Firefly Algorithm (FA) to determine the optimal initial cluster centres for the FCM (Nayak et al., 2014, Alsmadi, 2014). Thus, all applications that were relevant to fuzzy clustering (such as image segmentation) were improved. FA has a few drawbacks, including that it gets trapped into many local optimums. FA performs local searches as well, and it is sometimes not able to remove them since the firefly parameters are constant and they do not vary with time. Hence, the behaviour of the attraction coefficient and randomization coefficient in the firefly can be adjusted to determine the global search mobility for which random-based metaheuristic optimization methods are introduced. Random-based optimized clustering techniques, such as chaotic and levy Flights, are realized in FA to locate the global cluster centres as the beginning cluster value of FCM (Nayak et al., 2014, Alsmadi, 2014).

Chen et al. (2009) demonstrated a chaos–ant colony algorithm on the basis of an ant colony algorithm, making use of the gridding method and merging it with chaos theory. ACO is a brand new random optimization algorithm that uses artificial ants ejecting pheromones along the way, as portrayed by positive feedback, distributed computation, and a parallel algorithm. It is highly robust, and when using this method, it is easier to obtain a combination with other techniques in optimization. Slower convergence and easier trapping in local optimum are the few shortcomings, though it finds wide application in optimization issues. In the chaos-ant colony algorithm, some max-min ant system idea is helpful for limiting the pheromone strewn in the path. Enhancements are made during initialization and updating of the pheromone.

Min-Yuan and Kuo-Yu (2009) introduced the K-means with chaos genetic algorithm (KCGA) to lower the amount of computation required, as well as to improve the estimation accuracy of nonlinear optimizations, in which the initial population is developed by chaos mapping and then fine-tuned by competition. Within every iteration of this technique, along

with the development of GA, the K means clustering algorithm is employed to accomplish faster convergence; this results in the rapid generation of the population as well. The important aim of the paper is to demonstrate how improvements of the GA optimizer can be achieved by incorporating a hybridization strategy.

Ebrahimzadeh and Jampour (2013) generated pseudo-random numbers using the Lorenz chaotic system for operators of GA to avoid local convergence. In recent times, rapidly developing optimization algorithms have made use of GA to improve upon the results of optimization issues. Many GA procedures are based on 'Random' basic or evolutionary algorithms, although the main defects in the GA are local convergence and high tolerance in the results, which have happened due to being random.

Liu (2014) decided to focus on the use of PSO for cluster analysis. Clustering analysis is a widely known technique in the data-mining domain. It is mostly utilized to automatically find those classes or groups of unlabelled datasets. In standard PSO, the non-oscillatory route can be quick to cause a particle to stagnate, and it may also lead to premature convergence on suboptimal solutions that do not even guarantee provision of a locally optimal solution. In Liu's report, the Lévy mechanism was presented for the PSO algorithm and it was employed in the datasets. The results revealed that the new PSO model, named LPSO, was successful at enhancing data clustering.

Image de-noising and segmentation are the two most highly challenging areas in MR image segmentation of the cerebral tissues. The presence of noise not only deteriorates the visual quality but it also largely affects the accuracy of segmentation, which is significant for medical diagnostic procedures. Although conventional linear noise reduction techniques have been available for quite a long time, it was also found that MR images of the brain are chiefly degraded by Additive White Gaussian Noise Channel (AWGN). Without the de-noising, the image details are eroded which, in turn, leads to a reduction in the quality of the image and thus results in improper segmentation. In this chapter, the classification of important image segmentation algorithms is studied. Despite several years of research, there is no universally approved MR image segmentation algorithm. It can thus be deduced that segmentation of MR images of the brain is challenging in image processing and computer

vision. In this chapter, segmentation approaches utilizing clustering and optimization techniques are discussed. However, global optimization still remains a highly demanding issue in medical applications. The work reviewed thus far showed that there is a good research going on in the development of random-based optimized clustering techniques but the time complexity of these techniques is a big drawback, which makes it inadequate for practical/ real time use.

3.4 SUMMARY

This chapter offered an overview of all of the currently available methods for MR image pre-processing, MR image segmentation methods (as based on clustering), and classification methods (as based on ANN and SVM). While many reports have aimed to improve de-noising and segmentation results, many techniques have been proposed by making use of various procedures. The underlying merits and demerits of each one of the existing techniques have also been discussed. Since a detailed and systematic analysis of the available techniques was made, it will help guide the present research work. This is also essential when attempting to overcome the limitations of the existing techniques, as it will thus improve the accuracy of the segmentation and classification approaches used here, particularly with respect to cancer detection.

From the current state of the art, it is clear that even though several methodologies have been proposed to detect abnormalities in the breast at various stages, there are some limitations in the existing work. This study summarized these limitations as follows: the current systems (discussed in this chapter) provide low accuracy (85%–90%), the system suffers from high false-positive and false-negative rates, and the use of fewer features can lead to the wrong classification.

CHAPTER 4

ARTIFICIAL NEURAL NETWORK AND SUPPORT VECTOR MACHINES

4.1 INTRODUCTION

The main objective of this chapter is to provide an overview of the basic theories of ANN and SVM classifiers. In addition, this chapter also outlines the application of these two classifiers in different cases in the literature.

4.2 BACKGROUND OF ANN

Cluster analysis is used to group objects that have similar properties. The K-means algorithm is a well-known partitioning technique used to obtain clusters. The K-means algorithm primarily uses the Euclidean distance measure to group objects. The algorithm is not that efficient when the sample observations belong to a statistical population. This problem can be sorted out by defining a statistical distance measure, such as Mahalanobis distance, Fisher–Behrens distance, and so on. The statistical distance measures used by the K-means algorithm do improve the results to some extent. In the case of overlapping populations, traditional clustering techniques do not produce good results. These problems have been taken into account in this research work, and an attempt was made to improve the existing clustering techniques using the various learning principles suggested by ANN.

ANN learning algorithms are also currently being used for classification purposes. ANNs do not make any assumptions regarding the distribution of the population from which the sample units are drawn. In the present study, an ANN based classification technique was used for MRI data classification. The proposed technique works similar to the K-means algorithm, with some modifications. The neighbourhood concept of ANN is incorporated in the algorithm. The initial centres (weights) have to be chosen when initiating the algorithm, and it may be selected in different ways. Generally, initial weights are randomly chosen. The proposed algorithm is an iterative algorithm. A brief review of ANN and ANN-based classification methods is given in the next sections.

4.3 ANN-BASED CLASSIFICATION TECHNIQUES

A large number of ANN learning algorithms have been proposed for classification purposes. Pal et al. (1993) have proposed a generalization of the learning vector quantization (LVQ) method for clustering. Jain and Mao (1992) have further performed elaborate work in the projection and extraction of multivariate data. They proposed a number of networks and learning algorithms that provide new tools for feature extraction and data projection. Vesanto and Alhoniemi (2000) have also described two efficient training methods for Self Organization map (SOM) and a new procedure for clustering. These networks include a network for Sammon's nonlinear projection (SAMANN), a linear discriminant analysis (LDA) network, a nonlinear discriminant analysis (NDA) network, and a network for nonlinear projection (NP-SOM) based on Kohonen's SOM.

Gallinari et al. (1988; 1991) have studied the relationships between discriminant analysis and multilayer perceptrons used for classification purposes. Furthermore, Osman and Fahmy (1994) have expanded the available theoretical framework that establishes a link between discriminant analysis and the adaptive feed-forward layered linear output networks used as mean-square classifiers. A description of ANN in relation to cluster analysis is discussed below.

4.4 ANN AND CLUSTER ANALYSIS

The input layer consists of p input nodes, through which the sample input vectors are presented. The second set of m nodes associated with m clusters is termed the output layer. The nodes in both the input and output layers are connected. Each connection has a weight, denoted by w_{ji}, which is the strength of the connection from input node i to output node j. This setup is termed as a Multi -layer network in ANN (Figure 4.1).

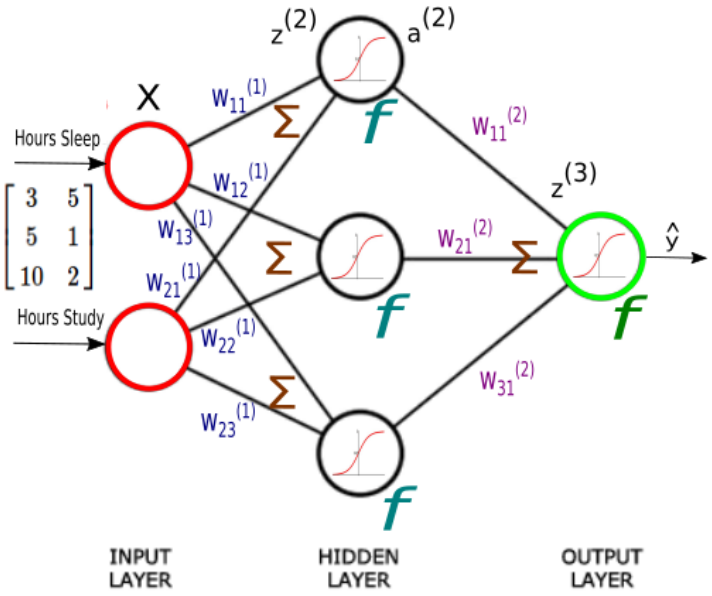

FIGURE 4.1: MULTI-LAYER ANN STRUCTURE

During cluster analysis, the objective is to find the weights (W), so that the sample units are assigned to the nodes to which they already belong, either in successive cycles or iterations based on some criterion. Generally, the initial weights are chosen at random or by some other method. Sample units are presented one after the other and are assigned to output nodes on the basis of a specified criterion. This is called a cycle. The weights are updated and again, the cycle is repeated until either the weights converge, or until a specified number of cycles has been completed. Since each node j is associated with a weight vector, W, similar to the discriminant coefficient, they are used to classify an input vector to a node that corresponds to a group or cluster.

4.5 ANN-BASED STATISTICAL CLUSTER ANALYSIS

A clustering algorithm that works perfectly on one type of datum may completely fail on other types of' data. In spite of numerous research efforts, data clustering, as a general principle that will work in all situations, remains a difficult – and essentially unsolved – problem. If the clusters in a set are compact and isolated in the sense that the between-cluster variation is much larger than the within-cluster variation, then any clustering method will be able to detect the clusters, irrespective of the cluster shape. Otherwise, the choice of distance measures can make a substantial difference in the clustering results. It has been found that most clusters in real datasets are not well isolated, as there may be overlapping clusters.

Partitioning techniques with Euclidean distance have the undesirable property where large clusters are split under some circumstances. Sometimes, this approach produces unusually large or small clusters. A Euclidean distance-based clustering algorithm favours clusters of equal size.

In cases where the clusters are of variable size, this method yields drastic results. In such situations, normalization of the data cannot solve the problem. It is easy to find examples of datasets in real-life applications that do not have well-separated clusters. The well-known Fisher–Iris data that consist of 150 four-dimensional patterns from three classes (Iris setosa, Iris versicolor, Iris virginica) do not have well-separated classes. It was found that the first species was well separated, while the other two species had overlapping features. As such, the data may sometimes be split into only two well-separated clusters using the existing clustering techniques. The traditional K-means partitioning technique may also fail to produce well-defined clusters in cases of overlapping populations; thus, an alternative approach should be taken into account.

One way to solve this problem is to introduce statistical distance measures, such as the Mahalanobis distance measure, in the clustering criterion. This statistical measure has a variance–covariance term, which takes care of' the variations within the cluster that arise due to the variables under consideration. However, the variance–covariance matrix may sometimes become singular if the cluster size is less than the dimension of the dataset. Mao and Jain (1996) have suggested using the regularized Mahalanobis distance measurement to solve the singularity problem by adding a small value along the diagonal of variance–covariance matrix. The K-means algorithm with statistical distance also does not have satisfactory results. Subsequently, one can opt for an ANN technique. ANN learning algorithms can be used as tools for clustering objects.

The unsupervised learning of ANNs has dealt with classification problems. Kohonen's SOM I (Kohonen, 1998) is often used to cluster the input dataset. In SOM, neighbouring cells in the network topology compete in terms of their activities by means of mutual lateral interactions and they adaptively develop into specific detectors of different input values. The SOM has the special property of effectively creating spatially organized "internal representations of various features of input values and their abstractions". SOM is a two-layered network that can organize a topological map from a random starting point. The resulting map shows the natural relationships among the patterns that are given to the network. The network combines

an input layer with a competitive layer of processing units and is trained by unsupervised learning. SOM uses the topological neighbourhood. Each node in the output layer has a set of nodes surrounding it, which are all taken as neighbours. The nodes in the input layer are connected to the nodes in the output layer with a 2D weight vector. The weight values correspond to the physical locations within the space occupied by the input sample units. Thus, the neighbouring units in the physical space may occupy unrelated locations in weight space. During training, a 2D point is selected at random to serve as the input vector. The weight vector of all units within the neighbourhood changes slightly towards the input value. As the training continues with different input points, the size of the neighbourhood decreases gradually until it encompasses only a single unit. Upon completion of the training, the weight vector for each unit will be approximately equal to the physical coordinates of the unit. In SOM, the neighbourhood is selected from a set of nodes surrounding the assigned node.

This results in a large number of nodes in the output layer. The drawbacks of the K-means algorithm and the self-organizing feature map algorithm have been kept in mind and an attempt is made to resolve them by proposing an ANN-based clustering technique, by combining features of both algorithms.

A good ANN-based clustering algorithm makes use of statistical distance measures, such as the Mahalanobis distance and Fisher–Behrens distance measures. To calculate the distances between input and output nodes, the variance–covariance matrix also participates in the assignment of sample units to the nodes. The winning node is the node that has a minimum distance with an input vector X. A neighbourhood of a point X is a set of nodes that are at a distance less than or equal to a pre-specified value.

In the present discussion, the neighbourhood of a point X in p-dimension is defined in terms of the maximum distance of the input vector X with all output nodes. The neighbourhood of X is the set of nodes that fall inside the sphere, and whose radius declines with increasing numbers of iterations or cycles. The radius of a neighbourhood can be calculated with each iteration t (Kohonen, 1998).

The neighbourhood can also be defined in many other ways, depending on the requirement. The logic behind using the aforementioned definition of a neighbourhood is as follows. All of the sample units are fixed in the p-dimensional sample space. In order to cluster these points, certain numbers of seed points (that represent clusters) are initially assumed amongst the sample units. Since the sample points are fixed, one can only move these reference points in

the sample space. These reference points are the nodes that have been associated with the weight vectors. In conventional clustering algorithms, only the reference point that is closest to the input vector X is updated or recalculated. However, we propose including even other nodes that are in the neighbourhood of X to obtain an updated, but smaller, learning coefficient P. A higher learning parameter 'an' is used with the winning node – that is, the node that is closest to X in the sample space. By using this concept, more than one reference point in the space is adjusted, but with different levels of accuracy, thereby providing an opportunity for other reference points to get trained.

4.6 ANN ARCHITECTURE

Figure 4.2 shows the different types of ANN architecture: (a) recurrent architecture and (b) feed-forward architecture.

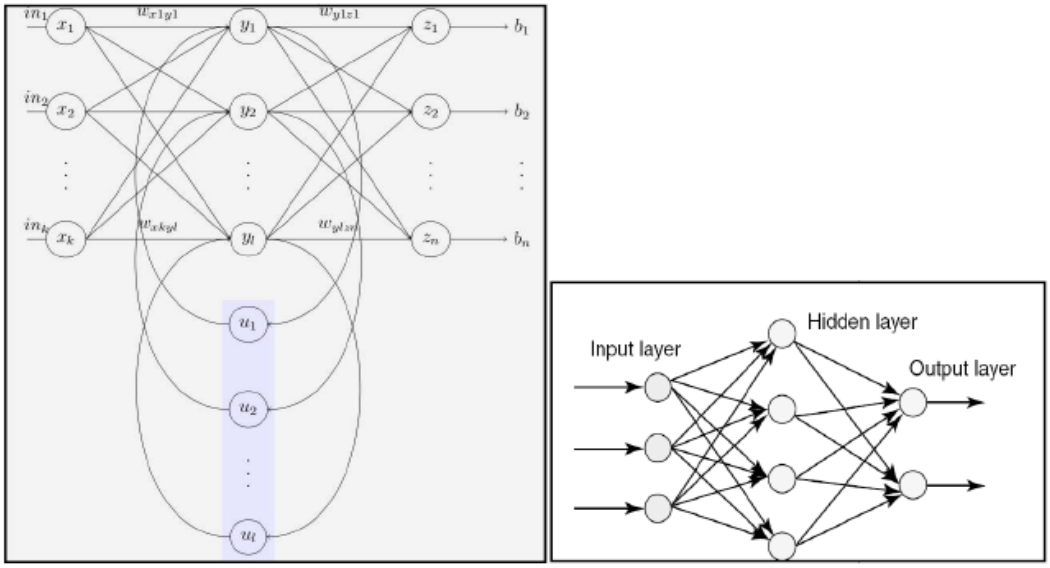

(a) (b)

FIGURE 4.2: RECURRENT NETWORK (A) AND FEED-FORWARD NETWORK (B)

When there is no connection between the output and input/hidden layer in the backward direction, then this connection provides a feed-forward ANN (FFANN). It consists of three layers: 1) an input layer, 2) a hidden layer, and 3) an output layer. The hidden layers are mainly employed to deal with signal processing (input signals). The input layer is used to feed the input signals, while the output layer is used to provide the required number of outputs. Though, FF-MLP (Multi-layer perceptron) can have more than one hidden layer.

Conversely, the recurrent network provides feedback from the forward layers to the backward layers. This network involves more weights, as there are more connections in this model when compared with FFANN.

4.7 NEURAL NETWORK LEARNING

Different learning rules (Jain et al., 1996) were suggested by different researchers to train the ANN. In a broad sense, the learning of the ANN configuration can be divided into three classes:

4.7.1 Supervised Learning

In this learning model, the desired set of outputs is provided along with the training dataset. This learning approach is useful when it has a sample training set and it wants the network to work according to that sample.

4.7.2 Unsupervised Learning

In this learning approach, a desired set of outputs is not provided alongside the training dataset. This learning method is useful when the system/user does not have a training data set with known outputs. In this method, ANN is allowed to establish its own rules.

4.7.3 Semi-supervised Learning

In this learning approach, only the direction of the output is provided; the actual output is not provided during training. Based on directional feedback, the ANN learns to adjust the various weights.

4.8 BACK-PROPAGATION LEARNING

In 1986, Rumelhart et al. (1986) proposed a popular error back-propagation learning algorithm. Since then, much work has been carried out in this area. The back-propagation algorithm (Haque et al., 2002; Devi et al., 2012) works on the principle of the gradient descent minimization rule. This is a supervised method of learning. The input and output dataset is provided to the ANN. The gradient is calculated with respect to the error in the desired and actual output, and then the ANN updates its weights according to this error gradient.

The complete training involves three main steps:

1. Inputting the training samples using an input layer;

2. Calculating the errors of the output layers; and

3. Adjusting the weights of the ANN to minimize that error.

Equation 4.1 shows the weight updation in the back-propagation algorithm. Here, 'e' represents the average of all the squared errors, $\boldsymbol{w_{ij}}$ represents new weights, $\boldsymbol{w_{ij}(n-1)}$ represents old weights, and η and α are the learning rate and momentum, respectively. The entire training session is an iterative process, and 'n' represents the current iteration number. A good choice for learning rate and momentum significantly affect the training process.

$$\boldsymbol{w_{ij} = -\eta * \frac{\delta e}{\delta wij} + \alpha * w_{ij}(n-1)} \quad (4.1)$$

Back-propagation in ANN (Haque et al., 2002; Devi et al., 2012) is a typical strategy that is used to prepare simulated neural systems; this approach is utilized in conjunction with an improvement technique, such as an angle plummet. The calculation rehashes a two-stage cycle involving engendering and weight refresh. At the point when an information vector is presented to the system, it is proliferated forward through the system, layer by layer, until it achieves the yielding layer. The yield of the system is then contrasted with the coveted yield, utilizing a misfortune work, and a blunder esteem is computed for each of the neurons in the yielding layer. The mistaken qualities are then proliferated in reverse, beginning from the yield, until every neuron has a related blunder esteem, which generally speaks to its commitment to the first yield.

Back-propagation utilizes these errors to determine the slope of the gradient work for the weights in the system. In the second stage, this slope is supplied to the streamlining strategy, which utilizes it to refresh the weights, while trying to limit the gradient work.

4.9 SUPPORT VECTOR MACHINES FOR PATTERN CLASSIFICATION

The goal of a pattern classification problem is to determine the class of an object using those features that separate the classes of given input data. This section provides a brief introduction to learning machines (different than ANN) known as support vector machines (SVMs) (Steve, 1998). This section restricts its discussion to two classes of binary classification problems.

SVMs are learning systems that use a hypothetical space of linear functions in a high-dimensional feature space, which is trained with a learning algorithm that was adopted from optimization theory. This algorithm implements a learning bias derived from statistical learning theory. This learning strategy, first introduced by (Vapnik et al. 1995), is a principled and very powerful method that, in the few years since its introduction, has already outperformed most other systems in a wide variety of applications. Presently, SVM is among the most popular tools used for the different type of classification tasks (Geng et al., 2016, Zare et al., 2016, Zhang et al., 2017).

Suppose there is a given training dataset {(xi, y;)},=1, 2,….m, where xi =($x_j^p \cdots$, x_i^n). Y in Rn denotes the input vector, and y_i belongs to {–1, 1}, which is it's the corresponding output class. The goal is to obtain a classifier that generalizes well on unseen data (i.e., it is able to predict well).

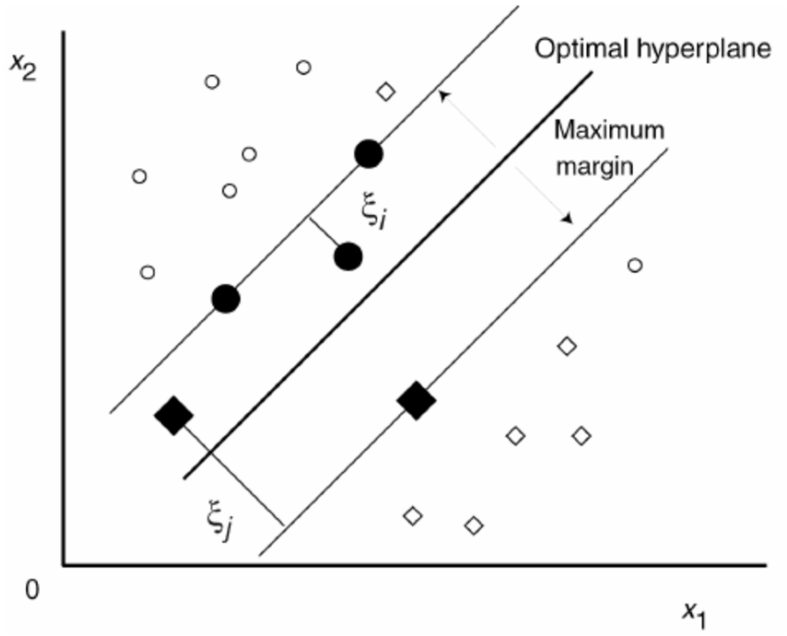

FIGURE 4.3: SVM FOR A LINEARLY SEPARABLE PROBLEM

In order to obtain a linear decision surface, or a hyperplane with a great potential for generalizability, one must first find the separating hyperplane with the maximal margin between the two classes of input data (i.e., the hyperplane that separates the two classes with the maximum distance to the closest points from each class of inputs; see Figure 4.4). This hyperplane is known as the optimal separating hyperplane.

The equation of the optimal hyperplane will be taken as:

$W \cdot x+b = 0,$ (4.2)

where the weight vector w in R_n and the offset (or bias) b belongs to R are unknown.

Then, determine the two hyperplanes that run parallel to the optimal hyperplane, and which are at equal distances from it, so that there are no input data points appearing between these parallel planes and other planes that are closest to the positive input dataset (and where the other is closest to the negative input dataset). Let us assume that the equation of these parallel planes will be:

$W \bullet x + b = 1$ and $W \bullet x + b = – 1.$ (4.3)

It can be verified that the margin is given whereby 11·11 is the norm. Then, the problem of maximizing the margin lies in finding the hyperplane that minimizes the ability to satisfy different constraints (as offered by the problem at hand) (Burges, 1998; Gunn, 1998; Cortes, 1995).

For the nonlinear support vector regression (SVR) model, the input data are mapped into a higher dimensional feature space via a kernel function K(-,-), and the linear support vector regression is performed in the feature space. Typically, let the input data be transformed into a higher dimensional feature space by the transformation ¢: Rn ~ RN, and let the support vector regression approximation function in the higher dimensional space be given by:

$F(x) = W \bullet ¢(x) + b.$ (4.4)

Then, the SVR formulation can be written as a constrained optimization problem.

4.10 CLASSIFICATION ALGORITHMS

Tumour classification is the final and most important step in automated cancer detection. In order to identify tumour-affected images, an efficient classification approach is required. To achieve this, geometrical features are extracted from the Region Of Interest (ROIs) using the specific characteristics of the tumour-affected areas.

Zheng and Qian (1996) proposed a computationally efficient mixed feature-based neural network (MFNN) to detect cancer in digitized mammograms. The MFNN employs features

computed in both the spatial and spectral domain, and it uses spectral entropy as a decision parameter. Back propagation with Kalman filtering (KF) was employed during network training to evaluate different features and related error analyses.

Furthermore, Dhawan et al. (1996) utilized two classes of corresponding gray-level picture structure highlights to group hard-to-analyze cases. The primary class of components included second-level histograms for the global surface and wavelet decay-based elements, which speak to the neighbourhood surface of the zone of intrigue. The second classification of components told about the arrangement of the main histogram levels. It was based on the measurements of the fragmented locales, size of elements and the separation of elements in the divided area. Different components in every classification were connected with the breast examination after effects of hard-to-analyze cases to determine the arrangement of elements that speak to the entire dark-level picture structure data. The component determination was performed utilizing a multivariate group investigation and the genetic algorithm (GA)-based hunt strategy. The chosen components were utilized to arrange for the use of a back-proliferation neural system and measurable parametric classifiers. A back-propagation ANN was utilized for classification purposes.

Hadjiiski et al. (1999) outlined a classifier that consolidated both an unsupervised and a regulated model. The unsupervised model depended on an adaptive resonance theory (ART2) organizational system, which grouped the masses into various separate classes. The classes were partitioned into two types: one containing a threatening tumour and the other containing a blend of dangerous and benevolent lesions. The threatening classes were grouped by ART2. The blended classes contributed to an administered linear discriminant classifier (LDA). Using this approach, some dangerous masses were isolated and characterized by ART2, while the less recognizable, amiable, and harmful masses were ordered by LDA.

Lo et al. (2002) managed a multiple circular path convolution neural network (MCPCNN) that was specificially engineered to examine tumours and tumour-like structures. To begin, each presumed tumour range was partitioned into segments. The characterized mass elements for every area were figured freely. These area elements were utilized on the info layer and they were facilitated by convolution parts of various sizes that proliferate signs to the second layer in the neural system frameworks. The convolution portions were prepared as required by displaying the preparation cases to the neural system.

The method provided by Zheng and Chan (1996 and 2001) was selected given that the algorithm provided a high level of sensitivity of 97.3%. The authors had adopted an artificial intelligence algorithm, which was a combination of techniques like fractal analysis, the multi-resolution Markov random field (MMRF) technique, and the binary decision tree. During fractal analysis, the blanket method was used to determine the roughness value of the surface, while MMRF was used for segmentation. This segmentation process was initialized using a clustering algorithm called the dogs-and-rabbits algorithm, which was an extension of the K-means clustering algorithm. The major difference between the K-means clustering algorithm and the dogs-and-rabbits algorithm was that the cluster centres were moved towards the data points in the latter case. Here, the concepts of cliques and neighbourhood systems were used.

El Naqa et al. (2002) further demonstrated that tumours can be identified by applying a successive enhancement learning (SEL) procedure, where support vector machine (SVM) training was adjusted iteratively by reincorporating misclassified samples.

Next, Campanini et al. (2004) presented a SVM-based featureless approach for tumour detection in digital mammograms. Instead of extracting features from ROIs, the authors used a multi-resolution, over-complete wavelet representation to codify the image with redundant information. Two SVM classifiers were used in this approach. First classifier was used to find a tumour and the second classifier was used to reduce the number of false positives.

Zhang et al. (2004) further proposed a system where a neural–genetic algorithm was used for feature selection, and where a neural network was used for classification. It also combined the computer-extracted statistical features from the mammogram with human-extracted features to classify different types of small-sized breast abnormalities.

Kinoshita et al. (2007) proposed an unsupervised learning approach in light of Kohonen's self-organizing map (SOM). The SOM was prepared to utilize visual elements that were identified with bosom thickness designs. An arrangement of elements was processed for every mammogram, which incorporated shape elements, surface elements, minute components, rakish projections, and morphological elements that were obtained from sectioned fibroglandular tissues.

The method developed by Dominguez and Nandi (2008) was selected as another approach, as it increased the SNR of the lesions being detected and it eliminated false-positive findings. They had proposed an algorithm to enhance mammograms with the objective of improving the segmentation of distinct structures of mammogram images. The enhancement algorithm used wavelet decomposition and reconstruction, morphological operations, and local scaling. After enhancement, region segmentation was performed and a set of features was computed from each of the segmented regions. A ranking system was used for classification purposes.

Islam et al. (2009) displayed a calculation known as the adaptive merging and growing algorithm (AMGA) when outlining ANNs. This calculation unifies and includes shrouded neurons during the preparation phase of ANNs. The union operation presented in AMGA was a sort of a blended mode operation, which prunes two neurons and ultimately includes one neuron. This versatile system consolidates or includes concealed neurons based on the learning capacity of shrouded neurons or on the preparation of ANNs. Keeping in mind the end goal of decreasing the measure of retraining subsequent to adjusting ANN models, AMGA prunes concealed neurons by consolidating associated shrouded neurons and includes shrouded neurons by part existing shrouded neurons.

Shukla et al. (2010) presented a method to detect breast cancer using soft computing tools like ANNs and neuro fuzzy systems. The feed-forward neural network was trained using three ANN algorithms: the back-propagation neural network (BPN), the radial basis function (RBF), and the adaptive neuro fuzzy inference system (ANFIS). The performance was compared by metrics such as accuracy of diagnosis, training time, the number of neurons, and the number of epochs.

Timp et al. (2010) subsequently presented an automated mass detection method to identify temporal changes in mammographic masses between two consecutive screening rounds. Two types of temporal features – difference features and similarity features – were designed to realize the interval change analysis. An SVM was employed as a classifier to detect the temporal changes in mammographic masses. Classification performance was evaluated with and without the use of temporal features. BPN, RBF, and SVM classifiers were used in this research due to their robustness and widely applicable characteristics.

In the literature review provided in this thesis, the methods that have explored various challenges associated with breast cancer detection in mammograms are reviewed. In the following section, three existing techniques that were used in the first three proposed approaches with modifications are discussed.

The method presented by Cascio et al. (2012) was selected for approach 1 since this method provides a segmented output without the loss of meaningful information. In this method, the ROI was obtained via segmentation by means of contour searching. In the classification step, feature extraction plays a fundamental role. Once the features were computed for each ROI, they were used as inputs in a supervised neural network. The output neuron provided the probability with which the ROI was pathological (or not). The authors obtained a sensitivity of 82%.

Some very recent applications of ANN and SVM in breast cancer classification have been reported elsewhere (e.g., Lam et al., 2014; Dheeba et al., 2014; Senapati et al., 2013; Bhardwaj et al., 2015; Zheng et al., 2014; Hu et al., 2013). In all of these cases, the results were quite good.

4.11 SUMMARY

ANN- and SVM-based clustering techniques are discussed in this chapter. This chapter explained the use of the self-organizing principle of ANN by first discussing the K-means algorithm. Statistical distance measures were used in the algorithm. The concept of the neighbourhood of an input vector X is introduced and used in the training phase. In ANN, the neighbourhood is defined for the nodes. In the present study, the neighbourhood of a point X is defined in terms of the maximum distance of input vector X with the output nodes. Generally, in traditional clustering algorithms, the reference point (node) alone, which is closest to the input vector X, is recalculated. By using the neighbourhood concept, more than one reference point in the space that falls within the neighbourhood of X is adjusted, thereby giving other reference points the opportunity to get trained. The initial weights can be chosen in different ways. The formation of clusters is dependent on the initial weights, as well as on the two gain terms, a and p. In the same way, this chapter also explained the theory of SVM and its related principles, along with its application in tumour classification.

CHAPTER 5

METHODOLOGY

5.1 INTRODUCTION

MRI is currently the most sensitive non-invasive method for detecting breast cancer; this modality has its own limitations, and its performance is dependent on the use of optimal feature selection for detection purposes. Few features extraction may not be sufficient enough to detect the abnormalities of breast cancer in its early stages. The integration of different features has been widely used to generate more diagnostic and clinical values in medical imaging. Since the early detection of cancer is likely a major factor that contributes to the reduction in mortality rates for certain cancers, image-guided and -targeted minimally invasive therapy has the promise to improve outcomes and reduce collateral effects. This thesis includes algorithms that were developed to perform pre-processing, segmentation, feature extraction, and classification. To classify tumours as benign or malignant, ANN and SVM classifiers were used and compared against each other. Figure 5.1 shows the flow diagram of a proposed methodology of the proposed breast cancer detection system.

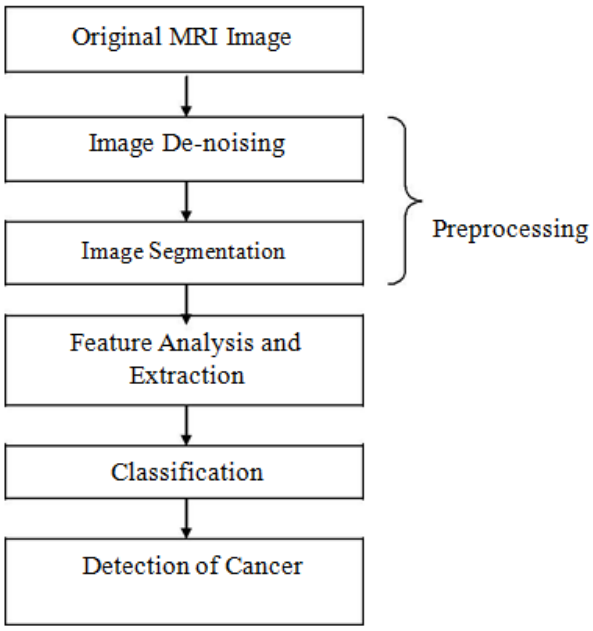

FIGURE 5.1: FLOW DIAGRAM SHOWING THE OVERALL METHODOLOGY OF ANALYSIS AND CLASSIFICATION OF BREAST CANCER FROM MRI IMAGES

5.2 DATASET, SOURCE, AND SOFTWARE

5.2.1 Dataset

The MR images of 56 patients are used in this study, patients were obtained from the medical imaging department via the picture archives of King Abdullah Medical City (KAMC), Saudi Arabia. 26 images were classified as featuring "malignant" tumours, and rest featured "benign" tumours (as classified by the medical specialist). All the images were used for image segmentation testing. The same MRI machine with the same sequence parameters was used to examine all of the patients. The images were obtained under well-controlled conditions by an experienced technician to ensure geometrically aligned orientations.

As the middle age women are more prone to breast cancers so data set is also collected from the patients of similar age range (25–45 years). Single MR image is taken from each patient. The MR image was saved in .png (lossless format) format of the size 352×352, bit depth of 24 bit with 96 dpi of resolution.

5.2.2 Source

The data used in this study were collected from the King Abdullah Medical City. A brief overview of King Abdullah Medical City is given below; then, details of the dataset that was used are provided.

The mammoth King Abdullah Medical City (KAMC) is the third referral master medical city in the nation of Saudi Arabia, following King Fahad Medical City and the King Fahad Specialist Hospital in Dammam.

The KAMC region is 800,000 square meters. It was developed by the National Project for Comprehensive Health Care, which aimed to provide health services under the guidance of excellent restorative administrations, which will satisfy the desires and aspirations of the authority. KAMC was established to meet each and every need of its inhabitants. The convenience limit of the five-storey building is 1,500 beds, of which 500 beds have been

dispensed to the pro-referral healing centre. The doctor's facility covers almost all medical specializations.

The medical complex has computerized operating rooms that are intended to be utilized by specialists, surgical inhabitants, anaesthetists, operating room attendants, and other surgical staff. This surgery bundle coordinates booking, clinics, and patient information to provide an assortment of organization and clinical reports. Aside from this, the expert referral clinic incorporates 500 beds for gynaecology, obstetrics, and paediatrics.

5.2.3 Software and System

MATLAB 2014a is used for all simulations. A computer system with an Intel i7 processing unit and 4 GB of RAM was utilized in this study.

5.3 AUTOMATIC BREAST CANCER DETECTION SYSTEM (ABCDS)

Breast cancer assessment with the assistance of MR images is a rather common clinical practice in the investigation and prediction of tumours, particularly among clinical experts. Pathologists perform a review of MR images under good lighting. The experts' level of experience directly affects the precision of their assessments. Changes in pathologists' opinions of the same MR image have been seen in clinical practice. In this broad facility, a pathologist conventionally handles 100 assessment cases at a time; each case includes nearly 2,000 MRI screens. In this way, assessments are a grim and time-consuming process. A computer-based assessment system can aid pathologists by providing second reviews, reducing their workload, and offering these assessments to cases that required a more detailed view, allowing clinicians to focus on analysis and prediction. The structure of a proposed automatic breast cancer detection system (ABCDS) is explained in this section.

The proposed ABCDS framework for MR image examination is shown in Figure 5.2. The primary step is image acquisition, and this is trailed by the image pre-processing step. Inside the image preparation stage, the ROI is initially segmented and followed by analysis of the nuclei, and by classification of the phase of the disease. The last step involves evaluating and offering recognizable proof. These methodologies are discussed in the following section.

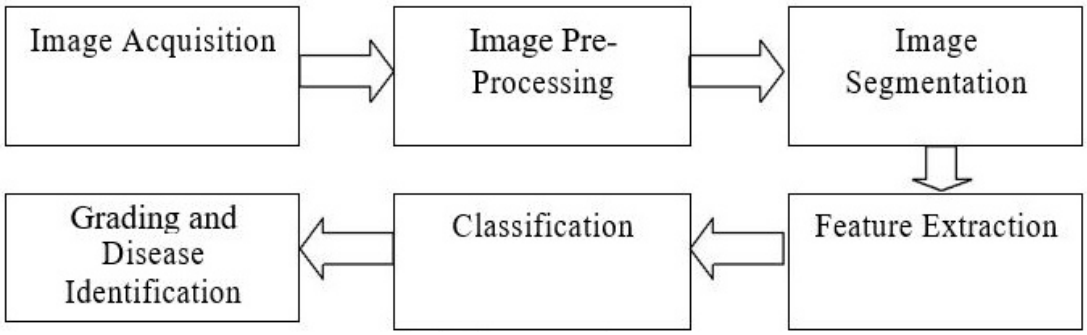

FIGURE 5.2: BLOCK DIAGRAM OF AN ACD SYSTEM'S STEPS

5.3.1 Image Acquisition

There has been tremendous growth in image acquisition methods. Ensuring that a clear picture with good resolution is obtained is always the preferred choice for any image-processing operation. MR images typically provide superior picture quality when compared with other methods, such as X-ray and ultrasound. An MR image captured from different angles can be clubbed together to generate a higher-resolution image. Such an image may be sent electronically so that a pathologist can "see" a portion of the scan without going anywhere.

Enhanced picture quality determines the accuracy of the radiologist's decision. Good bit resolution and spatial quality are the keys to obtaining better classification results. MRI of the breast in question utilizes a magnetic field; MRI features a good-quality detector and a computer to generate the inside view of the breast without making any types of cuts to the body. It is a very useful technique to screen those women at high risk for breast cancer, and it can also be used to assess the degree of malignancy or to further assess irregularities seen in the captured image.

5.3.2 Image Pre-processing and Segmentation

There are various parameters that can affect the quality of any captured image, and this is why there is a need to preprocess an image to make it suitable for any automatic decision-making approach. Instrumental twist, environmental conditions, different filters, and uneven illumination are some of the parameters that can affect the final decision. A pre-processing step ensures that all of the images inputted into the classifier are of similar quality, which ensures that better decisions can be produced by the classifier.

Filtering is generally used to reduce image noise and to uproot variables (different protests not held inside the ROI) from the background. Noise in the input image can be reduced utilizing morphological operations. Standard morphological operations are centred on the form and structure of an object (the structural components). The structural components can be

changed by applying mathematical morphological operations. The form and size of the structural components are situated as indicated by the segmentation or filtering undertaken.

A median filter is applied to the MRI image to ensure uniformity of the image. In addition, image rotation and alignment are also applied based on the average value of each row and pixel, so that only useful areas are processed for feature extraction. In the initial stages, the watershed segmentation divides the image into meaningful regions in a way that describes the structures in the MR image, such as large, continuous, bright and dark patches of similar intensity. The main focus of the smoothing operation is to make the image suitable for feature extraction.

Carrying out the precise, rapid, and reproducible delineation of breast lesions can be difficult, as the lesions may have complex topological structures and heterogeneous intensity distributions. The early detection of malignant breast tumours can be facilitated by the MRI scan, in combination with an appropriate automatic segmentation algorithm, which may enhance this imaging technique. Image segmentation is a procedure that partitions a picture into its constituent areas or items. Handling powerful picture division procedures for complex pictures is a standout option for the most troublesome cases. The reason for this is that segmentation divides the MR image into smaller portions of useful and non-useful regions. The main objective of this study is thus to develop a mechanism to automatically segment and facilitate the early detection of breast cancer based on the application of the watershed transform to MR images. The algorithm is divided into three major segments: pre-processing, watershed, and post-processing. The different segments are computed and the final image is cleared of all noise. The final modified image is generated after the final image is superimposed on the original MR image. This algorithm successfully resulted in the automatic segmentation of the MRI images, and it proved to be a beneficial tool for the early detection of breast cancer. This study showed that the results that were obtained automatically were in conformance with those obtained via manual detection, and they were also highly accurate. Image segmentation aims at labelling the tissue type and the ROI for further feature extraction. The objective of this work is to provide an automated tool that can help locate the tumour tissues in an MR image. There are multiple techniques available that can be leveraged to detect and identify various tumour tissues, but there are a few disadvantages associated with the available methods in the literature. Hence, a robust technique that can segment and de-noise MR images was developed by employing an efficient segmentation technique that can detect tumour tissues with accuracy. An automatic

watershed segmentation algorithm was developed using MR images so that it can aid in the early detection and classification of breast cancer.

5.3.3 Feature Extraction

Feature extraction is the more critical part of this automated detection system, as optimal feature extraction will ensure that the tumour type is accurately classified. The cancer cells are identified by image processing methods from the MRI data, and then feature extraction algorithms are applied on those data. Different features are calculated using various analytical operations, and those features include: total tumour area, a triangular area of the radial mapping of a tumour, triangular area of the uniform distribution of the radial mapping of a tumour, angular smoothness of the corners, and the counter-clockwise rotation to clockwise rotation ratio. These methods have been applied to 52 MRI sample data, of which 26 cases were benign and the rest were malignant. The results of these analyses show the correlation between the mathematical classification methods and those experts who classify cancers based on their experiences. Thus, these methods will provide supporting evidence when making a cancer diagnosis.

5.3.4 Classification

In this process, different classification methods were developed to identify malignant and benign cancer cells. ANN and SVM were employed on the dataset adopted herein to provide the classification. The classifier's ability to correctly classify cases was also tested against the k-fold cross validation test. This test was done to ensure that the classifiers are robust enough and not data or sequence dependent. ANN utilized the back-propagation error method during the training phase, and the SVM was also tested against various types of kernels.

5.4 SUMMARY

The overall discussion included the precise description of the different methodologies involved in understanding and detecting breast cancer in its early stages, as well as to classify different abnormalities of the breast. The feature-fusion methods that were involved in integrating the information that was extracted from the different approaches were also

discussed.

The methodology discussed herein proposed pre-processing and segmentation methods to extract the ROI. The feature-extraction procedure serves as the basis for classification. Overall, this chapter provided a detailed description of the techniques involved in the detection of breast cancer. Along with that, an analysis of the past research was also presented while addressing how further research should be conducted in this area. Such research initiatives have been undertaken by us, as presented in this thesis.

CHAPTER 6

AUTOMATIC SEGMENTATION

6.1 INTRODUCTION

This chapter discusses the Automatic segmentation algorithm developed in the proposed work, which comprises processes such as pre-processing, segmentation using clustering techniques, feature extraction, and classification techniques for tumour categorization.

Accurate tissue segmentation from MR image is an important step in the detection of breast cancer tumours. However, the accuracy of many segmentation algorithms is limited due to the presence of noise and intensity irregularities in MR images. Medical image segmentation has a huge impact on digital image processing, owing to its ability to enhance spatial resolution and image sharpening. It has been employed to derive helpful information from medical imaging data which, in turn, provides the most precise and reliable method for diagnosis. This procedure is a critical challenge given the existence of inhomogeneities in image intensities. The elimination of spatial intensity irregularities from MR images is a difficult task to achieve since these inhomogeneities could vary with different MRI acquisition parameters, as well as from one patient to another and from slice to slice. Conventional methods used in hospitals are based on the manual segmentation of the medical image under consideration. This again relies on the physician's ability to perceive and extract the required region from the image. This is made difficult given the minute variations and the strong resemblance between the actual and affected biological regions in the image.

The insufficient number of radiologists and the huge volume of MR images to be analyzed result in intensive labour; this approach is also highly uneconomical. This method depends on the expertise of the technician analyzing the images. Furthermore, the estimates also show that 10%–30% of tumours escape the eyes of the radiologists during routine screening (Taylor et al., 2008). There is a chance that the medical images might be tampered with due to issues that occur during the acquisition stage. Image segmentation can be defined as the partition or segmentation of a digital image into the same type of regions, with the important goal of simplifying the image under consideration into something that can be comprehended

and easily viewed for the visual analysis. Image segmentation is a highly significant process in medical image analysis.

Medical image segmentation plays a critical role in practical applications, such as in medical science. Medical images are important during object recognition when analyzing the human organs.

Various image segmentation algorithms have been proposed to achieve efficient and precise results. Of these proposed algorithms, the watershed segmentation approach is known as a classic technique in the field of topography, and it is considered the most useful method in medical imaging. This method was originally proposed by Digabel and Lantuejoul, 1977, and it was based on morphological concepts. However, the original algorithm has undergone various modifications, thus leading to improvements in its application. The theory of watershed segmentation is primarily based on the topographic representation of image intensity. Watershed segmentation also constitutes of other principal image segmentation methods, such as discontinuity detection, thresholding, and region processing. Overall, the watershed segmentation method is highly efficient and more stable when compared with other segmentation algorithms. The objective of the watershed transformation is to identify the watershed lines on a topographic surface.

The watershed algorithm is based on the geographic principles. A watershed is a land that separates various bodies of flowing water so that they ultimately converge at the same place. Since water tends to flow downhill, the borders of watersheds are elevated, serving as the boundary between land and water. Watersheds also serve as a barrier to protect the land from overflow.

Since radiologists are prone to making false-positive diagnoses in breast cancer cases, numerous attempts have been made to try to reduce these errors by developing image processing algorithms. Since contrast MRI is known to create high-resolution images of the breast, tumours can be more easily detected. The purpose of the automatic segmentation process is to detect the ROIs within MR images. A watershed transform algorithm is a powerful tool through which to achieve image segmentation. This study aimed to develop an automatic watershed segmentation algorithm for MR images to enhance their clarity, to increase the early detection rates of breast cancer, and to ultimately improve the diagnostic accuracy and capabilities of MRI when detecting breast cancer lesions.

6.2 METHODS

To enable meaningful segmentation while processing, the MRI was subjected to median filtering. This was followed by image rotation to orient and identify the pectoral muscles. A Sobel filter was applied in the water-shedding section to approximate a gradient map of the image. Post-processing consisted of masking the original images and recombining them into a single image. Figure 6.1 shows the steps followed by the watershed algorithm.

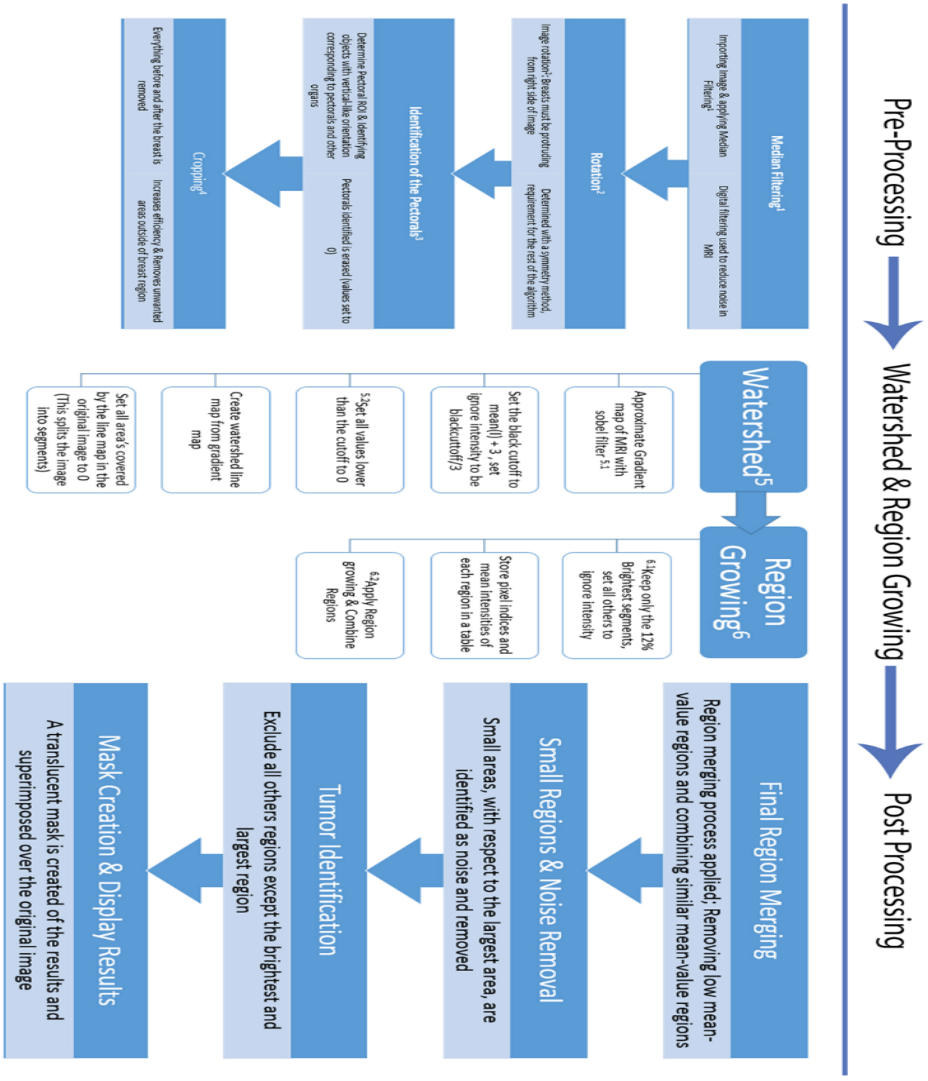

FIGURE 6.1: STEPS INVOLVED IN THE WATERSHED ALGORITHM: (A) PRE-PROCESSING, (B) WATERSHED, AND POST-PROCESSING

Below are the details of the method:

The method was separated into three major sections: pre-processing, watershed, and post-processing. In the first step, a median filtering technique was applied to remove the noise. Then, the image was rotated and the pectoral muscles were identified. A Sobel filter was applied in the watershed section to approximate a gradient map of the image. The final phase consisted of masking the original images and recombining them into a single image.

6.3 Pre-processing

6.3.1 median filter

Pre-processing involves the application of a median filter to the image. This filter sets the intensity of each pixel, and that of its direct neighbours, as its average intensity. During the initial stages, the watershed segmentation approach divides the image into meaningful regions in a way that describes the various structures in the MR image, including large continuous bright and dark patches of similar intensity. Smoothing the image during the pre-processing stage reduces the number of unusable regions. Figure 6.2 shows the original MRI in the right and post median filter in the left .

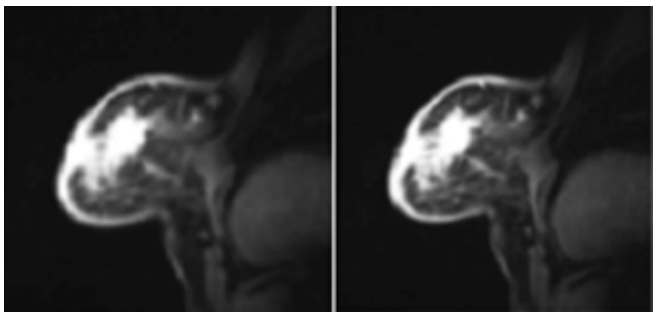

FIGURE 6.2: THE ORIGINAL MRI AND POST MEDIAN FILTER.

6.3.2 Rotation and Alignment

The algorithm determines the orientation of the image by summing up all the intensity values in a given row. It identifies the rows where the summations are above the threshold value and it proceeds to rotate the image if the row is located below the top 20% of the image. This is followed by the application of histogram equalization to improve the image contrast.

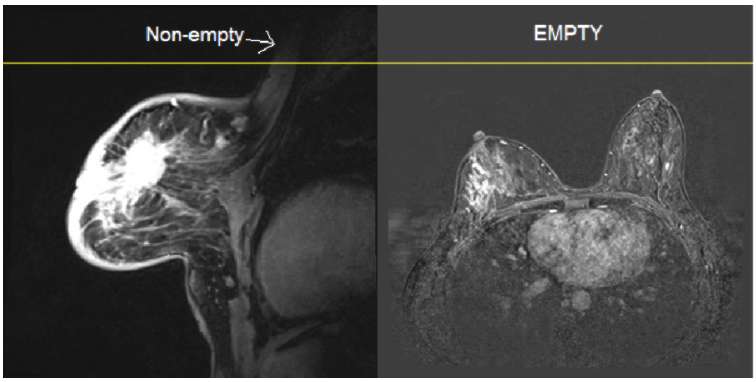

FIGURE 6.3: IMAGE ROTATION AND ALIGNMENT

Image rotation may result in the change of map position (x_0,y_0) to (x_2,y_2) in the output image, and it may rotate the image by angle degree, which is given as:

$$x_2 = \cos(\theta)*(x_1 - x_0) - \sin(\theta)*(y_1 - y_0) + x_0 \quad (6.1)$$

$$y_2 = \cos(\theta)*(x_1 - x_0) + \cos(\theta)*(y_1 - y_0) + y_0 \quad (6.2)$$

Where, (x_0, y_0) is central to the input image, (x_1, y_1) is the current pixel position, (x_2, y_2) is the new pixel position and θ is the rotation angle.

6.3.3 Identification of the Pectorals

The pectoral muscles are identified by determining the ROI, where the muscles are most likely to be found, such as the torso/breast border; the remaining portions left of the border are ignored. However, this approach appeared to be ineffective, as the pectoral muscles lie under the breast tissue. These remaining portions are then converted to a black-and-white image using a modified histogram-based threshold. This was followed by scanning the resulting image of the pectoral muscle to identify an area of minimum size and vertical orientation.

6.4 WATERSHED ALGORITHM

The Sobel filter was applied to the MRI, resulting in a gradient map of the image. In this gradient image, sharp changes in contrast, such as the edge between a dark and light region, appear as high-intensity points, while regions of monotonic intensity appear as dark patches. The gradient map is denoted by:

$$|G| = \sqrt{G_x^2 + G_y^2} \tag{6.3}$$

Each pixel location consists of two components: G_x and G_y. G_x and G_y are the variables that correspond to the result from the row mask and column mask respectively.

The watershed segmentation was applied to this gradient map. This algorithm poorly handles the monotone plateaus, resulting in their over-segmentation. However, these areas are monotonic, as they appear as a single dark patch surrounded by a high-intensity edge at the boundaries with better segmentation. A list of the regions created by segmentation was stored and filtered to locate the specific regions that could contain tumours.

This algorithm functions by marking any pixel below a certain threshold value in the original image as a potential background pixel. The pixels inside the largest connected region, where all pixels are below that value, are labelled as background pixels. The background regions are then removed from the list of breast regions.

This was followed by the removal of skin segments, as they tend to appear as extremely bright spots on the MR images. A distance map that defined the distance between each pixel in the breast, as well as the nearest background pixel, was generated to eliminate noise. The skin segments were also removed from the list of breast regions.

Thus, the resulting breast MRI was only composed of the inner breast regions. However, most of these regions on the MR image were dark, while any abnormalities (such as cancerous regions) appeared to be exceptionally bright. Therefore, these segments were also eliminated from the list of breast regions to be scanned. This algorithm resulted in the removal of 90% of darkest regions from the total list of breast regions. The remaining regions were those that could contain a tumour.

Regions growing: Based on the average intensity, the resulting segments were sorted and combined in order of highest to lowest intensity. First, the index of the region was converted to set the seed point. Using this seed point, the region-growing approach was applied to the segments to construct a new region. The regions are combined only when the grown region and new region are contained within each other. This process was applied multiple times to achieve ideal region growing, which formally defined the growth of additional regions, such as:

$$R = \bigcup_{i=1}^{n} R_i \quad (6.4)$$

Segmentation must be complete; that is, each pixel must be incorporated in a given region.

R_i is a connected region, *i= 1, 2,..., n* (6.5)

The points in a region must be connected in some predefined sense.

$$\cap R_i R_j = \emptyset \qquad \textit{for } i=1,2,...,n. \quad (6.6)$$

The regions must be disjointed.

$$P(R)=TRUE \qquad \textit{for } i=1,2,...,n. \quad (6.7)$$

Numerous properties must be satisfied by the pixels in a segmented region. In this case, $P(R_i)$ is true, if all pixels in R_i have the same intensity.

$P(R_i R_j)=FALSE$ for any adjacent region R_i and R_j (6.8)

Region R_i and R_j are different in the sense that predicate P

R_i $P(R_i)$ is a logical predicate defined over the points in the set and is Ø the null set.

6.5 POST-PROCESSING

After computing the different segments, some minimal areas (0.1% of the image size) were identified as noise and subsequently eliminated. A translucent mask was created from the resulting segments and superimposed over the MR image. Similarly, a different translucent colour mask was used to highlight the previously identified pectoral muscle in a separate image. At this point, the image was recombined with the previously cropped regions from the pre-processing stage and rotated back to its original orientation. The resulting image, including both the tumour ROI and the identified pectoral muscle, was displayed.

6.6 IMPLEMENTATION AND RESULTS

MATLAB 2014a was used for the implementation of this system; this program was run on an Intel i7 CPU with 4 GB of RAM. The automatic segmentation algorithm is successfully used to segregate the suspicious area from the total MR image. A representative case featuring each algorithm step is shown in Figure 6.4, where the sub- images show (1) the original MR image; (2) after the application of median filtering; (3) pectoral muscle identification; (4) application of the watershed algorithm and region-growing approach; and (5) the final results after masking the original image . The proposed method of segmentation introduced in this research was applied to all 55 patients to test the segmentation method and compering with (55 image that outlined by an expert).

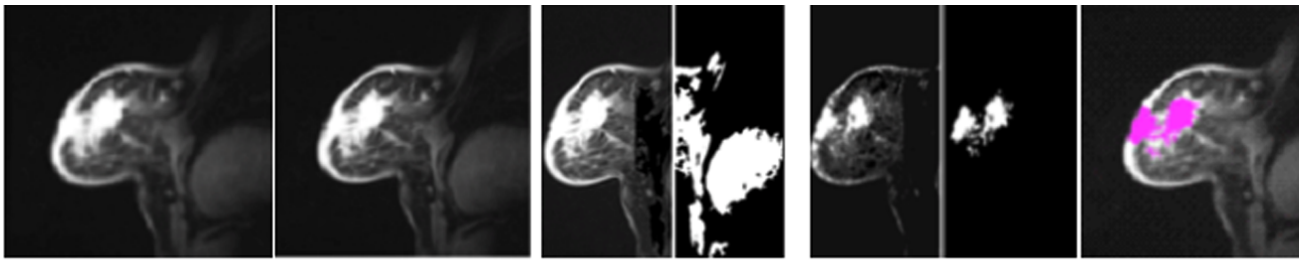

FIGURE 6.4: STEPWISE IMAGE PROCESSING USING THE WATERSHED ALGORITHM

Figure 6.5 shows the manual outline of a tumour where the outline covers the enclosed area. The software results clearly highlighted the entire area. The pixels in both the doctor-identified image and in the software output were compared. The accuracy of the differences between the two cases is calculated as:

$$Accuracy \ = (Number\ of\ different\ pixels\ /total\ number\ of\ pixels) \times 100 \qquad (6.9)$$

On an average, 97.52% of the region was contained within the outlined results, and there were some very mild cases where the software-detected regions fell slightly outside the detected region, as seen in the second set of results in Figure 6.5.

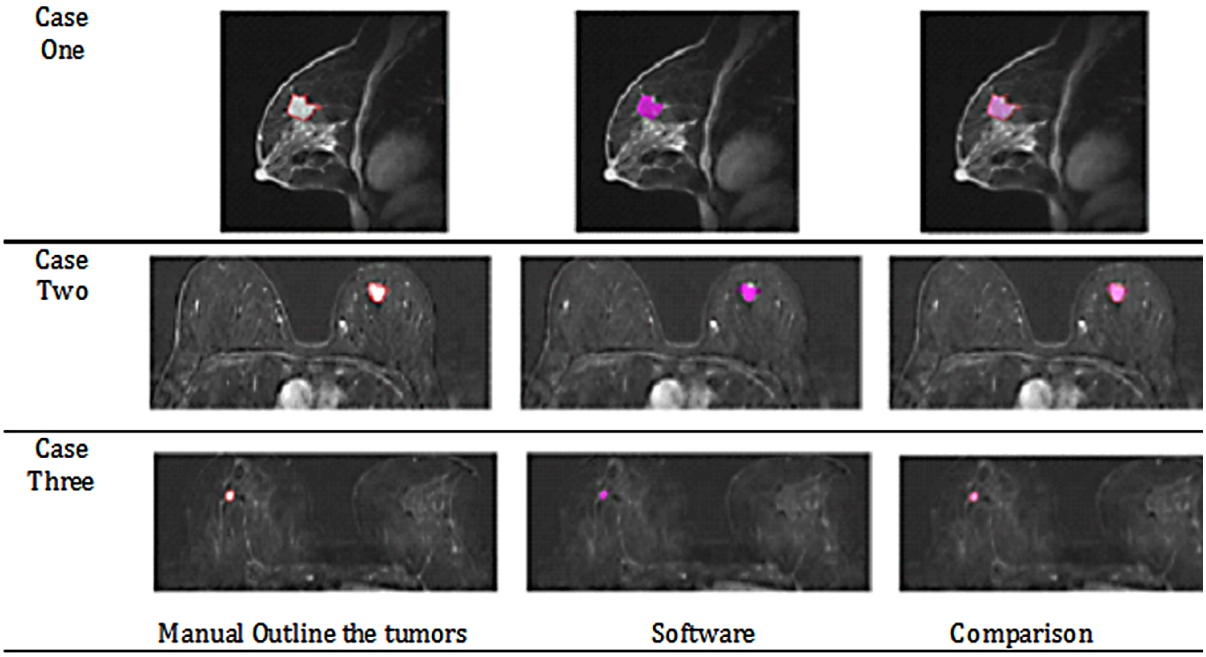

The expert-identified and software-generated tumour areas are shown in Figure 6.5. A numerical comparison of the same is also provided in Table 6.1. Table 6.1 further provides the average results for all 55 MR images, to ensure that more detailed comparisons can be made.

Table 6.1: Comparison of computer-identified and expert-identified tumour areas

MRI Image	Software-generated area (pix^2)	Expert-identified area (pix^2)
MRI Sample-1	82.9	83.1
MRI Sample-2	129	128.02
MRI Sample-3	76	77.01
MRI Sample-4	148.1	148.8
MRI Sample-5	111.2	110.8
Average of all 55 samples	3,451.45	3,524.48

6.7 DISCUSSION

This chapter described a novel method for the auto segmentation of areas corresponding to cancerous lesions in MR images of the breast. The areas suspected to represent cancerous lesions in the images were highlighted to facilitate further analysis to determine whether the detected lesions were indeed cancerous.

The analysis of MRI images, owing to their complexity, involves multiple steps that range from pre-processing to post-processing. Very limited automated algorithms are currently available for image segmentation, and they are based on the specific region under investigation and the type of imaging technique used. The automated algorithm described in this study involves a three-step process; it includes initial pre-processing, followed by the use of the watershed transform method for image segmentation, and a post-processing step. Pre-processing is an essential step where the Sobel technique for edge detection was used in conjunction with other pre-processing aids. This was followed by the use of the watershed transform technique for image segmentation. Then, the highlighted areas in the image are subjected to further analysis to determine whether they were cancerous or non-cancerous. The watershed algorithm was previously tested on standard digital images of mammograms, and it was found to be effective. Several studies hitherto have focused on testing various algorithms, including watershed algorithms, to enhance the sensitivity of mammography or other imaging techniques; however, very few studies have incorporated automated algorithms. This study is unique in that the proposed automated algorithm was used to process MR images for the evaluation of breast cancer, and this approach was tested against the manual isolation of a tumour's location from MR images. The results showed the considerable similarity between the results obtained by both the automated and manual processing approaches.

This study confirmed the previously reported findings, insofar as the watershed transform method can be used with foreground markers to segment MR images. The algorithm described in this study was capable of successfully executing the automatic segmentation of the MR images obtained in cases of suspected breast cancer. Furthermore, the automatic watershed segmentation technique was successful in identifying breast cancer lesions in the MRI images of all 52 patients evaluated. The tumour regions identified by the automated algorithm and those identified by manual processing of the MR images were compared by an independent expert, and they were found to be largely consistent; in fact, 97.52% of the tumour areas defined by the former method overlapped with the areas defined by the expert. In the remaining cases, the tumour areas defined by the software extended slightly beyond those identified by the manual analysis. Thus, our findings show that processing using the automated algorithm may be almost as effective as the manual processing of the MR images.

This is consistent with the findings of previous studies, which have shown that automatic image processing is accurate and at least as effective as manual analysis.

This study has a few limitations, which include the small sample size and the lack of more accurate techniques to confirm tumour margins. These drawbacks may be overcome by further investigating more large-scale populations comprising patients with different types of breast cancer. Furthermore, more accurate methods for tumour delineation should also be employed, possibly in conjunction with the combined use of multiple imaging modalities.

6.8 SUMMARY

Satisfactory results were obtained when applying the watershed algorithm in the segmentation of MRI scans. Our results indicate that the method described in this study may facilitate the early detection of breast cancer. The results obtained by employing the automatic algorithm were found to be in close agreement with those obtained by manual detection. The findings appear to be promising and justify the development of future studies, which will aim to develop and compare more accurate techniques to help further refine and enhance the accuracy of this current approach.

CHAPTER 7

CLASSIFICATION OF MR IMAGES

7.1 INTRODUCTION

MRI is a highly effective imaging modality when used in the early detection of breast cancer. Once an MRI scan is performed, an expert searches for signs of abnormalities; however, MR images are complex in appearance, and the signs of early disease are often small or subtle. This is the main reason why many missed diagnoses occur, as these errors are primarily attributable to human factors. To improve the accuracy of interpretation, or to help locate possible abnormalities, a variety of computer systems have been proposed. Some of the important signs of breast cancer that a specialist normally looks for are the size of a tumour, tumour complexity, and other recognizable features. MRI was repeatedly shown to be very useful in the timely detection of cancer, as it provides a clear picture of a tumour; however, even experts frequently fail to classify tumours as benign or malignant. As such, there is a need for an auto-classification method, which can help medical experts. Ensuring that the correct classification is made depends on efficient feature vector selection. This chapter first proposes two novel feature-extraction methods (radial mapping and uniform distribution of radial mapping), which can be used for breast cancer detection with the help of MRI. Both feature-extraction methods are applied to all MRI sample data, which comprise 26 cases of benign cancers and 26 cases of malignant cancers. The mathematical results (cancer type) of these feature-extraction methods are subsequently correlated with the opinions (classification) of medical experts. Thus, these features are used to classify breast cancer types. ANN is also employed to classify the tumours, particularly given its excellent non-linear classification ability. Furthermore, a five-fold cross-validation method is used to check the robustness of a classification scheme. The false-positive and false-negative rates of the classifier are also checked, and it turns out that these are quite low.

Correctly diagnosing a tumour is a rather difficult task that requires special effort. The early diagnosis of breast cancer provides patients with the chance to receive better treatment, thus enhancing their chance of survival. The World Health Organization's International Agency for Research on Cancer Working Group confirmed that the early detection and treatment of breast cancer are considered to be the most promising approaches to reduce mortality rates. There are currently four common ways to diagnosis breast cancer: BSE, clinical examination (CE), radiowave-based examination (RWBE), and MRI examination (MRIE).

MRIE is the most efficient approach when attempting to perform the early identification of a breast tumour. Breast cancer detection using an MRI scan primarily utilizes the principles of NMR, which states that "Certain atomic nuclei can absorb and emit radio frequency energy when placed in an external magnetic field". MRI scans the breast using an external magnetic field, which identifies potential tumour cells. Thereafter, an experienced radiologist analyzes the resulting MR images in order to classify a tumour as either benign or malignant. Several studies have shown that even for experienced radiologists, it is difficult to make clear distinctions between tumour types. Figure 7.1 shows MR image samples taken from both a benign and malignant tumour.

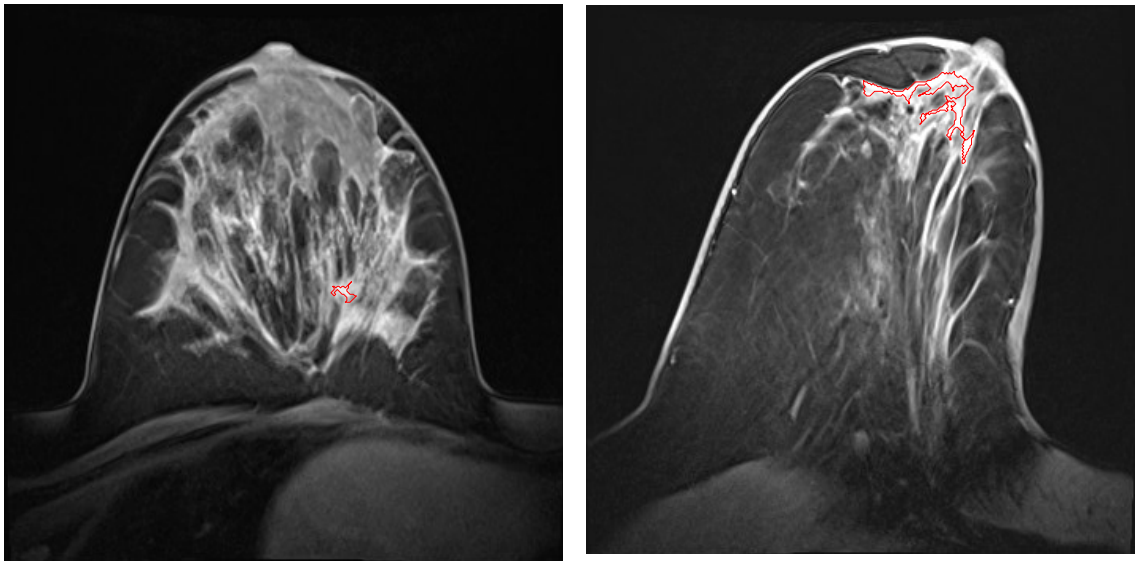

(a) **(b)**

FIGURE 7.1: SAMPLE MRI OF (A) A BENIGN AND (B) A MALIGNANT TUMOUR.

7.2 Feature Extraction

Correct feature selection is the most important part for improved classification. In this study, two new and better features are proposed. Along with that, three other features (that have been used in old literature) are also extracted. The five features extracted in this study are:

1. Total tumour area
2. Angular smoothness of the corners
3. Counter-clockwise rotation versus clockwise rotation ratio
4. Radial mapping of a tumour
5. Uniform distribution of radial mapping of a tumour

The last two feature extraction methods are novel and provide better insight of the tumour type and improve the classification accuracy.

7.2.1 Total Tumour Area

The total area covered by a tumour is one of the factors that can be used to classify tumour type. To calculate the tumour area, a reference point, such as the centre of gravity (CG), needs to be chosen. The CG position is calculated by equation 7.1 and 7.2:

$$CG_x = \frac{\sum_{i=1}^{n} x_i}{n} \quad (7.1)$$

$$CG_y = \frac{\sum_{i=1}^{n} y_i}{n} \quad (7.2)$$

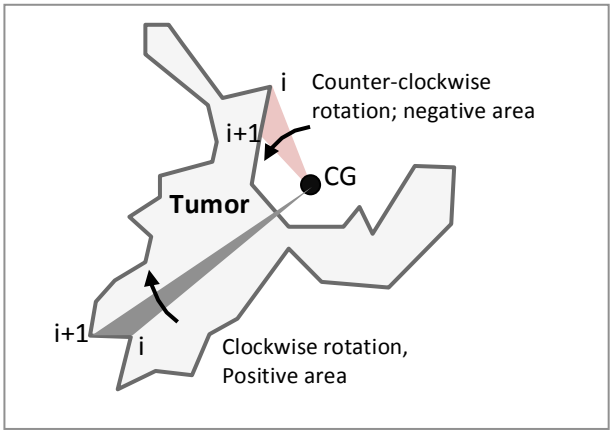

FIGURE 7.2: EXAMPLE OF HOW TO CALCULATE THE TUMOUR AREA WITH THE HELP OF TRIANGLES

This feature is calculated by adding small areas formed by three points as three points form a

triangle as shown in Figure 7.3. The three points are selected as any two consecutive points (where tumour changes its direction) on the borders of the segmented region and the reference point (CG). The areas of these triangles are assigned a positive sign if the two consecutive points are turned around the CG in a clockwise direction; otherwise, they are assigned a negative sign. These small triangular areas are summed to calculate the total tumour area. The area of each triangle (with corner names A, B, and C) is calculated, as shown in equation 7.3

$$\text{Area} = \frac{|X_A(Y_B - Y_C) + X_B(Y_C - Y_A) + X_C(Y_A - Y_B)|}{2} \tag{7.3}$$

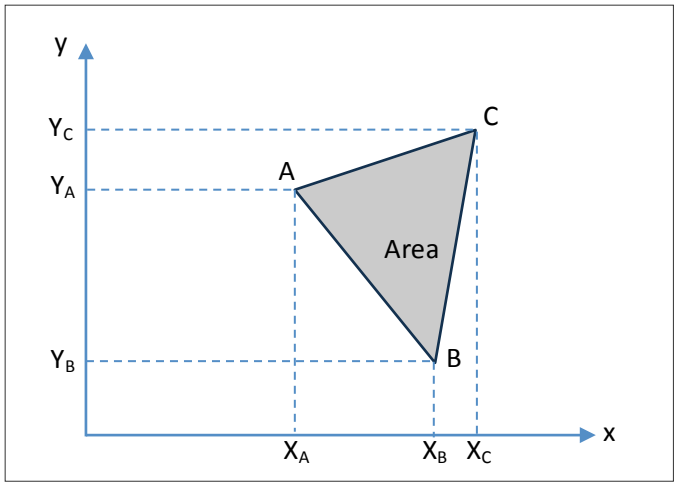

FIGURE 7.3: REFERENCE FIGURE FOR EQUATION 7.2

The complete feature calculation involves two steps, which are as follows:

First step: Calculation of the centre of gravity of the tumours and then selection of two consecutive points (where tumour changes its direction) on the contour.

Second step: Calculation of the each triangular area (CG and two points in the contour) with respective signs (positive/ negative) and addition of them to obtain a single value (feature).

7.2.2 Angular Smoothness of the Corners

The angular smoothness of the corners is derived from the angular deviation of the corners, as shown in Figure 7.4. For each of the three consecutive points, A, B, and C, the angular deviation is calculated by equations 7.4–7.6:

$$d_1 = [X_B - X_A; Y_B - Y_A; 0] \tag{7.4}$$

$$d_2 = [X_C - X_B; Y_C - Y_B; 0] \quad (7.5)$$

$$\text{Angular Dev} = \cos^{-1} \frac{\text{dot}(d_1, d_2)}{\text{norm}(d_1) * \text{norm}(d_2)} \quad (7.6)$$

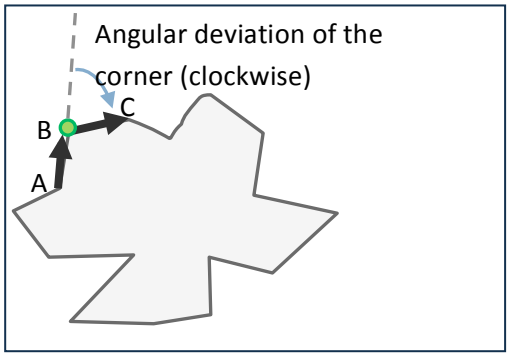

FIGURE 7.4 SAMPLE CALCULATION APPROACH TO DETERMINE THE ANGULAR DEVIATION OF THE CORNERS

Figure 7.5-A shows separated a cancer tumour from MR image, where Figure 7.5-B shows the plot of angular deviations with respect to each point, along with the associated variance. For a smooth shape (such as a perfect circle), the variance of this value will be zero (as all the deviation angles are the same); however, for shapes with many broken lines with different directions (clockwise or counter-clockwise), the variance will be a larger number.

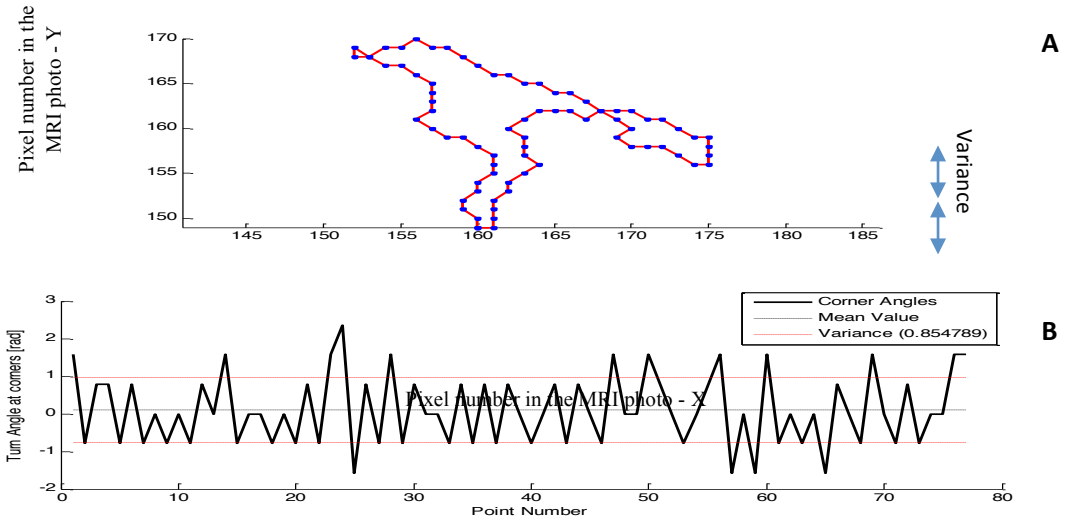

FIGURE 7.5: VARIANCE OF THE ANGULAR DEVIATION OF THE CORNERS

This feature basically provides two aspects of the tumour. It gives the idea about the tumour's shape and it also provides the variance value of the same.

7.2.3 Counter-clockwise rotation vs. clockwise rotation

The summation of the deviation angles (Figure 6.6) of all of the corners of a closed shape is 360 degrees (the clockwise rotations are regarded as positive, while the counter-clockwise rotations are regarded as negative). However, if we sum the clockwise rotations and counter-clockwise rotations separately, the ratio between these two values will represent the harshness or irregularity of the shape. For example, in the case of a circle, this ratio will be zero, while irregular shapes will yield some numerical value. To determine the direction of rotation, equation 7.7 is used (d_1 and d_2 are calculated by equations 7.4 and 7.5):

$$d_3 = \text{cross}(d_1; d_2) \begin{cases} \text{if } Z_{d3} < 0 & Clockwise \\ \text{if } Z_{d3} > 0 & Counter-clockwise \end{cases} \quad (7.7)$$

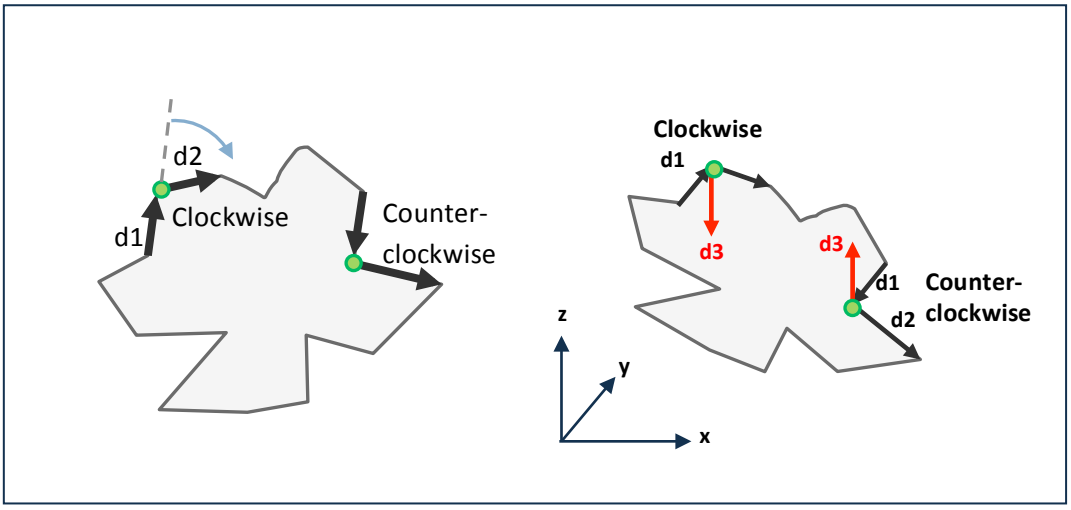

FIGURE 7.6: SAMPLE METHOD TO CALCULATE THE DIRECTION OF ROTATION

This feature calculates and provides all associated angles with Counter-clockwise rotation and clockwise rotations of the tumour area.

7.2.4 Radial Mapping of the Tumour

This novel feature present that some tumours have sharp angles at the corners, while the others have shallow and smooth corners. The shape of a tumour is first separated with the help of different image-processing methods (automatic segmentation). Figure 7.7A represent the plot of the shape of the tumour in respect to the Pixel number in the MRI photo – X and Y

coordinates where the corners of a tumour represented in points.

To determine the tumour type with the help of radial mapping, the shape of a tumour was mapped to a radial coordinate, where the angular and radial position of each corner was calculated relative to the CG.

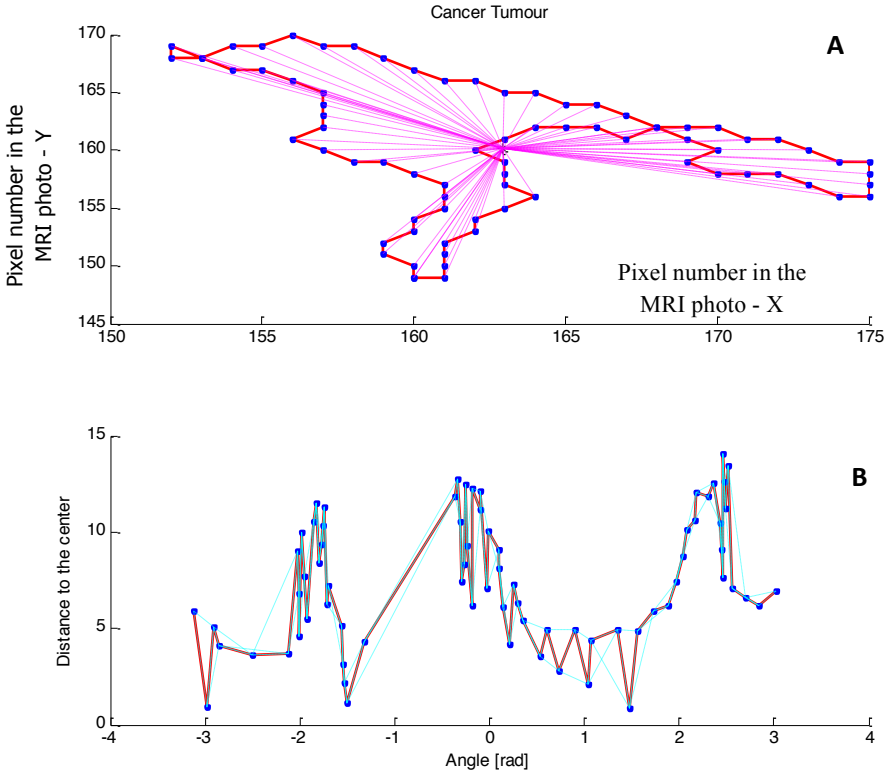

FIGURE 7.7 SEPARATED CANCER TUMOUR FROM THE MR IMAGE (A) AND RADIAL MAPPING OF A TUMOUR, AS BASED ON CALCULATING THE AREA OF A TRIANGLE (B)

The following steps summaries the Radial Mapping feature and its calculation:

Step one: First of all, the radial mapping is needed to be done. To map the points along the radial map, calculate the angle (θ) between the centre and the two points on the contour of the tumour shape (the number of points depends on the tumour shape) with the help of following equations:

$$R = \sqrt{(x - CG_x)^2 + \left(y - CG_y\right)^2} \tag{7.8}$$

$$\theta = \operatorname{atan2}\left(y - CG_y, x - CG_x\right) \tag{7.9}$$

Where R is the distance between the Centre of Gravity (CG) and each point (on the edges)
θ is the angle of the vector which connects CG to that point.
In the equations 7.8 and 7.9, the angle changes between $-\pi$ (radian) and $+\pi$ (radian), and the associated distances are calculated in pixels.

Step two: After mapping the tumour in the radial plane, the total area of the each triangle (which are created in step 1) is calculated to check the severity of cancer.

7.2.5 Uniform Distribution of Radial Mapping of the Tumour

When the tumour corners are mapped to the radial coordinate, the point distribution does not remain uniform, and the distance between each corner point varies with mapping. To ensure that there is a uniform distribution, an interpolation method is used in this proposed approach. This interpolation uses the spline function to interpolate the points between $-\pi$ and $+\pi$ for different values of $\Delta\theta$, as shown in Figure 7.8. The angles can easily be converted into degrees (-180 to 180 degree) also. For the sake of easy calculation and comparison, $\Delta\theta$ are used in terms of degree. The area of the triangles based on these uniformly distributed corner points (with different values of $\Delta\theta$ or different angular frequencies) behave as a function of $\Delta\theta$, as shown in Figure 7.8. Figure 7.8, uses radian on the X-axis for the plot so that it can be compared with the earlier plots but it uses degree for the uniform distribution factor ($\Delta\theta$) so that easy interpolation can be made possible.

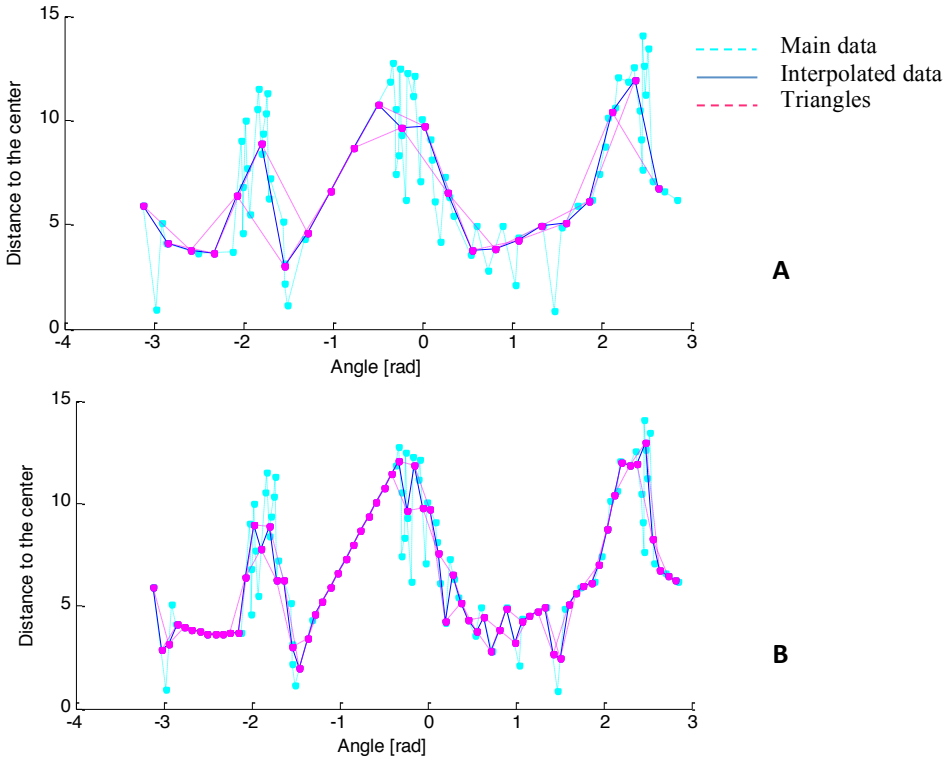

FIGURE 7.8: UNIFORM DISTRIBUTION OF RADIAL MAPPING OF A TUMOUR WITH ΔΘ=15°/0.83 RAD (A) AND ΔΘ=5°/0.027 RAD (B)

This feature has been tested with different values of Δθ (5°, 10°, 15°, 20°, 25°, and 30°). Table 7.1 shows the extracted features from sample data of benign tumour using different value of Δθ.

Table 7.1: Extracted features from sample data of benign tumour using different value of Δθ

Sample	Area (rad.pix) for Δθ=5°	Area (rad.pix) for Δθ=10°	Area (rad.pix) for Δθ=15°	Area (rad.pix) for Δθ=20°	Area (rad.pix) for Δθ=25°	Area (rad.pix) for Δθ=30°
Sample 1	1.60	2.02	2.98	4.27	4.68	7.76
Sample 2	1.55	2.19	3.65	5.36	6.37	6.70
Sample 3	1.46	2.01	2.75	3.92	4.14	3.42
Sample 4	10.34	11.16	10.34	15.65	13.98	19.96
Sample 5	1.48	4.18	6.04	7.04	8.78	10.74

Table 7.2: Extracted features from sample data of malignant tumour using different value of Δθ

Sample	Area (rad.pix) for Δθ=5°	Area (rad.pix) for Δθ=10°	Area (rad.pix) for Δθ=15°	Area (rad.pix) for Δθ=20°	Area (rad.pix) for Δθ=25°	Area (rad.pix) for Δθ=30°
Sample 1	20.46	18.61	19.39	28.44	30.29	20.13
Sample 2	11.39	17.16	15.95	16.52	17.09	26.92
Sample 3	8.11	14.94	17.67	26.08	25.95	32.02
Sample 4	18.25	21.25	22.41	17.54	27.08	23.66
Sample 5	24.41	14.62	22.34	20.94	16.78	38.91

These two tables presented above shows the extracted features for different values of Δθ, as well as for different datasets. For instance, one can clearly observe that the extracted features with Δθ =15° can itself be used to classify the type of tumour. For example: benign tumour generates a feature value somewhere between 2.75 to 10.34, whereas malignant tumour generates a feature value somewhere between 15.95 to 22.41. The use of other features along with this feature can make the prediction even better.

7.3 RESULTS AND DISCUSSIONS

Both of the proposed feature-extraction methods (radial mapping and uniform radial mapping) are applied to the 56 MRI. Figure 7.10 shows the obtained features from the "Malignant classified" MRI sample and result of some value of Δθ, while Figure 7.11 shows the features from the "Benign Classification" with a different value of Δθ.

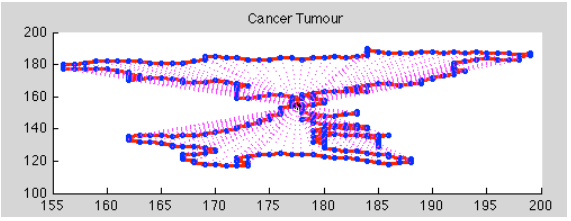

(a) Tumour shape after segmentation

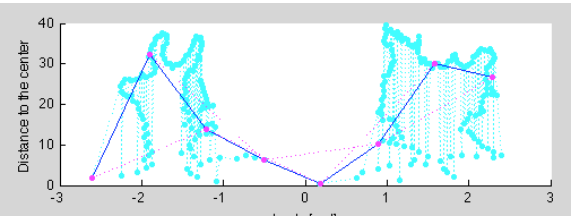

(b) Δθ=30°, Area = 38.75 rad.pix

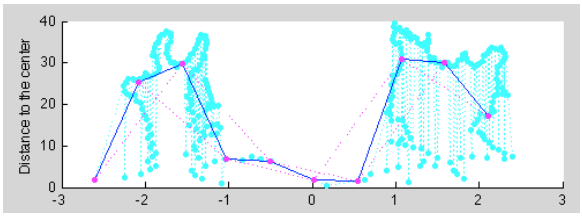

(c) $\Delta\theta = 20°$, Area = 38.91 rad.pix

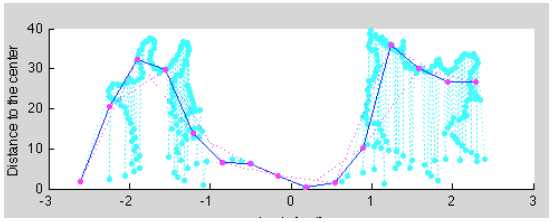

(d) $\Delta\theta = 15°$, Area = 20.92 rad.pix

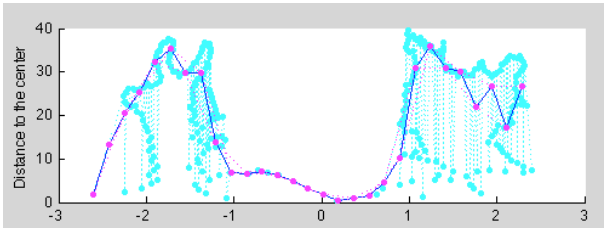

(e) $\Delta\theta = 10°$, Area = 14.65 rad.pix

FIGURE 7.10: OBTAINED FEATURES FROM A "MALIGNANT CLASSIFIED" MRI SAMPLE

In the above Figure 7.10 (a), it shows the tumour shape after segmentation is performed and rest of the images Figure 7.10 (b) - Figure 7.10 (e) shows the uniform radial mapped output with different values of $\Delta\theta$. The overall area (extracted feature) is also mentioned along with the every image.

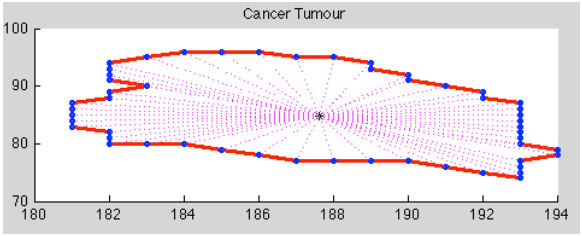

(a) Tumour shape after segmentation

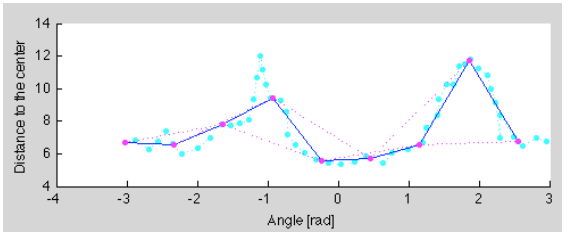

(b) $\Delta\theta = 30°$, Area = 9.20 rad.pix

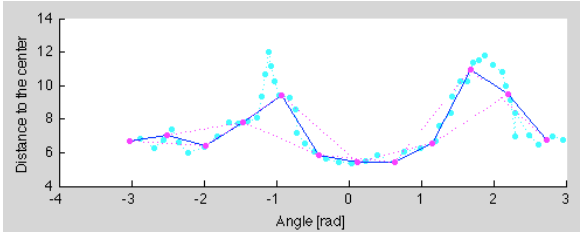

(c) $\Delta\theta = 20°$, Area = 6.10 rad.pix

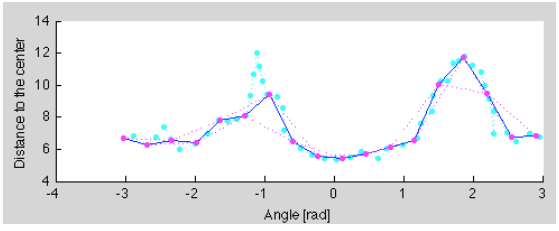

(d) $\Delta\theta = 5°$, Area = 4.26 rad.pix

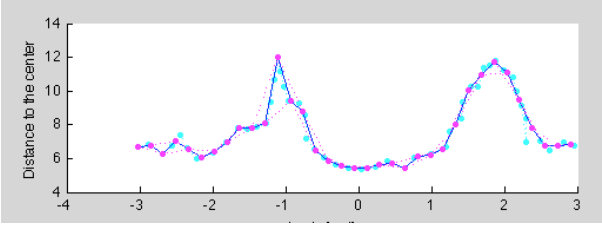

(e) $\Delta\theta = 10°$, Area = 2.70 rad.pix

FIGURE 7.11: OBTAINED FEATURES FROM A "BENIGN CLASSIFIED" MRI SAMPLE

In the above Figure 7.11 (a), it shows the tumour shape after segmentation is performed and rest of the images Figure 7.11 (b) - Figure 7.11 (e) shows the uniform radial mapped output with different values of $\Delta\theta$. The overall area (extracted feature) is also mentioned along with the every image.

In Benign case, the total area of the triangle turns out to be 9.20 rad.pix and 2.70 rad.pix for $\Delta\theta = 30°$ and $\Delta\theta = 10°$ respectively. This clearly indicates that the total area of triangle is much smaller in benign case as compared to malignant.

In this study, total five features are calculate for each MRI image. Figure 7.12 shows the selected MRI image along with extracted features.

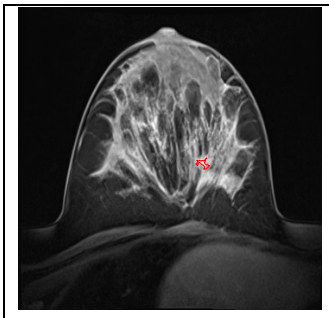 (a)	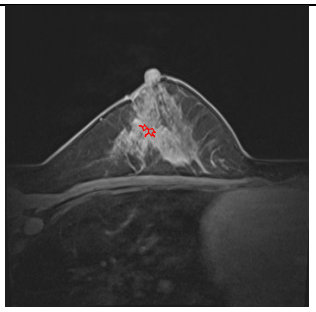 (b)
Tumour type: Benign Radial mapping area: 9.27 rad.pix Uniform radial mapping area (Δθ=15°) 7.58 rad.pix Tumour area: 62 pix^2 Variance of deviation angles: 0.95 rad^2 Counter-clockwise to clockwise ratio: 84.6%	Tumour type: Benign Radial mapping area: 6.69 rad.pix Uniform radial mapping area (Δθ=15°) 7.87 rad.pix Tumour area: 62 pix^2 Variance of deviation angles: 0.94 rad^2 Counter-clockwise to clockwise ratio: 86.7%
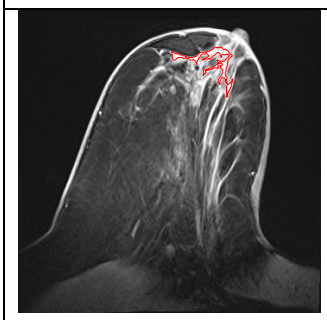 (c)	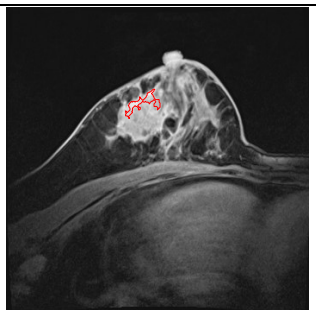 (d)
Tumour type: Malignant Radial mapping area: 32.58 rad.pix Uniform radial mapping area (Δθ=15°) 25.92 rad.pix Tumour area: 618 pix^2 Variance of deviation angles: 0.84 rad^2 Counter-clockwise to clockwise ratio: 100%	Tumour type: Malignant Radial mapping area: 16.6 rad.pix Uniform radial mapping area (Δθ=15°) 14.48 rad.pix Tumour area: 314 pix^2 Variance of deviation angles: 0.83 rad^2 Counter-clockwise to clockwise ratio: 93.9%

 (e) Tumour type: Malignant Radial mapping area: 38.53 rad.pix Uniform radial mapping area ($\Delta\theta$=15°) 37.31 rad.pix Tumour area: 1225 pix^2 Variance of deviation angles: 0.75 rad^2 Counter-clockwise to clockwise ratio: 97.1%	

FIGURE 7.12: SELECTED MRI SAMPLES AND THEIR CORRESPONDING EXTRACTED FEATURES

All of the features shown in Figure 7.12 are extracted from the 56 MRI samples in order to determine the most efficient feature that can aid health care professionals as they classify various tumour types. Figure 7.12 (a) and (b) represents samples of the benign type tumour, whereas (c), (d) and (e) shows malignant cases. Table 7.3 shows the extracted features from the "Benign" tumour MRI samples and Table 7.3 shows the extracted features from the "Malignant" tumour MRI samples.

Table 7.3: Extracted features from the "Benign" tumour MRI samples

Sample	Tumour Area (pix^2)	Radial Mapping Area (rad.pix)	Uniform Radial Mapping Area (rad.pix)	Variance of Deviation Angles (rad^2)	Counter-clockwise to Clockwise Ratio (%)
1	62	9.27	7.58	0.95	84.60%
2	62	6.69	7.87	0.94	86.70%

3	175	2.89	3.16	0.74	69.20%
4	78	10.32	4.44	1.22	77.80%
5	482	3	5.27	0.56	75.80%
6	70	4.4	2.65	0.68	76.50%
7	18.5	3.91	2.21	0.66	62%
8	33	5.19	2.98	0.7	73.30%
9	61	3.54	2.83	0.87	60%
10	82.5	3.31	2.15	0.92	63.60%
11	184	3.87	4.46	0.55	63.60%
12	82.5	8.1	3.81	0.76	66.70%
13	147.5	6.16	6.31	0.74	85.70%
14	76	2.34	1.99	0.69	52.90%
15	81	4.52	4	0.93	83.30%
16	98.5	3.73	3.47	0.63	61.90%
17	72	9.06	3.69	0.61	76.50%
18	16	3.17	1.18	0.99	33.30%
19	85.5	2.64	2.76	0.51	73.20%
20	134	6.1	4.81	0.68	73.30%
21	37	2.41	4.99	0.58	61.90%
22	55.5	2.74	2.12	0.51	42.90%
23	139	3.26	3.65	0.49	76.50%
24	24	4.7	1.69	0.95	52.90%
25	225.5	3.08	2.75	0.95	74.20%
26	194	3.64	4.36	0.64	78.40%
Average	**106.76**	**4.69**	**3.73**	**0.74**	**68.72%**

Table 7.4: Extracted features from the "Malignant" tumour MRI samples

Sample	Tumour Area (pix^2)	Radial Mapping Area (rad.pix)	Uniform Radial Mapping Area (rad.pix)	Variance of Deviation Angles (rad^2)	Counter-clockwise to Clockwise Ratio (%)
1	618	32.58	25.92	0.84	100%
2	314	16.6	14.48	0.83	93.90%
3	1,225.5	38.53	37.31	0.75	97.10%
4	1,040	29.47	17.76	0.75	94.10%
5	945.5	35.96	22.34	0.7	96.40%
6	2,708	35.88	34.82	0.69	100.00%
7	1,409	42.65	33.14	0.81	91.90%
8	1,792	9.09	17.67	0.61	95.20%
9	623.5	23.48	22.41	0.78	91.20%
10	768.5	4.01	12.64	0.76	92.70%
11	1,666	12.99	15.94	0.64	92.20%
12	595.5	24.46	19.39	0.7	100.00%
13	3,504.5	18.28	28.39	0.68	97.90%
14	4,690.5	70.63	80.99	0.69	97.40%
15	6,041	54.44	73	0.73	99.00%
16	3,938.5	11.76	29.71	0.67	97.30%
17	7,535.5	49.88	62.35	0.53	97.90%
18	9,982.5	40.14	73.92	0.52	97.10%
19	599	11.78	10.34	0.8	94.70%
20	1,451	15.86	24.65	0.77	93.70%
21	2,519.5	23.81	34.74	0.71	97.70%
22	1,304.5	35.9	36.85	0.66	93.20%
23	275	14.1	8.75	0.6	92.90%
24	595.5	24.46	19.39	0.7	100%

25	405	8.49	10.2	0.76	86.40%
26	208	16.6	14.48	0.83	93.90%
Average	**2,182.90**	**26.99**	**30.06**	**0.71**	**95.53%**

Once all of the features were calculated, a simple threshold classification was applied to these features by first calculating the average of the "Benign" (Table 7.3) and "Malignant" (Table 7.4) MRI samples, individually, and then calculating the average of these two averages (Table 7.5), which is known as the threshold value for classification.

Table 7.5: Calculation of the threshold values for classification

Sample	Tumour Area	Radial Mapping Area	Uniform Radial Mapping Area	Variance of Deviation Angles	Counter-clockwise to Clockwise Ratio
"Benign" Average	106.76	4.69	3.73	0.74	68.72%
"Malignant" Average	2,182.90	26.99	30.06	0.71	95.53%
Threshold	**1,144.83**	**15.84**	**16.895**	**0.725**	**82.13%**

The following classification rules can be concluded from the findings in Table 7.5:

- A tumour is "Malignant" if the total area covered by a tumour is >1,144.83 pix^2;
- A tumour is "Malignant" if the radial mapping area covered by a tumour is >15.84 rad.pix;
- A tumour is "Malignant" if the uniform radial mapping area covered by a tumour is >16.89 rad.pix;
- A tumour is "Malignant" if the variance of deviation angles is <0.725; and
- A tumour is "Malignant" if the counter-clockwise to clockwise ratio is >82.13%.

The individual features are used to separate the "Malignant" and "Benign" classes of 56 MRI samples with the help of the aforementioned criteria. Table 7.6 details the percentage of correct classifications.

Table 7.6: Percentage of the correct classification of MRI samples with different features

Feature Used	Correct Classification, %
Tumour Area	75.00%
Radial Mapping Area	84.61%
Uniform Radial Mapping Area	82.69%
Variance of Deviation Angles	44.23%
Counter-clockwise to Clockwise Ratio	88.46%

From Table 7.6, it is quite clear that the "radial mapping" area and the "uniform radial mapping" area are better features when compared with "Tumour area", as they provide more accurate classification. Classification accuracy can be further enhanced by combining the proposed feature-extraction methods with other features (tumour area, the variance of deviation angles, and the counter-clockwise to clockwise ratio).

7.4 CLASSIFICATION SYSTEM

Developing an approach that automates the detection of breast abnormalities is the need of the day. This not only helps radiologists to better understand the minute details of an irregularity, but it also aids in making rapid diagnoses. Speeding up the diagnostic process can enable radiologists to better serve larger patient populations within a specified time. The limitations of the diagnostic process traditionally followed by the radiologists can be properly addressed by introducing new computer-based algorithms. The existing methods have various limitations, such as non-optimal feature use, slow speeds, and poor accuracy rates. The use of multiple features helps us to retrieve the structural and functional features of the breast to detect the abnormal tissue patterns of breast cancer. ANN- and SVM-based classifiers have been designed, and they will be discussed in the next section.

7.4.1 ANN-based Classification

It is quite clear from the results (Table 7.5 and 7.6) of the simple threshold-based classification method that linear classifiers are not an optimal choice when analyzing our dataset, as it provides low accuracy. As such, an ANN-based classifier is implemented and used on this dataset instead.

Neural networks with 10 hidden layers nodes and 1,000 epochs (maximum) are used for this task. The hidden layers are fixed after multiple trails and cross validation to avoid over-fitting. A back-propagation mechanism is used for training proposes, while the mean squared error is used to calculate errors in the neural network's weight-updating process. Figure 7.13 shows the architecture of the designed ANN.

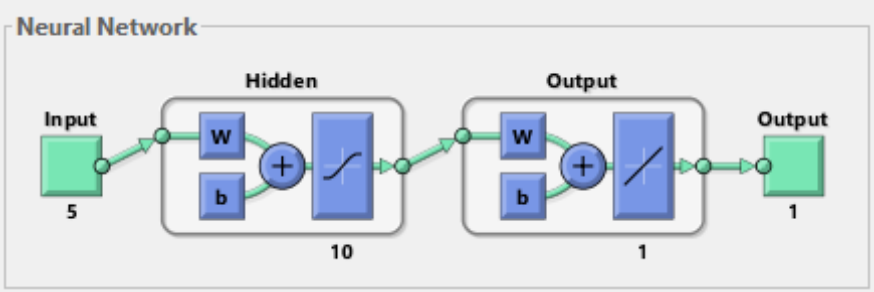

FIGURE 7.13: ANN ARCHITECTURE WITH A FIVE-FEATURE VECTOR

As already mentioned, five features are calculated in this work. Among them, three old features (Tumour Area, Variance of Deviation Angles, Counter-clockwise to Clockwise Ratio) and two new features (Radial Mapping Area, Uniform Radial Mapping Area) are there. The ANN is trained with three (old features) and five features (old + new features), one by one, to highlight the advantage of the new feature vectors over the old feature vectors. Figure 7.13 illustrates the different parameter settings of the ANN employed here.

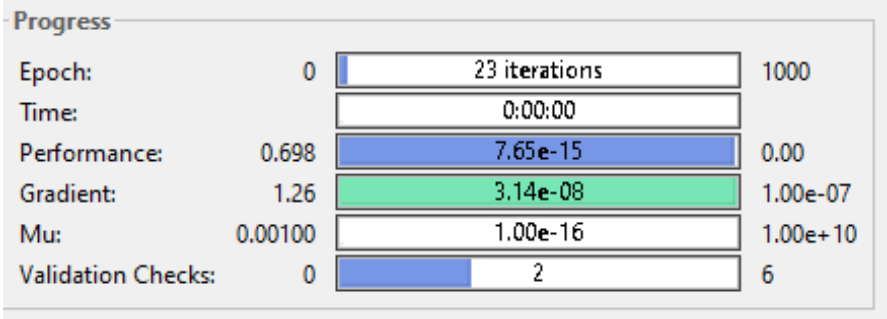

FIGURE 7.14: ANN PARAMETERS

Figure 7.15 shows the training, testing, and validation regression of the ANN when only three features are used. Figure 7.16 shows the training, testing, and validation regression of the ANN when only three features are used. The classification is enhanced when using a five-feature-based classification approach. To better examine the classification results, a five-fold cross-validation was also used in this study; the results are provided in the next section.

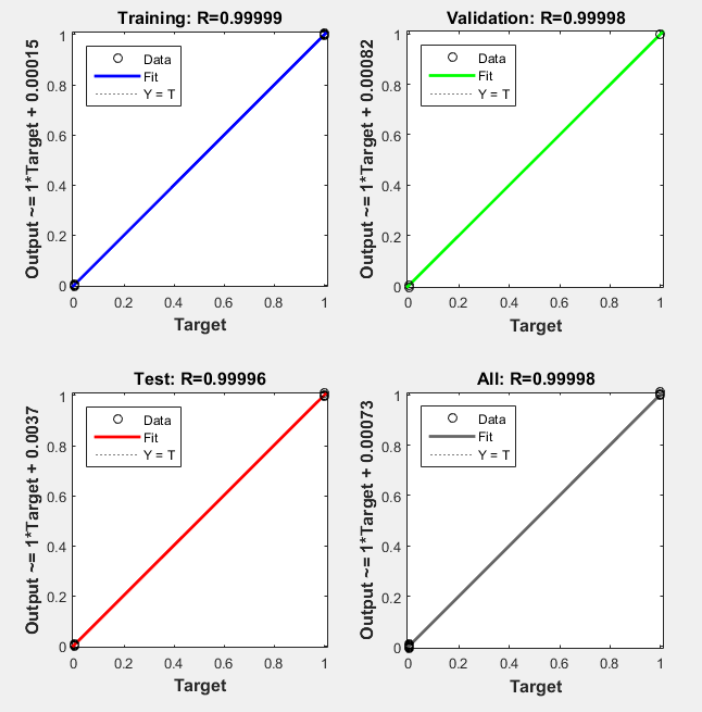

FIGURE 7.15: REGRESSION PLOT OF THE ANN CLASSIFIER WITH THREE INPUTTED FEATURE VECTORS

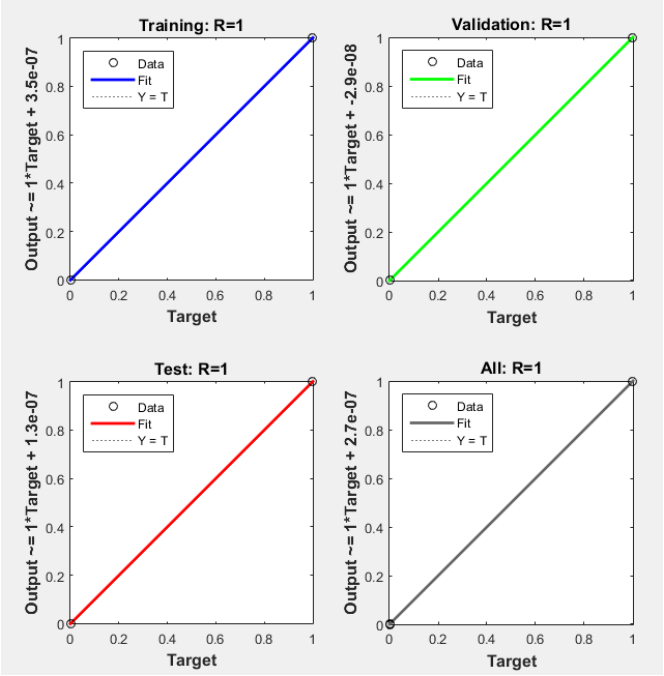

FIGURE 7.16: REGRESSION PLOT OF AN ANN CLASSIFIER WITH FIVE INPUTTED FEATURE VECTORS

7.4.2 K-fold Cross-validation

To avoid losing the generality of this approach, the performance of the ANN is tested on independent datasets generated using the training dataset itself. The results of the test are

shown in the tables. Although the results demonstrate a bit of variance with the different datasets, they are still within an acceptable range. It is quite evident from Tables 7.7 and 7.8 that the five-feature-based classification approach performs better than the three-feature-based classification method when employed on the same dataset.

Table 7.7: The degree of accuracy of each run and the average accuracy (three features)

Run	Accuracy
1	95.98
2	96.30
3	96.27
Average	**96.18**

Table 7.8: The degree of accuracy of each run and the average accuracy (five features)

Run	Accuracy
1	97.87
2	96.69
3	97.70
Average	**97.42**

7.4.3 False positive (FP), False Negative (FN)

The classifier is also tested against the false-positive and -negative results. A false positive is when a positive detection is made, even though there is no cancer; in other words, this is when “a malignant tumour” is detected, even though it is actually “a benign tumour”.

A false negative is the opposite of a false positive; this is when a negative class is detected, even though cancer is actually present. Table 7.9 shows the false-positive rate and the false-negative rate with multiple runs.

Table 7.9: The false-positive and false-negative rates

Run	False-positive Rate	False-negative Rate
1	0.06	0.04
2	0.05	0.05
3	0.06	0.05
Average	**0.056**	**0.046**

Mathematically, these parameters can be defined as:

$$FP = \frac{wrong\ positive\ results}{total\ positive\ results} \quad (7.8)$$

$$FN = \frac{wrong\ negative\ results}{total\ negative\ results} \quad (7.9)$$

$$TP = \frac{correct\ possitive\ results}{total\ positive\ results} \quad (7.10)$$

$$TN = \frac{correct\ negative\ results}{total\ negative\ results} \quad (7.11)$$

7.4.4 Sensitivity and Specificity

Sensitivity and specificity are two other parameters that show the robust and error-free nature of any system. These two parameters are defined as follows:

Sensitivity refers to the test's ability to correctly detect patients who do have the condition under consideration. In our case, a classification test is used to identify the cancer type, while the sensitivity of the test is the proportion of people who test positive for the disease among those who have it. Mathematically, sensitivity is expressed as:

$$Sensitivity = \frac{TP}{TP+FN} \quad (7.12)$$

Specificity refers to the test's ability to correctly detect patients without a condition. The specificity of a test is the proportion of healthy patients who are known as not having the disease, and who will actually test negative for it. Mathematically, specificity is expressed as:

$$Specificity = \frac{TN}{TN+FP} \quad (7.13)$$

The performance of the proposed system is also tested against these parameters, and the same is shown in Table 7.10.

Table 7.10: The sensitivity and specificity of the ANN classifier

Run	Sensitivity	Specificity
1	97.0260	97.1888
2	96.2356	97.4582
3	97.5564	96.2545
Average	**96.9393**	**96.9671**

7.5 CLASSIFICATION WITH SVM

To assess the possibility of improving classification, SVM was also tested on the dataset. K-fold cross-validation was also applied on the SVM classifier. Different kernels were used during the classification stage to check the accuracy, FP, FN, sensitivity, and specificity to select the best kernel. Table 7.11 shows the accuracy of five-feature SVM classifiers using a multi-layer perceptron (mlp) kernel. Table 7.12 shows the FP and FN rates of the SVM classifier (mlp kernel). Table 7.13 shows the sensitivity and specificity of the SVM classifier (mlp kernel).

Table 7.11: The accuracy of the SVM classifier (mlp kernel) with each run and the average accuracy

Run	Accuracy
1	86.73
2	86.53
3	89.61
Average	**87.62**

Table 7.12: The false-positive and false-negative rate of the SVM classifier (mlp kernel)

Run	FP	FN
1	0.52	0.86
2	0.54	0.86
3	0.36	0.72
Average	**0.47**	**0.81**

Table 7.13: The sensitivity and specificity of the SVM classifier (mlp kernel)

Run	Sensitivity	Specificity
1	84.07	89.60
2	84.07	89.20
3	86.66	92.80
Average	**84.93**	**90.53**

Table 7.14 shows the accuracies of the five-feature SVM classifier using the radial basis function (rbf) kernel. Table 7.15 shows the FP and FN rate of the SVM classifier (rbf kernel). Table 7.16 shows the sensitivity and specificity of the SVM classifier (rbf kernel).

Table 7.14: The accuracy of the SVM classifier (rbf kernel) with each run and the average accuracy

Run	Accuracy
1	96.15
2	96.73
3	96.53
Average	**96.47**

Table 7.15: The false-positive and false-negative rate of the SVM classifier (rbf kernel)

Run	FP	FN
1	0.38	0.02
2	0.34	0
3	0.36	0
Average	**0.36**	**0.006**

Table 7.16: the sensitivity and specificity of the SVM classifier (rbf kernel)

Run	Sensitivity	Specificity
1	99.62	92.40

2	100	93.20
3	100	92.80
Average	**99.87**	**92.80**

Table 7.17 shows the accuracies of the five-feature SVM classifier using the linear kernel. Table 7.18 shows the FP and FN rate of the SVM classifier (linear kernel). Table 7.19 shows the sensitivity and specificity of the SVM classifier (linear kernel).

Table 7.17: The accuracy of the SVM classifier (linear) with each run and the average accuracy

Run	Accuracy
1	98.65
2	98.65
3	98.26
Average	**98.52**

Table 7.18: The false-positive and false-negative rate of the SVM classifier (linear)

Run	FP	FN
1	0	0.14
2	0	0.14
3	0	0.18
Average	**0**	**0.15**

Table 7.19: The sensitivity and specificity of the SVM classifier (linear)

Run	Sensitivity	Specificity
1	97.40	100
2	97.40	100
3	96.66	100
Average	**97.15**	**100**

Table 7.20 shows the accuracy rates of the five-feature SVM classifier using the quadratic kernel. Table 7.21 shows the FP and FN rates of the SVM classifier (quadratic kernel). Table 7.22 shows the sensitivity and specificity of the SVM classifier (quadratic kernel).

Table 7.20: The accuracy of the SVM classifier (quadratic kernel) with each run and the average accuracy

Run	Accuracy
1	96.53
2	95.96
3	96.73
Average	**96.40**

Table 7.21: The false-positive and false-negative rates of the SVM classifier (quadratic kernel)

Run	FP	FN
1	0.20	0.16
2	0.20	0.22
3	0.20	0.14
Average	**0.2**	**0.17**

Table 7.22: Showing the sensitivity and specificity of the SVM classifier (quadratic kernel)

Run	Sensitivity	Specificity
1	97.03	96.00
2	95.92	96.00
3	97.40	96.00
Average	**96.78**	**96.00**

Table 7.23 shows the accuracies of the five-feature SVM classifier using the polynomial order-3 (P-3) kernel. Table 7.24 shows the FP and FN rate of the SVM classifier (P-3 kernel). Table 7.25 shows the sensitivity and specificity of the SVM classifier (P-3 kernel).

Table 7.23: The accuracy of the SVM classifier (P-3 kernel) with each run and the average accuracy

Run	Accuracy
1	95.96
2	95.76
3	96.73
Average	**96.15**

Table 7.24: The false-positive and false-negative rate of the SVM classifier (P-3 kernel)

Run	FP	FN
1	0.28	0.14
2	0.30	0.14
3	0.20	0.14
Average	**0.26**	**0.14**

Table 7.25: The sensitivity and specificity of the SVM classifier (P-3 kernel)

Run	Sensitivity	Specificity
1	97.40	94.40
2	97.40	94.00
3	97.40	96.00
Average	**97.40**	**94.80**

From the above tables, it is quite evident that linear kernel-based SVM provides the highest degree of accuracy, sensitivity, and specificity when compared to other kernels, as well as when compared with the neural network-based classifier. This implies that SVM (as a classifier) in MRI breast cancer using the feature extraction in this study is a preferable choice for this automated system.

7.6 AUTOMATED SYSTEM

A complete automated cancer classification system was developed in the current study. Figure 7.17 shows a snapshot of the developed system. The MR images are inserted into this system, which classifies the image using features as either “malignant” or “benign”.

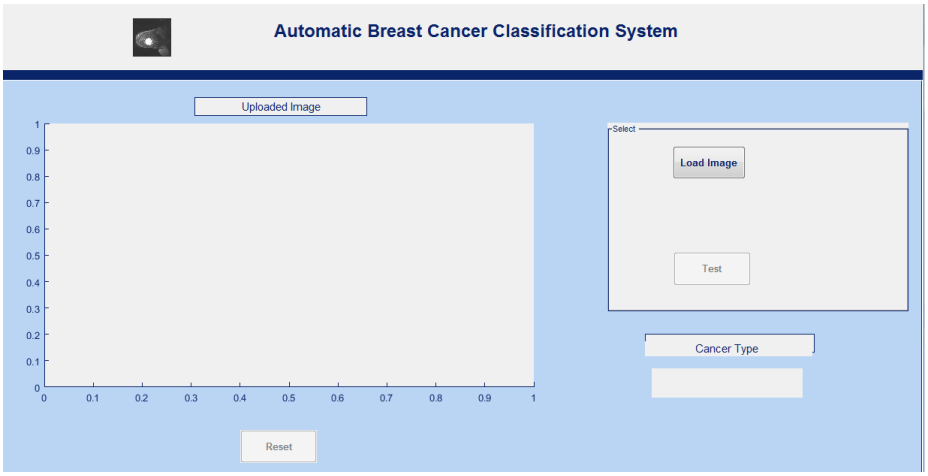

FIGURE 7.17: A FULLY AUTOMATIC CLASSIFIER FOR BREAST CANCER

Figures 7.18 and 7.19 show the operation of an automatic classifier; both images illustrate the detection of two different tumour types.

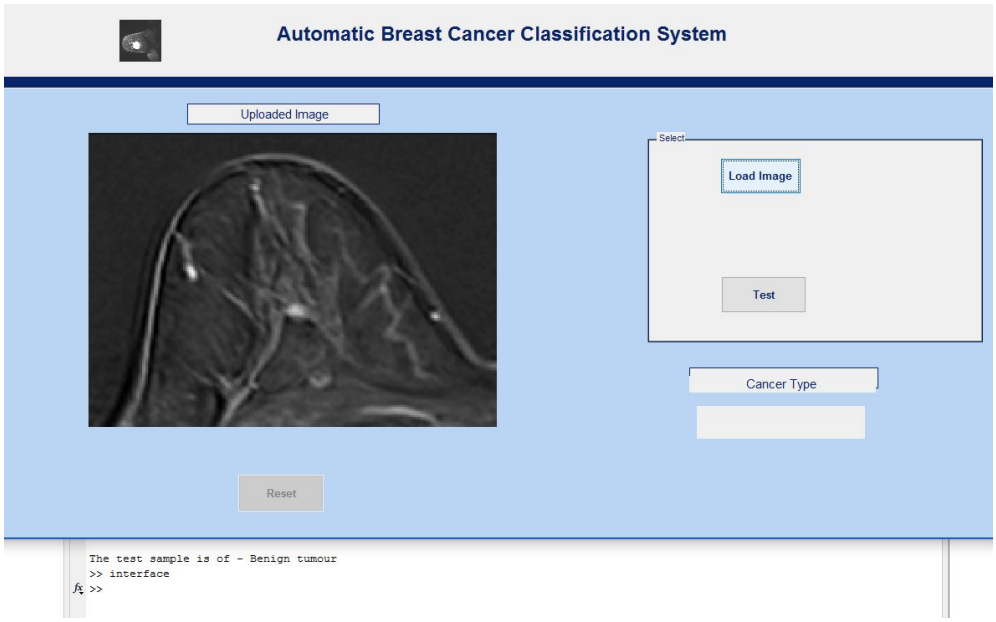

FIGURE 7.18: BENIGN CANCER DETECTION USING THE BREAST CANCER CLASSIFICATION SYSTEM

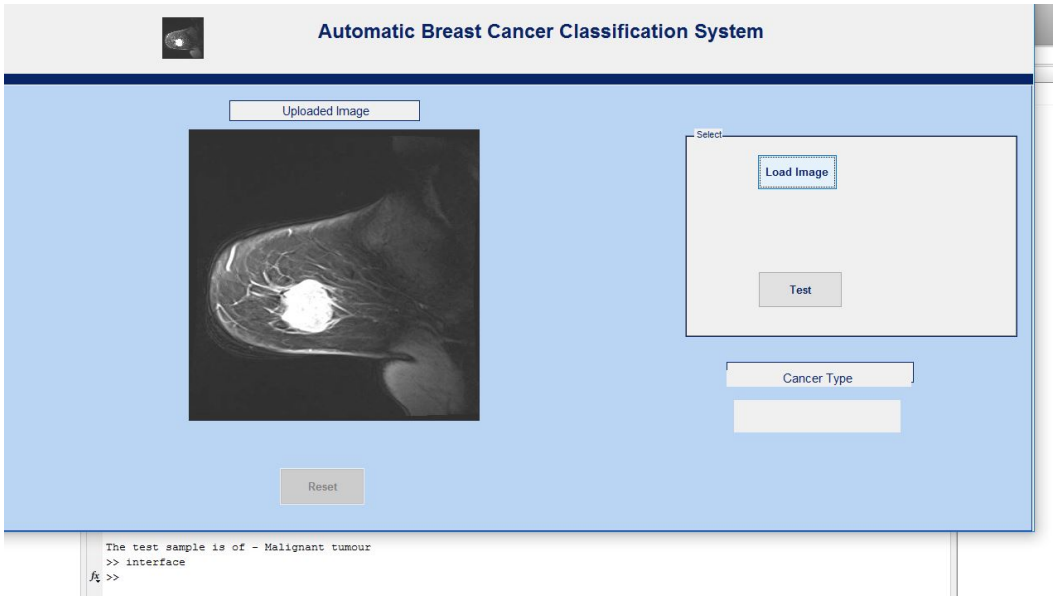

FIGURE 7.19: MALIGNANT CANCER DETECTION USING THE BREAST CANCER CLASSIFICATION SYSTEM

7.7 SUMMARY

This chapter proposed two novel and efficient feature-extraction methods, which are further used with threshold-based classification, to identify malignant and benign cancer cells. Image-processing methods were applied to identify the tumour area in the MRI samples. The proposed feature-extraction methods were also compared with the earlier proposed feature-extraction methods (total area of a tumour, angular smoothness of the corners, and counter-clockwise to clockwise rotation ratio) for classification accuracy. The use of the proposed feature vectors in the classification system enabled it to outperform a classifier that is only used in earlier feature vectors. In addition, the proposed features will also be applied to different classifiers in order to obtain better results.

CHAPTER 8

CONCLUSIONS AND FUTURE DIRECTIONS

8.1 Introduction

This concluding chapter of the thesis provides a summary of the research, discusses the research contribution to knowledge and provides directions for future research in this realm of study.

8.2 Research Summary

The research work described in this thesis employs numerous image-processing techniques to analyze suspicious tissue patterns for the early detection of breast cancer. With the critical review of the research filed, it become clear that none of the study on the breast had produced optimal performance in all cases. Moreover, it was also found out from the review that there has been a pressing need to improve the accuracy and sensitivity rate of these approaches for the early detection of breast cancer.

Although much attention has been directed toward ensuring technical quality assurance, which will guarantee optimal image quality across most breast screening methods (including for mammograms, ultrasound, and MRI), the quality of interpretation seems to be the weakest link in the diagnostic process. Thus, there was a need to develop tools or algorithms that assist experts in quick and accurate decision making. In order to increase detection and diagnostic accuracy, as well as to reduce the amount of labour required, computer-aided methodologies (algorithms) have been developed. These computer-aided algorithms are able to make certain diagnoses in a more quantitative. Such methodologies or algorithms are also developed to assist medical professionals in the timely evaluation of medical images, while also helping them to detect abnormalities in the breast at earlier stages. In general, these methodologies employ computers to assist doctors to interpret medical images. In particular, these methodologies, which automatically detect or classify abnormalities in the breast, can be very useful for breast cancer control, and they can provide doctors with a second perspective that is both highly consistent and repeatable.

The techniques proposed herein not only improve image quality, but they also help to increase the image contrast; further, they automatically determine tumour location, greatly reduce the human workload associated with making diagnoses, and improve the accuracy of detection and diagnosis. Application of computer-aided algorithms during the pre-processing stage helps to separate suspicious regions (which may contain abnormalities) from the background region. In other words, such pre-processing methodologies partition the images acquired from the MRI scan into several non-intersecting regions, while extracting ROIs and suspicious tissue candidates from these images. Generally, a computer-based breast cancer detection system uses some image-processing methods, like image segmentation, classification, and so forth, to detect breast cancer in its early stages. This research was focused on the development of a method that can detect and classify breast tumours using an ANN and SVM based classifier. The performance of this classifier was also checked via a cross-validation test. The false-positive and false-negative rates were also determined, and they were found to be very low.

8.3 Research contribution

This research work made a significant contribution in the field of automated breast cancer detection system development. Present work developed a system that can segment and classify the tumours in breast cancer automatically. The developed system can made a correct diagnosis for the type of the breast tumours. The introductory chapter of the report provided a list of objectives to meet in order to achieve the research aim. Based on these objectives, the following aims were accomplish in this research:

- It provided the novel feature extraction method.
- It combined many feature extraction to classify the type of the tumour.
- It provided an automatic segmentation and classification system.
- It also provided a high accuracy classification system.
- It gave relatively low number of false-positive and false-negative rate during classification.

As stated in chapter 1, there was a limitation of using MRI in breast cancer image processing research. The use of MRI in this study can positively improve the field of medical image research. In other words, by exploring complex and automated stages to segment and classify the tumour (using multi feature extraction), a better automated model can be developed. As far as present study is concerned, breast cancer automatic segmentation was successfully

provided the suspicious area with 97% accuracy. The developed model is tested against the 55 images that were pre-marked (classified) by the experts of the field.

Moreover, in terms of the exploration for classifier and feature extraction, this research did not just apply simple feature extraction as often seen in research within this area of study. It developed a new feature extraction method to classify the tumours more accurately. The radial mapping and uniform radial mapping feature was clearly improved the classfication accuracy of the system.

These feature extraction methods were combined with ANN and SVM methods to provide accurate and error free classifications.

8.4 FUTURE AVENUES

Although this study has made numerous positive contributions, it is important to acknowledge the study's limitations. Since early detection is the only approach that can be used to successfully manage or treat breast cancer, which is a highly life-threatening condition, much effort must be made to improve the accuracy with which various systems identify sites of structural distortion, while also quantitatively assessing the cancer detection rate. Improved methods are needed to ensure the early detection of breast cancer. In fact, increased sensitivity is required to reduce the mortality rate associated with this disease, while also improving the prognosis of breast cancer patients.

To improve the accuracy with which lesions are detected at the breast boundary region, novel segmentation approaches are required. One possible solution may be to impose shape restrictions on the growing mass. Further, one can also improve the performance and accuracy of the results by applying this approach to high-quality digital mammogram images.

It is important to note that the MRI-based breast cancer detection methods proposed herein were tested on a small set of clinical MRI images, as there is a lack of standard MRI datasets. Future work should validate the results reported here in larger datasets.

The current state of the art says that most of the work that has been carried out on the detection of breast cancer include a single modality concept. However, as was discussed in previous chapters, the features retrieved from one modality are not sufficient for classifying and detecting the abnormalities associated with early-stage breast cancer. Future research

should be carried out to design and test image-processing algorithms that extract features from other modalities (like mammograms, ultrasound images, CT, PET, and so on), while also combining these features at different levels to improve detection rates and accuracy.

REFERENCES

Abinaya, K. S. & Pandiselvi, T. (2014) Brain tissue segmentation from magnetic resonance image using particle swarm optimization algorithm. *International Journal of Computer Science and Mobile Computing*. 172 (3), 404–408.

Aharon, M., Elad, M. & Bruckstein, A. M. (2006) K-SVD: An algorithm for designing over complete dictionaries for sparse representation. *IEEE Transactions on Signal Processing*. 54, 4311–4322.

Aharon, M., Elad, M. & Bruckstein, A.M. (2006) K-SVD: An algorithm for designing over complete dictionaries for sparse representation. *IEEE Transactions on Signal Processing*. 54, 4311–4322.

Aldroubi, A., & Unser, M. (eds.). (1996) *Wavelets in medicine and biology*. Boca Raton, Florida: CRC Press.

Alshanbari, H., Amin, S., Shuttleworth, J., Slman, K. and Muslam, S. (2015). Automatic segmentation in breast cancer using watershed algorithm. International Journal of Biomedical Engineering and Science, 2(2).

Alsmadi, M.K., 2014. A hybrid firefly algorithm with fuzzy-c mean algorithm for mri brain segmentation. Am J Appl Sci, 11(9), pp.1676-1691.

Anand, C. S. & Sahambi, J. S. (2008) MRI de-noising using bilateral filter in redundant wavelet domain. *IEEE International Conference on TENCON*. 1–6.

Anitha, M., Selvy, P. T. & Palanisamy, V. (2012) Automated detection of white matter lesions in MRI brain images using spatio-fuzzy and spatio-possibilistic clustering models. *International Journal on Computer Science and Engineering*. 2(2), 1–11.

Ashburner, J., & Friston, K. J. (2000) Voxel-based morphometry—the methods. *Neuroimage*. 11(6), 805–821.

Bagg, H.J., 1936. Further studies on the relation of functional activity to mammary carcinoma in mice. The American Journal of Cancer, 27(3), pp.542-550.

Barker, A. D., Sigman, C. C., Kelloff, G. J., Hylton, N. M., Berry, D. A. & Esserman, L. J. (2009) I-SPY 2: An adaptive breast cancer trial design in the setting of neoadjuvant chemotherapy. *Clinical Pharmacology & Therapeutics*. 86(1), 97–100.

Beale, R. & Pryke, A. (2006) Knowledge through evolution. *Advances in Applied Artificial Intelligence*. 234.

Benson, J. R., Jatoi, I., Keisch, M., Esteva, F. J., Makris, A. & Jordan, V. C. (2009) Early breast cancer. *The Lancet*. 373(9673), 1463–1479.

Bhardwaj, A. & Tiwari, A. (2015) Breast cancer diagnosis using genetically optimized neural network model. *Expert Systems with Applications*. 42(10), 4611–4620.

Bhonsle, D., Chandra, V. & Sinha, G. R. (2012) Medical image de-noising using bilateral filter. *International Journal of Image, Graphics and Signal Processing*. 4(6), 36.

Billing, A., Buchner, A., Stief, C. & Roosen, A. (2015) Preoperative mp-MRI of the prostate provides little information about staging of prostate carcinoma in daily clinical practice. *World Journal of Urology*. 33(7), 923–928.

Bittner, J.J., 1941. The milk influence in tumor formation. Biology of the Laboratory Mouse, ed. G. Snell, p.321.

Boccignone, G., Chianese, A. & Picariello, A. (2000) Computer aided detection of microcalcifications in digital mammograms. *Computers in Biology and Medicine*. 30(5), 267–286.

Boyd, N. F., Guo, H., Martin, L. J., Sun, L., Stone, J., Fishell, E., ... & Yaffe, M. J. (2007) Mammographic density and the risk and detection of breast cancer. *New England Journal of Medicine*. 356(3), 227–236.

Boyle, P. (1997). Global burden of cancer. The Lancet, SII23.

Buades, A., Coll, B. & Morel, J. M. (2005) A non-local algorithm for image de-noising . *IEEE International Conference on Computer Vision and Pattern Recognition*. 2, 60–65.

Burbank, F., Parker, S. H., & Fogarty, T. J. (1996) Stereotactic breast biopsy: improved tissue harvesting with the Mammotome. *The American Surgeon*. 62(9), 738–744.

Burges, C. J. (1998) A tutorial on support vector machines for pattern recognition. *Data Mining and Knowledge Discovery*. 2(2), 121–167.

Cabeen, R. P. & Laidlaw, D. H. (2014) Bilateral filtering of multiple fiber orientations in diffusion MRI. *Computational Diffusion MRI, Mathematics and Visualization*. 193–202.

Campanini, R., Dongiovanni, D., Iampieri, E., Lanconelli, N., Masotti, M., Palermo, G., ... & Roffilli, M. (2004) A novel featureless approach to mass detection in digital mammograms based on support vector machines. *Physics in Medicine and Biology*. 49(6), 961.

Cascio, D., Magro, R., Fauci, F., Iacomi, M. & Raso, G. (2012) Automatic detection of lung nodules in CT datasets based on stable 3D mass–spring models. *Computers in Biology and Medicine*. 42(11), 1098–1109.

Cavalieri, E. and Rogan, E., 2014. The molecular etiology and prevention of estrogen-initiated cancers: Ockham's Razor: Pluralitas non est ponenda sine necessitate. Plurality

should not be posited without necessity. Molecular aspects of medicine, 36, pp.1-55.

Chen, P. F. (2009) *Image segmentation/registration: A variational framework for 2-D and 3-D applications*. pages.128.

Choe, R., Corlu, A., Lee, K., Durduran, T., Konecky, S.D., Grosicka□Koptyra, M., Arridge, S.R., Czerniecki, B.J., Fraker, D.L., DeMichele, A. and Chance, B., 2005. Diffuse optical tomography of breast cancer during neoadjuvant chemotherapy: a case study with comparison to MRI. Medical physics, 32(4), pp.1128-1139.

Chughtai, M.S., 1964. THERMOMETRY AND THERMOGRAPHY IN BREAST TUMORS (Doctoral dissertation, Department of Experimental Surgecy, MCGill University, Montreal, Canada).

Cortes, C. & Vapnik, V. (1995) Support-vector networks. *Machine Learning*. 20(3), 273–297.

Coupé, P., Yger, P., Prima, S., Hellier, P., Kervrann, C. & Barillot, C. (2008) An optimized blockwise non local means de-noising filter for 3D magnetic resonance images. *Transactions on Medical Imaging*. 27(4), 425–441.

Dale, B. M., Brown, M. A. & Semelka, R. C. (2015) *MRI: Basic principles and applications*. Hoboken, New Jersey: John Wiley & Sons.

de Paredes, E. S. (1994) Evaluation of abnormal screening mammograms. *Cancer*. 74(S1), 342–349.

Deepika, G. L. (2014) Brain tumor segmentation of noisy MRI images using anisotropic diffusion filter. *International Journal of Computer Science and Mobile Computing*. 3(7), 744–750.

Denison, C. M. & Lester, S. C. (2016) Essential components of a successful breast core needle biopsy program: Imaging modalities, sampling techniques, specimen processing, radiologic/pathologic correlation, and appropriate follow-up. In: *A comprehensive guide to core needle biopsies of the breast*. Switzerland: Springer International Publishing. pp. 3–47.

Devi, C. J., Reddy, B. S. P., Kumar, K. V., Reddy, B. M. & Nayak, N. R. (2012) ANN approach for weather prediction using back propagation. *International Journal of Engineering Trends and Technology*. 3(1), 19–23.

Dhawan, A. P., Chitre, Y. & Kaiser-Bonasso, C. (1996) Analysis of mammographic microcalcifications using gray-level image structure features. *IEEE Transactions on Medical Imaging*. 15(3), 246–259.

Dheeba, J., Singh, N. A. & Selvi, S. T. (2014) Computer-aided detection of breast cancer on mammograms: A swarm intelligence optimized wavelet neural network approach.

Journal of Biomedical Informatics. 49, 45–52.

Digabel, H. and Lantuéjoul, C., 1978, October. Iterative algorithms. In Proc. 2nd European Symp. Quantitative Analysis of Microstructures in Material Science, Biology and Medicine (Vol. 19, No. 7, p. 8). Stuttgart, West Germany: Riederer Verlag.

Dominguez, A. R. & Nandi, A. K. (2008). Detection of masses in mammograms via statistically based enhancement, multilevel-thresholding segmentation, and region selection. *Computerized Medical Imaging and Graphics*. 32(4), 304–315.

Ebrahimzadeh, R. & Jampour, M. (2013) Chaotic genetic algorithm based on lorenz chaotic system for optimization problems. *International Journal of Intelligent Systems and Applications*. 5(5), 19.

Einstein, A. J., Henzlova, M. J. & Rajagopalan, S. (2007) Estimating risk of cancer associated with radiation exposure from 64-slice computed tomography coronary angiography. *JAMA*. 298(3), 317–323.

El-Naqa, I., Yang, Y., Wernick, M. N., Galatsanos, N. P. & Nishikawa, R. M. (2002). A support vector machine approach for detection of microcalcifications. *IEEE Transactions on Medical Imaging*. 21(12), 1552–1563.

Eyal, E., Badikhi, D., Furman-Haran, E., Kelcz, F., Kirshenbaum, K. J. & Degani, H. (2009) Principal component analysis of breast DCE-MRI adjusted with a model-based method. *Journal of Magnetic Resonance Imaging*. 30(5), 989–998.

Ferlay, J., Héry, C., Autier, P. & Sankaranarayanan, R. (2010) Global burden of breast cancer. In: *Breast cancer epidemiology*. New York: Springer. pp. 1–19.

Fisher, R. A. (1936) The use of multiple measurements in taxonomic problems. *Annals of Eugenics*. 7(2), 179–188.

Fraser, K. C., Meltzer, J. A., Graham, N. L., Leonard, C., Hirst, G., Black, S. E. & Rochon, E. (2014) Automated classification of primary progressive aphasia subtypes from narrative speech transcripts. *Cortex*. 55, 43–60.

Gallea, R., Ardizzone, E. & Pirone, R. (2008) Noise filtering using edge-driven adaptive anisotropic diffusion. *IEEE Symposium on Computer Based Medical Systems*. 29–34.

Gallinari, P., Thiria, S. & Soulie, F. F. (1988) Multilayer perceptrons and data analysis. In: *Neural networks*. Utah: Snowbird.

Gallinari, P., Thiria, S., Badran, F. & Fogelman-Soulie, F. (1991) On the relations between discriminant analysis and multilayer perceptrons. *Neural Networks*. 4(3), 349–360.

Garg, S. & Kaur, J. (2013) Improving segmentation by de-noising brain MRI images

through interpolation median filter in ADTVFCM. *International Journal of Computer Trends and Technology*. 4(2), 187–188.

Garnica, C., Boochs, F. and Twardochlib, M., 2000. A new approach to edge-preserving smoothing for edge extraction and image segmentation. International Archives of Photogrammetry and Remote Sensing, 33(B3/1; PART 3), pp.320-325.

Geng, Y., Chen, J., Fu, R., Bao, G. and Pahlavan, K., 2016. Enlighten wearable physiological monitoring systems: On-body rf characteristics based human motion classification using a support vector machine. IEEE transactions on mobile computing, 15(3), pp.656-671.

Gerig, G., Kubler, O., Kikinis, R. & Ferenc, A. (1992) Nonlinear anisotropic filtering of MRI data. *IEEE Transactions on Medical Imaging*. 11, 221–232.

Ghassabeh, Y. A., Forghani, N. & Forouzanfar, M. (2007) MRI fuzzy segmentation of brain tissue using IFCM algorithm with genetic algorithm optimization. *International Conference on Computer Systems and Applications*. 665–668.

Goldhirsch, A., Glick, J. H., Gelber, R. D., Coates, A. S., Thürlimann, B. & Senn, H. J. (2005) Meeting highlights: International expert consensus on the primary therapy of early breast cancer 2005. *Annals of Oncology*. 16(10), 1569–1583.

Gopinath, N. (2011) Graph based image segmentation method for identification of cancer in prostate MRI image. *Journal of Computer Applications*. 4(4), 104–108.

Graber, M., Gordon, R. & Franklin, N. (2002) Reducing diagnostic errors in medicine: What's the goal? *Academic Medicine*. 77(10), 981–992.

Greenberg, S. & Kogan, D. (2006) Improved structure-adaptive anisotropic filter. *Pattern Recognition Letters*. 27(1), 59–65.

Guleryuz, O. G. (2007) Weighted averaging for de-noising with overcomplete dictionaries. *IEEE Transactions on Image Processing*. 16(12), 3020–3034.

Guleryuz, O. G. (2007) Weighted averaging for de-noising with over complete dictionaries. *IEEE Transactions on Image Processing*. 16, 3020–3034.

Gunn, S. R. (1998) Support vector machines for classification and regression. *ISIS Technical Report*. 14, 85–86.

Gunn, Steve R. "Support vector machines for classification and regression." ISIS technical report 14 (1998): 85-86.

Hadfield, G., 1958. The Application of Physiological Principles to Hormone-Dependent Breast Cancer:* Imperial Cancer Research Fund Lecture delivered at the Royal College of Surgeons of England on 14th May 1957. Annals of the Royal College of Surgeons

of England, 22(2), p.73.

Hadjiiski, L., Sahiner, B., Chan, H. P., Petrick, N., & Helvie, M. (1999) Classification of malignant and benign masses based on hybrid ART2LDA approach. *IEEE Transactions on Medical Imaging*. 18(12), 1178–1187.

Handley, W.S., 1931. Genesis of Cancer. Kegan Paul; London.

Haque, M. E. & Sudhakar, K. V. (2002) ANN back-propagation prediction model for fracture toughness in microalloy steel. *International Journal of Fatigue*. 24(9), 1003–1010.

Harris A., L., A Grant, J.R., 2005. A Father's Journey, a Daughter's Voyage, a Cancer Journal: Father I Daughter We, 9780595343485, iUniverse, https://books.google.co.in/books?id=9DJbr9kGgFUC

Harris, J. R., Lippman, M. E., Veronesi, U. & Willett, W. (1992) Breast cancer. *New England Journal of Medicine*. 327(6), 390–398.

Hasebroock, K. M. & Serkova, N. J. (2009) Toxicity of MRI and CT contrast agents. *Expert Opinion on Drug Metabolism & Toxicology*. 5(4), 403–416.

Health Quality Ontario. (2007). Screening Mammography for Women Aged 40 to 49 Years at Average Risk for Breast Cancer: An Evidence-Based Analysis. Ontario Health Technology Assessment Series, 7(1), 1–32.

Heywang, S. H., Lipsit, E. R., Glassman, L. M. & Thomas, M. A. (1984). Specificity of ultrasonography in the diagnosis of benign breast masses. *Journal of Ultrasound in Medicine*. 3(10), 453–461.

http://www.kamc.med.sa/index.php/en/

Hu, C., Wang, J., Zheng, C., Xu, S., Zhang, H., Liang, Y., Bi, L., Fan, Z., Han, B. & Xu, W. (2013) Raman spectra exploring breast tissues: Comparison of principal component analysis and support vector machine-recursive feature elimination. *Medical Physics*. 40(6).

Hu, J., Pu, Y., Wu, X., Zhang, Y. & Zhou J. (2012) Improved DCT-based nonlocal means filter for MR images de-noising. *Computational and Mathematical Methods in Medicine*. 14.

Hwuang, E., Danish, S., Rusu, M., Sparks, R., Toth, R. & Madabhushi, A. (2013) Anisotropic smoothing regularization (AnSR) in Thirion's Demons registration evaluates brain MRI tissue changes post-laser ablation. *Engineering in Medicine and Biology Society*. 4006–4009.

Islam, M. M., Sattar, M. A., Amin, M. F., Yao, X. & Murase, K. (2009) A new adaptive merging and growing algorithm for designing artificial neural networks. *IEEE Transactions on Systems, Man, and Cybernetics, Part B (Cybernetics)*. 39(3), 705–722.

Jain, A. K. & Mao, J. (1992) Artificial neural network for nonlinear projection of multivariate data. *Neural Networks*. 3, 335–340.

Janghel, R. R., Shukla, A., Tiwari, R. & Kala, R. (2010) Breast cancer diagnosis using artificial neural network models. In: *Information sciences and interaction sciences (ICIS)*, 2010 3rd International Conference, Chicago, IL. pp. 89–94.

Jemal, A., Siegel, R., Ward, E., Hao, Y., Xu, J., Murray, T. and Thun, M.J., 2008. Cancer statistics, 2008. CA: a cancer journal for clinicians, 58(2), pp.71-96.

Jemal, A., Siegel, R., Ward, E., Murray, T., Xu, J. and Thun, M.J., 2007. Cancer statistics, 2007. CA: a cancer journal for clinicians, 57(1), pp.43-66.

Jones, D. K., Symms, M. R., Cercignani, M. & Howard, R. J. (2005) The effect of filter size on VBM analyses of DT-MRI data. *Neuroimage*. 26(2), 546–554.

Jordanov, M., Bregman, J., Montgomery, K. & Heidel, M. (2015) Curbside radiology consults: How does the time allotted for review, level of training, and subspecialization affect interpretation accuracy? *Clinical Imaging*. 39(3), 497–503.

Jozwik, K.M. and Carroll, J.S., 2012. Pioneer factors in hormone-dependent cancers. Nature Reviews Cancer, 12(6), pp.381-386.

Kalavathi, P. & Sowdeeswari, P. (2016) Edge enhanced anisodiffusion filter for de-noising Gaussian noise in medical images. *International Journal of Control Theory and Applications*. 9(27), 203–210.

Kaur, M. K. & Mittal, R. (2014) An efficient scheme for brain tumor detection of MRI brain images using Euclidean distance. *Journal of Emerging Technologies in Web Intelligence*. 6(4), 429–434.

Kavitha, D., Karthikeyan, T. and Swaminathan, L.A., 2013. A New Algorithm of Automatic white Matter Segmentation Based on MRI Brain Images. International Journal of Advanced Information Science and Technology (IJAIST) ISSN: 2319:2682Vol.10, No.10, February 2013 pp. 64-72

Kinoshita, S. K., de Azevedo-Marques, P. M., Pereira Jr, R. R., Rodrigues, J. A. H. & Rangayyan, R. M. (2007) Content-based retrieval of mammograms using visual features related to breast density patterns. *Journal of Digital Imaging*. 20(2), 172–190.

Kohonen, T. (1998). The self-organizing map. Neurocomputing, 21(1), 1-6.

Kolb, T. M., Lichy, J. & Newhouse, J. H. (2002) Comparison of the performance of screening mammography, physical examination, and breast us and evaluation of factors that influence them: An analysis of 27,825 patient evaluations 1. *Radiology*. 225(1), 165–175.

Kopans, D. B. (2007) *Breast imaging*. Philadelphia, Pennsylvania: Lippincott

Williams & Wilkins.

Kriege, M., Brekelmans, C. T., Boetes, C., Besnard, P. E., Zonderland, H. M., Obdeijn, I. M., ... & Muller, S. H. (2004) Efficacy of MRI and mammography for breast-cancer screening in women with a familial or genetic predisposition. *New England Journal of Medicine*. 351(5), 427–437.

Lam, S. W., Jimenez, C. R., & Boven, E. (2014) Breast cancer classification by proteomic technologies: Current state of knowledge. *Cancer Treatment Reviews*. 40(1), 129–138.

Lawrence, M.S., Stojanov, P., Mermel, C.H., Garraway, L.A., Golub, T.R., Meyerson, M., Gabriel, S.B., Lander, E.S. and Getz, G., 2014. Discovery and saturation analysis of cancer genes across 21 tumor types. Nature, 505(7484), p.495.

Lee, E.K., Han, G.Y., Park, H.W., Song, Y.J. and Kim, C.W., 2010. Transgelin promotes migration and invasion of cancer stem cells. Journal of proteome research, 9(10), pp.5108-5117.

Liberman, L. & Menell, J. H. (2002) Breast imaging reporting and data system (BI-RADS). *Radiologic Clinics of North America*. 40(3), 409–430.

Lienhart, R. & Wernicke, A. (2002) Localizing and segmenting text in images and videos. *IEEE Transactions on Circuits and Systems for Video Technology*. 12(4), 256–268.

Lim, S.S., Vos, T., Flaxman, A.D., Danaei, G., Shibuya, K., Adair-Rohani, H., AlMazroa, M.A., Amann, M., Anderson, H.R., Andrews, K.G. and Aryee, M., 2012. A comparative risk assessment of burden of disease and injury attributable to 67 risk factors and risk factor clusters in 21 regions, 1990–2010: a systematic analysis for the Global Burden of Disease Study 2010. The lancet, 380(9859), pp.2224-2260.

Liu, R. W., Shi, L., Huang, W., Xu, J., Yu, S.C. & Wang, D. (2014) Generalized total variation-based MRI Rician de-noising model with spatially adaptive regularization parameters. *Magnetic Resonance Imaging*. 32(6), 702–720.

Liu, R., Chen, Y., Jiao, L. & Li, Y. (2014) A particle swarm optimization based simultaneous learning framework for clustering and classification. *Pattern Recognition*. 47(6), 2143–2152.

Lo, S. C. B., Li, H., Wang, Y., Kinnard, L. & Freedman, M. T. (2002) A multiple circular path convolution neural network system for detection of mammographic masses. *IEEE Transactions on Medical Imaging*. 21(2), 150–158.

MacMahon, B. and Feinleib, M., 1960. Breast Cancer in Relation to Nursing and Menopausal History 2. JNCI: Journal of the National Cancer Institute, 24(3), pp.733-753.

Madhukumar, S. and Santhiyakumari, N., 2015. Evaluation of k-Means and fuzzy C-means segmentation on MR images of brain. The Egyptian Journal of Radiology and Nuclear Medicine, 46(2), pp.475-479.

Mairal, J., Sapiro, G. & ELAD, M. (2008) Learning multiscale sparse representations for image and video restoration. *Multiscale Modeling Simulation*. 7, 214–241.

Malladi, R. & Sethian, J. A. (1996) A unified approach to noise removal, image enhancement, and shape recovery. *IEEE Transactions on Image Processing*. 5(11), 1554–1568.

Manjón, J.V., Coupé, P., Martí-Bonmatí, L., Collins, D. L. & Robles, M. (2010) Adaptive non-local means de-noising of MR images with spatially varying noise levels. *Journal of Magnetic Resonance Imaging*. 31, 192–203.

Mann, R. M., Balleyguier, C., Baltzer, P. A., Bick, U., Colin, C., Cornford, E., ... & Gilbert, F. J. (2015) Breast MRI: EUSOBI recommendations for women's information. *European Radiology*. 25(12), 3669–3678.

Mao, J. & Jain, A. K. (1992) Texture classification and segmentation using multiresolution simultaneous autoregressive models. *Pattern Recognition*. 25(2), 173–188.

Mao, J. & Jain, A. K. (1996). A self-organizing network for hyperellipsoidal clustering (HEC). *IEEE Transactions on Neural Networks*. 7(1), 16–29.

Mathers, C.D., Stevens, G.A., Boerma, T., White, R.A. and Tobias, M.I., 2015. Causes of international increases in older age life expectancy. The Lancet, 385(9967), pp.540-548.

McPhee, K. C., Denk, C., Al-Rekabi, Z. & Rauscher, A. (2011) Bilateral filtering of magnetic resonance phase images. *Magnetic Resonance Imaging*. 29(7), 1023–1029.

McPherson, C. P., Swenson, K. K. & Lee, M. W. (2002). The effects of mammographic detection and comorbidity on the survival of older women with breast cancer. *Journal of the American Geriatrics Society*. 50(6), 1061–1068.

Meena, A. & Raja, R. (2013) *Symmetry based cluster approach for automatic recognition of the epileptic focus in brain using PET scan image analysis*. arXiv preprint.

Mehrabi, A., Hafezi, M., Arvin, J., Esmaeilzadeh, M., Garoussi, C., Emami, G., Kössler-Ebs, J., Müller-Stich, B. P., Büchler, M. W., Hackert, T. & Diener, M. K. (2015) A systematic review and meta-analysis of laparoscopic versus open distal pancreatectomy for benign and malignant lesions of the pancreas: It's time to randomize. *Surgery*. 157(1), 45–55.

Min-Yuan, C. & Kuo-Yu, H. (2009) K-means clustering and chaos genetic algorithm for nonlinear optimization. In: *Proceedings of The International Symposium on Automation*

and Robotics in Construction (ISARC).

Moein, S. (ed.). (2014) *Medical diagnosis using artificial neural networks*. *Hershey*, Pennsylvania: IGI Global.

Muir, Robert. "The evolution of carcinoma of the mamma." The Journal of Pathology 52, no. 2 (1941): 155-172.

Nakano, S., Sakamoto, H., Ohtsuka, M., Mibu, A., Sakata, H. & Yamamoto, M. (2007) Evaluation and indications of ultrasound-guided vacuum-assisted core needle breast biopsy. *Breast Cancer*. 14(3), 292–296.

Nayak, J., Nanda, M., Nayak, K., Naik, B. and Behera, H.S., 2014. An improved firefly fuzzy c-means (FAFCM) algorithm for clustering real world data sets. In Advanced Computing, Networking and Informatics-Volume 1 (pp. 339-348). Springer, Cham.

Neha, T. & Sahu, O. P. (2014) MRI brain tumor segmentation using improved ACO. *International Journal of Electronic and Electrical Engineering*, 7(1), 85–90.

Noble, J. A. (2010) Ultrasound image segmentation and tissue characterization. *Proceedings of the Institution of Mechanical Engineers, Part H: Journal of Engineering in Medicine*. 224(2), 307–316.

Nowak, R. D. (1999) Wavelet-based Rician noise removal for magnetic resonance imaging. *IEEE Transactions on Image Processing*, 8(10), 1408–1419.

Osman, H. & Fahmy, M. M. (1994) Probabilistic winner-take-all learning algorithm for radial-basis-function neural classifiers. *Neural Computation*. 6(5), 927–943.

Pal, N. R., Bezdek, J. C. & Tsao, E. K. (1993) Generalized clustering networks and Kohonen's self-organizing scheme. *IEEE Transactions on Neural Networks*. 4(4), 549–557.

Palma, C. A. & Cappabianco, F. A. (2014) Anisotropic diffusion filtering operation and limitations - magnetic resonance imaging evaluation. *IFAC Proceedings Volumes*. 19(1), 3887–3892.

Pan, S., Liu, W., Jin, K., Liu, Y. & Zhou, Y. (2014) Ultrasound-guided vacuum-assisted breast biopsy using Mammotome biopsy system for detection of breast cancer: Results from two high volume hospitals. *International Journal of Clinical and Experimental Medicine*. 7(1), 239.

Pandit-Taskar, N., Gemignani, M. L., Lyall, A., Larson, S. M., Barakat, R. R. & Rustum, N. R. A. (2010). Single photon emission computed tomography SPECT-CT improves sentinel node detection and localization in cervical and uterine malignancy. *Gynecologic Oncology*. 117(1), 59–64.

Parker, S. H., Klaus, A. J., Mc Wey, P. J., Schilling, K. J., Cupples, T. E., Duchesne,

N., ... & Harness, J. K. (2001) Sonographically guided directional vacuum-assisted breast biopsy using a handheld device. *American Journal of Roentgenology*. 177(2), 405–408.

Parker, S.L., Tong, T., Bolden, S. and Wingo, P.A., 1996. Cancer statistics, 1996. CA: A cancer journal for clinicians, 46(1), pp.5-27.

Perona, P. & Malik, J. (1990) Scale-space and edgedetection using anisotropic diffusion. *IEEE Transactions on Pattern Analysis and Machine Intelligence*. 12(7), 629–639.

Ponto, L. L. B., Menda, Y., Magnotta, V. A., Yamada, T. H., Denburg, N. L. & Schultz, S. K. (2015) Frontal hypometabolism in elderly breast cancer survivors determined by [18F] fluorodeoxyglucose (FDG) positron emission tomography (PET): A pilot study. *International Journal of Geriatric Psychiatry*. 30(6), 587–594.

Rabbani, H., Nezafat, R. & Gazor, S. (2009) Wavelet-domain medical image de-noising using bivariate laplacian mixture model. *IEEE Transactions on Biomedical Engineering*. 56(12), 2826–2837.

Rack, B., Schindlbeck, C., Jückstock, J., Andergassen, U., Hepp, P., Zwingers, T., et al. (2014) Circulating tumor cells predict survival in early average-to-high risk breast cancer patients. *Journal of the National Cancer Institute*. 106(5), pii: dju066.

Rodby, K. A., Robinson, E., Danielson, K. K., Quinn, K. P. & Antony, A. K. (2016) Age-dependent characteristics in women with breast cancer: Mastectomy and reconstructive trends at an urban academic institution. *The American Surgeon*. 82(3), 227–235.

Rosenblatt, F. (1958) The perceptron: A probabilistic model for information storage and organization in the brain. *Psychological Review*. 65(6), 386.

Rosenblatt, F. (1962) *Principles of neurodynamics*: *Perceptrons and the theory of brain mechanisms*. Washington: Spartan Books.

Rumelhart, D. E., Smolensky, P., McClelland, J. L. & Hinton, G. (1986) Sequential thought processes in PDP models. *Parallel Distributed Processing: Explorations in the Microstructures of Cognition*. 2, 3–57.

Saslow, D., Boetes, C., Burke, W., Harms, S., Leach, M. O., Lehman, C. D., ... & Smith, R. A. (2007) American Cancer Society guidelines for breast screening with MRI as an adjunct to mammography. *CA: A Cancer Journal for Clinicians*. 57(2), 75–89.

Sauter, E. R., Ross, E., Daly, M., Klein-Szanto, A., Engstrom, P. F., Sorling, A., Malick, J. & Ehya, H. (1997) Nipple aspirate fluid: A promising non-invasive method to identify cellular markers of breast cancer risk. *British Journal of Cancer*. 76(4), 494.

Schelling, M., Avril, N., Nahrig, J., Kuhn, W., Romer, W., Sattler, D., ... & Schwaiger, M. (2000) Positron emission tomography using [18F] fluorodeoxyglucose for

monitoring primary chemotherapy in breast cancer. *Journal of Clinical Oncology*. 18(8), 1689–1695.

Schwartz, T., Stark, A., Pang, J., Awuah, B., Kleer, C. G., Quayson, S., et al. (2013) Expression of aldehyde dehydrogenase 1 as a marker of mammary stem cells in benign and malignant breast lesions of Ghanaian women. *Cancer*. 119(3), 488–494.

Selvy, P. T., Palanisamy, V. & Radhai, M. (2013) A proficient clustering technique to detect CSF level in MRI brain images using PSO algorithm. *WSEAS Transactions on Computers*. 12(7), 298–308.

Senapati, M. R., Mohanty, A. K., Dash, S. & Dash, P. K. (2013) Local linear wavelet neural network for breast cancer recognition. *Neural Computing and Applications*. 22(1), 125–131.

Senkus, E., Kyriakides, S., Ohno, S., Penault-Llorca, F., Poortmans, P., Rutgers, E., Zackrisson, S. & Cardoso, F. (2015). Primary breast cancer: ESMO Clinical Practice Guidelines for diagnosis, treatment and follow-up. *Annals of Oncology*. 26(suppl 5), v8–v30.

Serres, S., Soto, M. S., Hamilton, A., McAteer, M. A., Carbonell, W. S., Robson, M. D., ... & Weissensteiner, T. (2012). Molecular MRI enables early and sensitive detection of brain metastases. *Proceedings of the National Academy of Sciences*. 109(17), 6674–6679.

Sharma, A. & Gulista. (2011) Performance comparison of K-means & canny edge detection algorithm on MRI images. *International Journal of Mobile Network Communications & Telematics*. 1(1).

Sickles, E. A., Filly, R. A., Callen, P. W. (1983) Breast detection with sonography and mammography. *AJR*. 140, 843–845.

Slichter, C. P. (2013). *Principles of magnetic resonance* (Vol. 1). Springer Science & Business Media.

Soesanti, I., Susanto, A., Widodo, T. S. & Tjokronagoro, M. (2011) Optimized fuzzy logic application for MRI brain images segmentation. *International Journal of Computer Science & Information Technology*. 3(5), 137–146.

Sölétormos, G., Nielsen, D., Schiøler, V., Mouridsen, H. & Dombernowsky, P. (2004). Monitoring different stages of breast cancer using tumour markers CA 15-3, CEA and TPA. *European Journal of Cancer*. 40(4), 481–486.

Somasundaram, I. K. & Shankar, S. (2014) Automated skull stripping method using clustering and histogram analysis for MRI human head scans. *International Journal of Advanced Research in Computer Science and Technology*. 2(3), 117–122.

Sommers, C.L., Walker-Jones, D., Heckford, S.E., Worland, P., Valverius, E., Clark,

R., McCormick, F., Stampfer, M., Abularach, S. and Gelmann, E.P., 1989. Vimentin rather than keratin expression in some hormone-independent breast cancer cell lines and in oncogene-transformed mammary epithelial cells. Cancer research, 49(15), pp.4258-4263.

Sonka, M., Hlavac, V. & Boyle, R. (2014) *Image processing, analysis, and machine vision*. Canada: Cengage Learning.

Stark, A. M., Schem, C., Maass, N., Hugo, H. H., Jonat, W., Mehdorn, H. M. & Held-Feindt, J. (2010) Expression of metastasis suppressor gene maspin is reduced in breast cancer brain metastases and correlates with the estrogen receptor status. *Neurological Research*. 32(3), 303–308.

Strauss, L., Bostel, F., Clorius, J. H., Raptou, E., Wellman, H. & Georgi, P. (1982) Single-photon emission computed tomography (SPECT) for assessment of hepatic lesions. *Journal of Nuclear Medicine: Official Publication, Society of Nuclear Medicine*. 23(12), 1059–1065.

Tabik, S., Garzon, E. M. & Garcia, I. (2006) Multiprocessing of anisotropic nonlinear diffusion for filtering 3D images. *International Conference on Parallel, Distributed, and Network-Based Processing*. 7.

Tamijeselvy, P., Palanisamy, V. & Elakkiya, S. (2013a) A novel approach for the prediction of epilepsy from 2D medical images using case based reasoning classification model. *WSEAS Transactions on Computers*. 243–254.

Tamijeselvy, P., Palanisamy, V. & Sri Radhai, M. (2013b) Image segmentation using clustering technique and swarm intelligence. *Journal of Global Research in Computer Science*. 4(4), 200–203.

Taylor, P. (2008) From patient data to medical knowledge: The principles and practice of health informatics. Hoboken, New Jersey: John Wiley & Sons.

Taylor, R. H., Menciassi, A., Fichtinger, G. & Dario, P. (2008) Medical robotics and computer-integrated surgery. In: *Springer handbook of robotics*. Berlin Heidelberg: Springer. pp. 1199–1222.

Theilmann, R. J., Borders, R., Trouard, T. P., Xia, G., Outwater, E., Ranger-Moore, J., ... & Stopeck, A. (2004) Changes in water mobility measured by diffusion MRI predict response of metastatic breast cancer to chemotherapy. *Neoplasia*. 6(6), 831–837.

Tiede, B. and Kang, Y., 2011. From milk to malignancy: the role of mammary stem cells in development, pregnancy and breast cancer. Cell research, 21(2), pp.245-257.

Timp, S., Varela, C. & Karssemeijer, N. (2010) Computer-aided diagnosis with temporal analysis to improve radiologists' interpretation of mammographic mass lesions.

IEEE Transactions on Information Technology in Biomedicine. 14(3), 803–808.

Tristán-Vega, T., Garcia Perez, V., Aja-Fernández, S. & Westin, C. F. (2012) Efficient and robust nonlocal means de-noising of MR data based on salient features matching. *Computer Methods and Programs in Biomedicine*. 105(2), 131–144.

Ueda, S., Tsuda, H., Asakawa, H., Shigekawa, T., Fukatsu, K., Kondo, N., ... & Abe, Y. (2008) Clinicopathological and prognostic relevance of uptake level using 18F-fluorodeoxyglucose positron emission tomography/computed tomography fusion imaging (18F-FDG PET/CT) in primary breast cancer. *Japanese Journal of Clinical Oncology*. 38(4), 250–258.

Valerio, M., Donaldson, I., Emberton, M., Ehdaie, B., Hadaschik, B. A., Marks, L. S., ... & Ahmed, H. U. (2015) Detection of clinically significant prostate cancer using magnetic resonance imaging–ultrasound fusion targeted biopsy: A systematic review. *European Urology*. 68(1), 8–19.

Van Heertum, R. L., Scarimbolo, R., Ford, R., Berdougo, E. & O'Neal, M. (2015) Companion diagnostics and molecular imaging-enhanced approaches for oncology clinical trials. *Drug Design, Development and Therapy*. 9, 5215.

Varghees, V. N., Manikandan, M. S. & Gini, R. (2012) Adaptive MRI image de-noising using total-variation and local noise estimation. *International Conference on Advances in Engineering, Science and Management*. 506–511.

Vesanto, J. & Alhoniemi, E. (2000) Clustering of the self-organizing map. *IEEE Transactions on Neural Networks*. 11(3), 586–600.

Vorherr, H., 2012. The breast: morphology, physiology, and lactation. Elsevier.

Walker, S. A., Miller, D. & Tanabe, J. (2006) Bilateral spatial filtering: Refining methods for localizing brain activation in the presence of parenchymal abnormalities. *Neuro Image*. 33(2), 564–569.

Wang, Y. & Zhou, H. (2006) Total variation wavelet-based medical image de-noising . *International Journal of Biomedical Imaging*. 1–6.

Wells, C. J., O'Donoghue, C., Ojeda-Fournier, H., Retallack, H. E. & Esserman, L. J. (2013) Evolving paradigm for imaging, diagnosis, and management of DCIS. *Journal of the American College of Radiology*. 10(12), 918–923.

Wiest-Daesslé, N., Prima, S., Coupé, P., Morrissey, S. P. & Barillot, C. (2008) Rician noise removal by non-local means filtering for low signal-to-noise ratio MRI: Applications to DR-MRI. *MICCAI*. 11, 171–179.

Wood, D.A. and Darling, H.H., 1943. A cancer family manifesting multiple

occurrences of bilateral carcinoma of the breast. Cancer Research, 3(8), pp.509-514.

Woods, K., Bowyer, K. W. & Sallam, M. Y. (2002) Evaluating detection algorithms. In: Strickland, R. N. (ed.). *Image-processing techniques for tumor detection*. New York: CRC Press.

World Health Organization. (2007) *Cancer control: knowledge into action: WHO guide for effective programmes* (Vol. 2). Geneva, Switzerland: World Health Organization.

Yang, D., Gross, C.P. and Yu, J.B., 2013. Changes in Early-and Late-Stage Colorectal Cancer Incidence During the Era of Screening: 1976-2009. International Journal of Radiation Oncology• Biology• Physics, 87(2), p.S331.

Yang, L. and Jacobsen, K.H., 2008. A systematic review of the association between breastfeeding and breast cancer. Journal of women's health, 17(10), pp.1635-1645.

Yaroslavsky, L.P., Egiazarian, K. & Astola, J. (2000) Transform domain image restoration methods: Review, comparison and interpretation. *TICSP*. 155.

Zanaty, E. A. (2013) An adaptive fuzzy C-means algorithm for improving MRI segmentation. *Open Journal of Medical Imaging*. 3(4), 125.

Zare, M., Rezvani, Z. and Benasich, A.A., 2016. Automatic classification of 6-month-old infants at familial risk for language-based learning disorder using a support vector machine. Clinical Neurophysiology, 127(7), pp.2695-2703.

Zhang, P., Verma, B. & Kumar, K. (2004) A neural-genetic algorithm for feature selection and breast abnormality classification in digital mammography. *Neural Networks*. 3, 2303–2308.

Zhang, X., Hou, G., Ma, J., Yang, W., Lin, B., Xu, Y., Chen, W. & Feng, Y. (2014) De-noising MR images using non-local means filter with combined patch and pixel similarity. *PloS One*. 9(6).

Zhang, Y., Liu, B., Ji, X. and Huang, D., 2017. Classification of EEG signals based on autoregressive model and wavelet packet decomposition. Neural Processing Letters, 45(2), pp.365-378.

Zhen, L. & Chan, A. K. (2001) An artificial intelligent algorithm for tumor detection in screening mammogram. *IEEE Transactions on Medical Imaging*. 20(7), 559–567.

Zheng, B., Qian, W., & Clarke, L. P. (1996) Digital mammography: mixed feature neural network with spectral entropy decision for detection of microcalcifications. *IEEE Transactions on Medical Imaging*. 15(5), 589–597.

Zheng, B., Yoon, S. W. & Lam, S. S. (2014) Breast cancer diagnosis based on feature extraction using a hybrid of K-means and support vector machine algorithms. *Expert Systems*

with Applications. 41(4), 1476–1482.

Zheng, L., Chan, A. K., McCord, G., Wu, S. & Liu, J. S. (1999) Detection of cancerous masses for screening mammography using discrete wavelet transform-based multiresolution Markov random field. *Journal of Digital Imaging*. 12, 18–23.